Chaotic Modeling and Simulation (CMSIM) 1: 67-80, 2012

A Nonlinear Schrödinger-like Equation in the Statistical Theory of Spheroidal Bodies

Alexander M. Krot[1]

[1] Laboratory of Self-Organization Systems Modeling, United Institute of Informatics Problems of National Academy of Sciences of Belarus, Minsk, Belarus
(E-mail: alxkrot@newman.bas-net.by)

Abstract: A statistical theory is proposed for initial gravitational interactions of particles inside the forming cosmological bodies (molecular clouds), which have fuzzy contours and are represented by spheroidal forms. The equation for quasi-equilibrium gravitational compression of a spheroidal body in a vicinity of its mechanical equilibrium is considered initially. According to the proposed model of quasi-equilibrium gravitational compression an antidiffusion mass flow arises inside a slowly compressible gravitating spheroidal body. In this connection, the notions of antidiffusion mass flow density as well as antidiffusion particle velocity in a spheroidal body are introduced. The equations for calculating the partial derivative of the antidiffusion velocity (in the cases of absence or presence of an ordinary hydrodynamic velocity) as well as the complete derivative of the common (hydrodynamic plus antidiffusion) velocity with respect to time are obtained. As shown in this work, these equations are more general than the analogous equations derived in Nelson' stochastic mechanics. They are used for the derivation of nonlinear time-dependent Schrödinger-like equation describing a gravitational formation of a cosmological body.
Keywords: Molecular clouds, Initial gravitational interactions, Spheroidal bodies, Quasi-equilibrium gravitational compression, Antidiffusion mass flow, Antidiffusion velocity, Nonlinear Schrödinger-like equation.

1 Introduction

A statistical theory of slowly compressible gravitating cosmological body formed by a numerous of interacted particles isolated from an influence of external fields and bodies has been proposed in the works [1–6]. Within framework of this theory, the forming cosmological bodies are shown to have fuzzy contours and are represented by spheroidal forms (unlike ordinary macroscopic bodies having distinct contours). In this connection a new notion of theoretical mechanics called a *spheroidal body* has been introduced in the works [1–6] (in addition to the well-known notion as mass point). A mass point m_0 does not possess any geometrical sizes, on the contrary, a spheroidal body with mass M has infinitely long sizes (in the physical sense of infinity, of course). By analogy with the well-known dilemma "particle–wave" (solved by means of corpuscular–wave dualism principle in the case of quantum mechanical particles) it is appropriate to consider a new concept "mass point–spheroidal

Received: 21July 2011 / Accepted 27 December 2011

ISSN 2241-0503

body". Let us note that a cosmological body can be considered as a mass point at long distance of its observation or as a spheroidal body at short distance respectively.

In such spheroidal bodies, under the condition of critical values of mass density (or parameter of gravitational compression α [5, 6]) the centrally symmetric gravitational field arises. The tension, force, potential and energy of the gravitating spheroidal body have been determined to be of probability character [1, 2]. It has been pointed out that a spheroidal body has a clearly outlined form if the potential energy of gravitational interaction of its particles is sufficiently great and the body's mass itself is relatively small. Obviously, the spheroidal body (like the well-known objects in the theoretic physics as a single mass point, an absolutely rigid body etc.) is an *idealized* notion.

A process of slow-flowing-in time initial gravitational contraction of a spheroidal body has been investigated [3, 7]. Within framework of model of this process, the equations have been derived for description of a slow-flowing quasi-equilibrium gravitational compression of a spheroidal body in a vicinity of unstable mechanical equilibrium (initial and quasi-equilibrium) state [3, 7].

This paper considers the slow-flowing process of an initial gravitational condensation of a spheroidal body leading to origin of its gravitational field. The process of initial quasi-equilibrium gravitational compression of a spheroidal body in space within framework of the proposed "vibrating strainer" model can be interpreted on the basis of Wiener process in a space-frequency domain [8–10].

Recently L. Nottale [11, 12] has developed a new theory of the scale relativity. In Nottale's theory, both direct and reverse Wiener processes are considered in parallel; that leads to the introduction of a twin Wiener (backward and forward) process as a single complex process [11, 12]. For the first time backward and forward derivatives for the Wiener process were introduced within framework of statistical mechanics of Nelson [13, 14]. Both Nelson's statistical mechanics and Nottale's scale relativistic theory investigate families of virtual trajectories which being continuous but nondifferentiable. The important point in Nelson's works [13, 14] is that a diffusion process can be described in terms of a Schrödinger-type equation, with help of the hypothesis that any particle in the empty space, under the influence of any interaction field, is also subject to a universal Brownian motion (i.e. from the mathematical view-point, a Markov–Wiener process) [15] based on the quantum nature of space-time in quantum gravity theories or on quantum fluctuations on cosmic scale [16–18].

In the previous works [1–6], it was supposed that a weakly gravitating spheroidal body is isolated from influence of other fields and bodies, it is homogeneous in its chemical structure and has the temperature close to the absolute zero. In this paper we accept the same methodology supposing that the following assumptions are used:

1. The spheroidal body under consideration is homogeneous in its chemical structure, i.e. it consists of N identical particles with the mass m_0.

2. The spheroidal body is not subjected to an influence of external fields and bodies.

3. The spheroidal body is isothermal and has temperature T close to the absolute zero, besides $T_{\deg} < T$, where $T_{\deg} = (h^2 / m_0 k_B) n^{2/3}$ is a degeneration temperature [19], h is the Planck's constant, k_B is the Boltzmann's constant, n is a concentration of particles.

4. The spheroidal body is weakly gravitating, i.e. it occurs in a state close to a state of instable mechanical equilibrium (when a hydrodynamic mass flow is absent though a weak mass flow takes place [20, 21]), therefore the process of gravitational contraction (compression) appears slowly developing in time (the case of *unobservable* velocities of particles composing the spheroidal body [4, 22]).

In compliance with these requirements, an attempt to derive a nonlinear equation describing a gravitational formation of a cosmological body based on model of self-organizing processes into a spheroidal body is made in this paper.

2 The density of antidiffusion mass flow and antidiffusion velocity into a slow-flowing gravitational compressible spheroidal body

As shown in the papers [3, 6], the dynamics of a slowly evolving process of initial gravitational condensation of a spheroidal body from an infinitely distributed substance is described by the *antidiffusion equation*:

$$\frac{\partial \rho}{\partial t} = -\mathrm{G}(t)\nabla^2 \rho, \tag{1}$$

where ρ is a mass density of the spheroidal body and

$$\mathrm{G}(t) = \frac{1}{2\alpha^2} \cdot \frac{d\alpha}{dt} \tag{2a}$$

is a *gravitational compression function*, generally speaking (or a gravitational compression coefficient in some particular cases [3, 7]), α is a *parameter of gravitational compression* (slowly changing in time t), besides $\alpha > 0$ [1–7]. The solution of Eq. (1) gives us the mass density function of a *non-rotating* spheroidal body:

$$\rho(r,t) = \rho_0(t)\mathrm{e}^{-\frac{\alpha(t)}{2} r^2}, \tag{2b}$$

where $\rho_0(t) = M\left(\frac{\alpha(t)}{2\pi}\right)^{3/2}$, M is a mass of the spheroidal body, r is a radial coordinate.

We are going to use the general equation (1) of the slow-flowing gravitational compression; for this we shall rewrite it taking into account that

gravitational compression function $\mathrm{G}(t)$ does not depend on the space variable *r*, therefore:

$$\frac{\partial\rho}{\partial t} = -\nabla\left(\mathrm{G}(t)\nabla\rho\right) = -\mathrm{div}\left(\mathrm{G}(t)\mathrm{grad}\,\rho\right), \tag{3a}$$

whence

$$\frac{\partial\rho}{\partial t} + \mathrm{div}\left(\mathrm{G}(t)\,\mathrm{grad}\,\rho\right) = 0\,. \tag{3b}$$

The relation (3b) reminds completely the continuity equation expressing the law of conservation of mass in a nonrelativistic system [23]:

$$\frac{\partial\rho}{\partial t} + \mathrm{div}\,\vec{j} = 0\,, \tag{4a}$$

where $\vec{j}$ is a continuum flow density. In this connection, the value in round brackets of Eq. (3b) has the sense of a mass flow density (like a conductive flow) $\vec{j}$ arising at the slow-flowing gravitational compression of spheroidal body [3, 4, 7]:

$$\vec{j} = \mathrm{G}(t)\,\mathrm{grad}\rho\,. \tag{4b}$$

For the first time, conductive (owing to diffusion or thermal conductivity) flows in dissipative systems were investigated by I. Prigogine in his works (see, for example, [20, 21]). As it follows from Eq. (4b) directly, there exists an *antidiffusion mass flow density* in a slowly compressible gravitating spheroidal body [3, 6]. Applying the equation of continuity (4a) to this antidiffusion flow density (4b) we obtain again the well-known linear antidiffusion equation (1). Since ρ is a function of the space variable r, then in the spherical system of coordinates $\mathrm{grad}\,\rho = \dfrac{\partial\rho}{\partial r}\vec{e}_r = \dfrac{\partial\rho}{\partial r}\cdot\dfrac{\vec{r}}{r}$. Taking into account the fact that according to (2) the mass density ρ is an exponentially decreasing function, then its derivative $\dfrac{\partial\rho}{\partial r} < 0$. Consequently, the direction of the antidiffusion flow density vector $\vec{j}$ is directly opposite to the basis vector $\vec{e}_r$, i.e. the vector $\vec{j}$ is directed to the spheroidal body center.

Like the particle momentum operator $\hat{p} = i\hbar\nabla$ in the quantum mechanics [24–26], we can introduce from Eq. (4b) a *velocity operator* in the case of *unobservable* velocities of particles composing a spheroidal body [4, 22]:

$$\hat{v} = \mathrm{G}(t)\nabla\,, \tag{5}$$

i.e. $\hat{v}$ is the operator of unobservable antidiffusion velocity. Taking into account this Eq. (5) the antidiffusion mass flow density (4b) of slow-flowing gravitational contraction of spheroidal body (with unobservable velocities of particles) can be written as follows [4, 22]:

$$\vec{j} = \hat{v}\rho\,. \tag{6}$$

According to Eq. (6) the continuity equation (4a) takes the form:

$$\frac{\partial\rho}{\partial t} + \mathrm{div}(\hat{v}\rho) = 0\,. \tag{7}$$

As it has been mentioned above, I. Prigogine, G. Nicolis, P. Glansdorff studied the so-called conductive (diffusive and thermal conductive) flows [20, 21] satisfying equations analogous to Eqs.(4a), (7). In this connection, along with the velocity operator $\hat{v}$ let us introduce a conductive velocity for the antidiffusion mass flow density or, simply say, *antidiffusion velocity*:

$$\vec{u} = \mathrm{G}(t)\frac{\nabla\rho}{\rho} = \mathrm{G}(t)\,\mathrm{grad}\ln\rho. \tag{8}$$

Obviously, the antidiffusion velocity $\vec{u}$ of the antidiffusion mass flow density satisfies the well-known continuity equation of the kind:

$$\frac{\partial\rho}{\partial t} + \mathrm{div}(\rho\vec{u}) = 0\,. \tag{9}$$

Using this continuity equation (9) we can calculate the partial derivative of the antidiffusion velocity (8) with respect to time:

$$\begin{aligned}
&\frac{\partial\vec{u}}{\partial t} = \{\frac{d\mathrm{G}(t)}{dt}\}\,\mathrm{grad}\ln\rho + \mathrm{G}(t)\,\mathrm{grad}\,\{\frac{1}{\rho}\frac{\partial\rho}{\partial t}\} = \\
&= \frac{d\mathrm{G}(t)}{dt}\{\frac{1}{\mathrm{G}(t)}\vec{u}\} + \mathrm{G}(t)\nabla\{\frac{1}{\rho}(-\mathrm{div}(\rho\vec{u}))\} = \\
&= \{d\ln\mathrm{G}(t)/dt\}\vec{u} - \mathrm{G}(t)\nabla\{\nabla\vec{u} + \vec{u}\frac{\nabla\rho}{\rho}\} = \\
&= -\mathrm{G}(t)\,\mathrm{grad}(\mathrm{div}\,\vec{u}) - \mathrm{grad}(\vec{u}^{\,2}) + \{d\ln\mathrm{G}(t)/dt\}\vec{u}.
\end{aligned} \tag{10}$$

An advantage of the antidiffusion velocity notion (8) versus the velocity operator notion (5) to be introduced is contained in the fact that the antidiffusion velocity of particles inside a slow-flowing gravitational compressible spheroidal body can become *observable* one if the mass density of spheroidal body is very

small. Indeed, according to Eq. (8) if the mass density $\rho \to 0$ then the antidiffusion velocity $\vec{u} \to \infty$ (under condition that $\mathrm{grad}\rho$ be finitary). The condition of smallness for the mass density ρ takes place in the molecular clouds of distributed gas-dust substance in space [27]. Thus, as a result of spheroidal body formation from an initial weakly condensed gas-dust cloud it might be a sharp *increase* of the antidiffusion velocity of particles into the forming spheroidal body under condition of finiteness of the mass density gradient. In this case it is reasonable to rewrite Eq. (10) based on the familiar formulas of vector analysis [23]:

$$\frac{1}{2}\mathrm{grad}\,\vec{u}^{\,2} = (\vec{u}\cdot\nabla)\vec{u} + [\vec{u}\times\mathrm{rot}\,\vec{u}], \tag{11a}$$

$$\nabla^2\vec{u} = \mathrm{grad}(\mathrm{div}\,\vec{u}) - \mathrm{rot}(\mathrm{rot}\,\vec{u}). \tag{11b}$$

Taking into account Eq. (8) we can see that $\mathrm{rot}\,\vec{u} = 0,$ whence

$$\mathrm{grad}\,\vec{u}^{\,2} = 2(\vec{u}\cdot\nabla)\vec{u}, \tag{12a}$$

$$\nabla^2\vec{u} = \mathrm{grad}(\mathrm{div}\vec{u}). \tag{12b}$$

Substituting Eqs.(12a,b) in Eq. (10) we obtain:

$$\frac{\partial\vec{u}}{\partial t} = -\mathrm{G}(t)\nabla^2\vec{u} - 2(\vec{u}\cdot\nabla)\vec{u} + \{d\ln\mathrm{G}(t)/\mathrm{dt}\}\vec{u}. \tag{13}$$

Taking into account Eq. (12a) again, the equation (13) can be written as follows:

$$\frac{\partial\vec{u}}{\partial t} + (\vec{u}\cdot\nabla)\vec{u} = -\mathrm{grad}(\vec{u}^{\,2}/2) - \mathrm{G}(t)\nabla^2\vec{u} + \{d\ln\mathrm{G}(t)/\mathrm{dt}\}\vec{u}. \tag{14}$$

The obtained equation (14) is similar to the Navier-Stokes' equation of motion of a viscous liquid [23] under conditions that a gas-dust substance of spheroidal body is isolated from influence of external fields and $\mathrm{G}(t) = \mathrm{G_S} = const.$

Now let us estimate the antidiffusion velocity (8) of particles into a spherically symmetric slow-flowing gravitational compressible spheroidal body taking account of its mass density function (2):

$$\vec{u}(\vec{r},t) = \mathrm{G}(t)\,\mathrm{grad}\,\{\ln\rho_0(t) - \alpha(t)\vec{r}^{\,2}/2\} = -\mathrm{G}(t)\alpha(t)\vec{r}. \tag{15}$$

We can see that the antidiffusion velocity $\vec{u}$ is expressed by the very simple relation (15) in the case of a spherically symmetric spheroidal body. Apropos, using approach proposed by W. Ebeling for the first time [28] the equation for spherical autowaves of magnitude of gravitational field strength

$\vec{a} = \dfrac{\partial \vec{u}}{\partial t} + (\vec{u}\nabla)\vec{u}$ of a slowly contracting spheroidal body has been derived in the work [29]. The obtained Eq. (15) reminds the formula the velocity of autowave front propagation [29] for gravitational strength magnitude in a remote zone of slowly compressible gravitating spheroidal body.

Along with the antidiffusion velocity $\vec{u}$ there exists an ordinary hydrodynamic velocity $\vec{v}$ (or a *convective* velocity in the sense of Prigogine [20]). In principle, the hydrodynamic velocity $\vec{v}$ of mass flow arises as a result of powerful gravitational contraction of a spheroidal body on the next stages of its evolution. The growing magnitude of gravitational field strength $\vec{a}$ induces the significant (i.e. observable) value of hydrodynamic velocity $\vec{v}$ of mass flows moving into spheroidal body. This means that the value of antidiffusion velocity (8) becomes much less than the value of hydrodynamic velocity, i.e.

$$|\vec{u}| << |\vec{v}| \ . \tag{16}$$

Under this condition (16), a common (hydrodynamic and antidiffusion) mass flow density inside a spheroidal body satisfies the hydrodynamic equation of continuity [23]:

$$\frac{\partial \rho}{\partial t} + \mathrm{div}(\rho \vec{v}) = 0 \, . \tag{17}$$

Taking into account Eq. (17) we can also calculate the partial derivative of the antidiffusion velocity (8) with respect to time in accord with the condition (16):

$$\begin{aligned} \frac{\partial \vec{u}}{\partial t} &= \{\frac{d\mathrm{G}(t)}{dt}\} \mathrm{grad} \ln \rho + \mathrm{G}(t) \, \mathrm{grad} \, \{\frac{1}{\rho}\frac{\partial \rho}{\partial t}\} = \\ &= \frac{d\mathrm{G}(t)}{dt}\{\frac{1}{\mathrm{G}(t)} \cdot \vec{u}\} + \mathrm{G}(t)\nabla\{\frac{1}{\rho}(-\mathrm{div}(\rho \vec{v}))\} = \\ &= \{d \ln \mathrm{G}(t) / dt\}\vec{u} - \mathrm{G}(t)\nabla\{\nabla \vec{v} + \vec{v}\frac{\nabla \rho}{\rho}\} = \\ &= -\mathrm{G}(t) \, \mathrm{grad}(\mathrm{div}\vec{v}) - \mathrm{grad}(\vec{v}\vec{u}) + \{d \ln \mathrm{G}(t) / dt\}\vec{u}. \end{aligned} \tag{18}$$

As known from a fluid-like description [23], the complete time-derivative of the common (hydrodynamic plus antidiffusion) velocity $\vec{v} + \vec{u}$ inside a spheroidal body defines the common acceleration (or gravitational field strength of spheroidal body) including the partial time-derivatives and convective derivatives:

$$\vec{a} = \frac{d(\vec{v} + \vec{u})}{dt} = \frac{\partial \vec{v}}{\partial t} + (\vec{v} \cdot \nabla)\vec{v} + \frac{\partial \vec{u}}{\partial t} + (\vec{u} \cdot \nabla)\vec{u}. \tag{19a}$$

Taking into account Eq. (14) as well as Eq. (12a), the complete acceleration (19a) can be represented in the form:

$$\vec{a} = \frac{d(\vec{v}+\vec{u})}{dt} = \frac{\partial \vec{v}}{\partial t} + (\vec{v}\cdot\nabla)\vec{v} - (\vec{u}\cdot\nabla)\vec{u} - \mathrm{G}(t)\nabla^2\vec{u} + \{d\ln \mathrm{G}(t)/dt\}\vec{u}. \quad (19b)$$

Let us note since the mass density of spheroidal body is directly proportional to the probability volume density function according to the relation [1–6]:

$$\rho = M\Phi,$$

where Φ is a probability volume density function to locate a particle into spheroidal body, M is a mass of spheroidal body, then antidiffusion velocity (8) (or (15)) can be defined by the probability volume density function:

$$\vec{u} = \mathrm{G}(t)\frac{\nabla \Phi}{\Phi} = \mathrm{G}(t)\,\mathrm{grad}\ln \Phi. \quad (20)$$

Obviously, the antidiffusion velocity (20) of probability volume flow density also satisfies Eqs.(10), (14), (15), (18) and (19a,b).

3 A nonlinear Schrödinger-like equation in the statistical theory of spheroidal bodies

Considerations in the works [1–6] point to an *initial quasi-equilibrium gravitational compression* occurring in a forming spheroidal body. Within framework of the proposed "vibrating strainer" model [8–10], interactions of oscillating particles inside a spheroidal body lead to the coherent displacement of particles and, as a consequence, to a resonance increase of the parameter of gravitational compression $\alpha(t)$. This means *that nonlinear phenomena* arise owing to self-organization processes [21] into a spheroidal body under its formation. These nonlinear phenomena induce nonlinear autowaves satisfying a *nonlinear* Schrödinger-like equation.

Now let us note besides the well-known linear undulatory Schrödinger equation there are its generalizations in the Nelson's statistical mechanics and the Nottale's scale relativity [11–14]. Moreover, it is not difficult to see [10] that both these equations of Schrödinger can be derived in the special case of a constant $\mathrm{G}(t)$ in the antidiffusion equation (1) when $\mathrm{G}(t) = -\hbar/2m_0$ and $\mathrm{G}(t) = -\gamma M/2\upsilon$ respectively. Obviously, this paper considers the general case of $\mathrm{G}(t)$ according to Eq. (2a), which is different from the Nelson's and Nottale's considerations. In this connection let us calculate the partial derivatives (relative to t) of antidiffusion velocity and ordinary hydrodynamic velocity with the aim to obtain a *nonlinear* Schrödinger-like equation by analogy with the Nelson's and Nottale's theories.

So, now let us consider again Eqs.(18), (19b) derived within framework of the statistical theory of gravitating spheroidal bodies. Taking into account the

simple formulas (12a), (12b), (20), these Eqs. (18), (19b) can be rewritten in the form:

$$\frac{\partial \vec{u}}{\partial t} = -\mathrm{G}(t)\,\mathrm{grad}(\mathrm{div}\vec{v}) - \mathrm{grad}(\vec{v}\vec{u}) + \{d\ln \mathrm{G}(t)/dt\}\vec{u}; \qquad (21a)$$

$$\frac{\partial \vec{v}}{\partial t} = \vec{a} - (\vec{v}\cdot\nabla)\vec{v} + \mathrm{grad}(\vec{u}^{\,2}/2) + \mathrm{G}(t)\,\mathrm{grad}(\mathrm{div}\vec{u}) - \{d\ln \mathrm{G}(t)/dt\}\vec{u}. \qquad (21b)$$

Let us investigate some special solution of Eqs. (21a, b) in the case that the acceleration (or gravitational field strength) comes from a gravitational field potential of spheroidal body, i.e.

$$\vec{a} = -\mathrm{grad}\,\varphi_g\,, \qquad (22a)$$

under the assumption that the hydrodynamic velocity $\vec{v}$ is a gradient of a statistical action $\Im$:

$$\vec{v} = 2\mathrm{G}(t)\,\mathrm{grad}\,\Im\,. \qquad (22b)$$

Indeed, Eq. (18) points to a possible justification of Eq. (22b); in the special case of a constant $\mathrm{G}(t)$ as $\hbar/2m_0$ Eq. (22b) becomes the Nelson's formula [13]: $\vec{v} = \dfrac{\hbar}{m_0}\mathrm{grad}\,\Im\,.$

In this connection, $\mathrm{rot}\,\vec{v} = 0$, i.e. $(\vec{v}\cdot\nabla)\vec{v} = \mathrm{grad}(\vec{v}^{\,2}/2)$. Since $\vec{u}$ is also a gradient due to Eq. (20) as well as $\vec{a}$ and $\vec{v}$ according to Eqs. (22a,b), so that Eqs. (21a, b) become the following:

$$\mathrm{grad}\frac{\partial(\mathrm{G}(t)\ln\Phi)}{\partial t} = -\mathrm{G}(t)\,\mathrm{grad}(\mathrm{div}\vec{v}) - \mathrm{grad}(\vec{v}\vec{u}) + \\ + \{d\ln \mathrm{G}(t)/dt\}\mathrm{G}(t)\,\mathrm{grad}\ln\Phi; \qquad (23a)$$

$$\mathrm{grad}\frac{\partial(2\mathrm{G}(t)\Im)}{\partial t} = -\mathrm{grad}\varphi_g - \mathrm{grad}(\vec{v}^{\,2}/2) + \mathrm{grad}(\vec{u}^{\,2}/2) + \\ + \mathrm{G}(t)\,\mathrm{grad}(\mathrm{div}\vec{u}) - \{d\ln \mathrm{G}(t)/dt\}\mathrm{G}(t)\,\mathrm{grad}\ln\Phi. \qquad (23b)$$

Integrating these Eqs.(23a,b) and taking into account a simplification $\{d\ln \mathrm{G}(t)/dt\}\cdot \mathrm{G}(t) = d\,\mathrm{G}(t)/dt$, we can find that

$$\frac{\partial(\mathrm{G}(t)\ln\Phi)}{\partial t} = -\mathrm{G}(t)\mathrm{div}\vec{v} - \vec{v}\vec{u} + \{d\,\mathrm{G}(t)/dt\}\cdot\ln\Phi; \qquad (24a)$$

$$\frac{\partial(2\mathrm{G}(t)\Im)}{\partial t} = -\varphi_g - \vec{v}^2/2 + \vec{u}^2/2 + \mathrm{G}(t)\mathrm{div}\vec{u} - \{d\,\mathrm{G}(t)/dt\}\cdot\ln\Phi. \quad (24b)$$

Let us carry out a change of dependent variable:

$$\Re = \frac{1}{2}\ln\Phi; \quad (25a)$$

$$\Psi = \mathrm{e}^{\Re + i\Im}, \quad (25b)$$

where $\Im$ is defined by Eq. (22b), $i = \sqrt{-1}$. Obviously, as it follows from Eqs. (25a,b) directly

$$\Psi = \sqrt{\Phi}\cdot\mathrm{e}^{i\Im}, \quad (26)$$

so that $\Phi = \Psi\Psi^* = |\Psi|^2$ as usually. According to the first change (25a) it is not difficult to see that

$$\frac{\partial(2\mathrm{G}(t)\,\Re)}{\partial t} = -2\mathrm{G}^2(t)\nabla^2\Im - 4\mathrm{G}^2(t)\nabla\Re\cdot\nabla\Im + 2\{d\,\mathrm{G}(t)/dt\}\cdot\Re; \quad (27a)$$

$$\frac{\partial(2\mathrm{G}(t)\Im)}{\partial t} = -\varphi_g + 2\mathrm{G}^2(t)(\nabla\Re)^2 - 2\mathrm{G}^2(t)(\nabla\Im)^2 + \\ + 2\mathrm{G}^2(t)\nabla^2\Re - 2\{d\,\mathrm{G}(t)/dt\}\cdot\Re. \quad (27b)$$

Let us rewrite these two Eqs. (27a, b) as one. To this end, after multiplication of the second Eq. (27b) on imaginary unit and then addition both of Eqs. (27a, b), we can obtain the following:

$$\frac{\partial}{\partial t}\left[2\mathrm{G}(t)(\Re + i\Im)\right] = -i\varphi_g + i2\mathrm{G}^2(t)(\nabla^2\Re + i\nabla^2\Im) + \\ + i\left[\sqrt{2}\mathrm{G}(t)\nabla(\Re + i\Im)\right]^2 + 2(1-i)\{d\,\mathrm{G}(t)/dt\}\cdot\Re. \quad (28)$$

Taking into account the second change (25b) we can see that

$$\Re + i\Im = \ln\Psi; \quad 2\Re = \ln\Psi + \ln\Psi^* = \ln|\Psi|^2;$$

$\nabla(\Re + i\Im) = \nabla\ln\Psi = \nabla\Psi/\Psi$; $\nabla^2(\Re + i\Im) = \nabla^2\Psi/\Psi - (\nabla\Psi)^2/\Psi^2$, so that Eq. (28) takes the form:

$$\frac{\partial}{\partial t}\left[2\mathrm{G}(t)\ln\Psi\right] = -i\varphi_g + i2\mathrm{G}^2(t)\cdot\frac{\nabla^2\Psi}{\Psi} + (1-i)\{d\,\mathrm{G}(t)/dt\}\cdot\ln|\Psi|^2. \quad (29)$$

After some transformations and simplifications Eq. (29) can be represented as follows:

$$i2\mathrm{G}(t)\frac{\partial\Psi}{\partial t} = \varphi_g\Psi - 2\mathrm{G}^2(t)\cdot\nabla^2\Psi + \\ + i(1-i)2\{d\,\mathrm{G}(t)/dt\}\cdot\Psi\ln|\Psi| - i2\{d\,\mathrm{G}(t)/dt\}\cdot\Psi\ln\Psi, \tag{30}$$

whence we can obtain a nonlinear time-dependent Schrödinger-like equation of the kind:

$$i2\mathrm{G}(t)\frac{\partial\Psi}{\partial t} = [-2\mathrm{G}^2(t)\cdot\nabla^2 + \varphi_g]\Psi + 2\frac{d\,\mathrm{G}(t)}{dt}[\ln|\Psi| - i\ln\frac{\Psi}{|\Psi|}]\Psi. \tag{31}$$

Let us note that $\mathrm{G}(t) = \mathrm{G}_\mathrm{S} = const$ in the *virial* (relative mechanical) *equilibrium* states of spheroidal body [3, 6], so the nonlinear time-dependent Schrödinger equation (31) becomes linear one in these special cases: for example, the time-dependent Schrödinger equation is a particular case of Eq. (31) if $\mathrm{G}(t)$ satisfies the Nelson's basic assumption [13] as well as the generalized time-dependent Schrödinger equation in the form of Nottale is a special case of Eq. (31). A specific particular case of Eq. (31) also corresponds to the Nottale's generalized time-dependent Schrödinger equation with a slowly varying diffusion coefficient δD depending on time. So, the Nelson's and Nottale's considerations are appropriate mainly in the case of gravitational interaction of particles in a spheroidal body being in a virial equilibrium state.

Thus, the derived nonlinear time-dependent Schrödinger equation (31) describes not only the mentioned states of virial mechanical equilibrium $(\mathrm{G}(t) = \mathrm{G}_\mathrm{S} = const)$ or quasi-equilibrium gravitational compression state close to mechanical equilibrium with a slowly varying antidiffusion coefficient $(\mathrm{G}(t) = G/t^2)$ but *gravitational instability states* with the considered resonance increase of gravitational compression of spheroidal body leading to formation of a cosmological body.

4 Conclusions

The main contribution of this paper is to show that gravitational compression of a spheroidal body is described by *nonlinear* Schrödinger-like equation as well as to obtain this nonlinear Schrödinger-like equation.

In Section 2, the equation (1) for the gravitational compression of a spheroidal body is considered initially. This Section investigates the density of antidiffusion mass flow into a slow-flowing gravitational compressible spheroidal body. Here the notion of *antidiffusion velocity* (8) inside a slowly

compressed spheroidal body is introduced. The equations (10), (18) for calculating the partial derivative of the antidiffusion velocity with respect to time (in the cases of absence or presence of the ordinary hydrodynamic velocity) are obtained. The equation (19b) relative to the complete time-derivative of the common (hydrodynamic plus antidiffusion) velocity is also derived.

In this paper, interconnections of the proposed statistical theory of spheroidal bodies with Nelson's statistical mechanics and Nottale's scale relativistic theory are investigated. Really, both Nelson's statistical mechanics and Nottale's scale relativistic theory introduce so-called mean forward and mean backward derivatives [11-14]. It is remarkable that, in the proposed statistical theory of spheroidal bodies, the main equations (relative to *antidiffusion velocity*) have been obtained *without introducing* any *mean forward* nor *mean backward derivatives* of stochastic processes. In this regard, the proposed statistical theory differs profoundly from Nelson' stochastic mechanics [13, 14] as well as from Nottale's scale relativistic theory [11, 12, 16, 30, 31].

Moreover, the obtained main Eqs.(18), (19b) are *more general* than analogous equations in Nelson' stochastic mechanics. Indeed, within framework of the proposed statistical theory of spheroidal bodies the generalized Schrödinger equations can also be derived as in Nottale's scale relativistic theory (in the case of a constant $\mathrm{G}(t)$ the derived nonlinear Schrödinger-like equation (31) becomes the generalized Schrödinger equation). So, the Nelson's and Nottale's considerations are appropriate mainly in the case of gravitational interaction of particles in a spheroidal body being in a *virial* equilibrium state.

As noted in Section 3, this paper investigates more general dynamical states of gravitating spheroidal body. Really, the derived nonlinear time-dependent Schrödinger-like equation (31) describes not only the mentioned states of virial mechanical equilibrium $(\mathrm{G}(t) = \mathrm{G}_{\mathrm{S}} = const)$ or quasi-equilibrium gravitational compression state close to mechanical equilibrium with a slowly varying antidiffusion coefficient $(\mathrm{G}(t) = G / t^2)$, but *gravitational instability states* with a resonance increase of gravitational compression of spheroidal body leading to formation of a cosmological body.

Thus, the *linear* Schrödinger equation as well as its generalizations are mentioned in this work in connection with the Nelson's statistical mechanics and the Nottale's scale relativity only. Moreover, both these equations of Schrödinger have been derived in the special case of a constant of gravitational compression function $\mathrm{G}(t)$ in the proposed antidiffusion equation when $\mathrm{G}(t) = -\hbar / 2m_0$ and $\mathrm{G}(t) = -\gamma M / 2\upsilon$ respectively. In this connection the derived equations for calculating the partial derivatives (relative to t) of antidiffusion velocity and ordinary hydrodynamic velocity are used to obtain a *nonlinear* Schrödinger-like equation by analogy with Nelson's and Nottale's theories. Indeed, nonlinear phenomena arise owing to self-organization processes into a spheroidal body under its formation. These nonlinear

phenomena lead to nonlinear autowaves satisfying a nonlinear Schrödinger-like equation.

As mentioned above, the obtained result (relative to the nonlinear time-dependent Schrödinger-like equation (31)) has been suggested in accordance with similar conclusions of El Naschie [15] and Ord [32] that the Schrödinger equation could be universal, i.e. that it may have a large domain of applications, but with interpretations different from that of standard quantum mechanics. This main conclusion formulated with point of view of these modern quantum gravity theories confirms entirely correctness of the considered approach based on the statistical theory of spheroidal bodies.

References

1. A.M. Krot. The statistical model of gravitational interaction of particles. *Uspekhi Sovremennoï Radioelektroniki* (special issue "Cosmic Radiophysics", Moscow) 8: 66-81, 1996 [in Russian].
2. A.M. Krot. Use of the statistical model of gravity for analysis of nonhomogeneity in earth surface. In: *Proceedings of the SPIE's 13th annual international symposium "AeroSense"*, Orlando, Florida, USA, 5-9 April 1999, vol. 3710, 1248-1259, 1999.
3. A.M. Krot. Statistical description of gravitational field: a new approach. In: *Proceedings of the SPIE's 14th annual international symposium "AeroSense"*, Orlando, Florida, USA, 24-28 April 2000, vol. 4038, 1318-1329, 2000.
4. A.M. Krot. Gravidynamical equations for a weakly gravitating spheroidal body. In: *Proceedings of the SPIE's 15th annual international symposium "AeroSense"*, Orlando, Florida, USA, 16-20 April 2001, vol. 4394, 1271-1282, 2001.
5. A.M. Krot. On the principal difficulties and ways to their solution in the theory of gravitational condensation of infinitely distributed dust substance. In: *Proceedings of the 2007 IAG general assembly "Observing our Changing Earth"*, Perugia, Italy, 2-13 July 2007/Edited by Sideris MG. Berlin, Heidelberg: Springer, vol.133, 283-292, 2009.
6. A.M. Krot. A statistical approach to investigate the formation of the solar system. *Chaos, Solitons & Fractals* 41(3): 1481-1500, 2009.
7. A.M. Krot. The model of slow-gravitating spheroidal body based on statistical approach. In: *Proceedings of the 2nd world conference on mathematics & computers in physics* (MCP 2000), Vouliagmeni, Athens, Greece, 10-15 July 2000, 5181-5188.
8. A.M. Krot. A quantum mechanical approach to description of gravitating body. In: *Proceedings of the 34th scientific assembly of the committee on space research (COSPAR) – the 2nd world space congress-2002*, Houston, Texas, USA, October 10-19, 2002.
9. A.M. Krot. Exploring gravitational interaction of particles based on quantum mechanical principles: an oscillator approach. In: *Proceedings of the European Geoscinces Union (EGU) general assembly*, Vienna, Austria, Geophysical research abstracts, vol.8: 00220, 2-7 April 2006 [SRef-ID: 1607-7962/gra/ EGU06-A-00220].
10. A.M. Krot. A quantum mechanical approach to description of initial gravitational interactions based on the statistical theory of spheroidal bodies. *Nonlinear Sci. Lett.* A. 1(4): 329-369, 2010.
11. L. Nottale. Scale relativity, fractal space-time, and quantum mechanics. *Chaos, Solitons & Fractals* 4:361-388, 1994.

12. L. Nottale. Scale-relativity and quantization of the universe: I. Theoretical framework. *Astron* & *Astrophys* 327:867-889, 1997.
13. E. Nelson. Derivation of the Schrödinger equation from Newtonian mechanics. *Phys Rev* 150(4):1079-1085, 1966.
14. E. Nelson. *Quantum fluctuations*. Princeton (NJ): Princeton University Press, 1985.
15. M.S. El Naschie, E. Rössler, I. Prigogine, editors. *Quantum mechanics, diffusion and chaotic fractals.* Oxford: Pergamon Press, 1995.
16. L. Nottale, M.S. El Naschie, S. Athel, G. Ord. Fractal space–time and Cantorian geometry in quantum mechanics. *Chaos, Solitons & Fractals* 7(6), 1996 [a special issue].
17. G. Ord. Classical particles and the Dirac equation with an electromagnetic force. *Chaos, Solitons & Fractals* 8:727-741, 1997.
18. E.G. Sidharth. *The chaotic universe*. New York: Nova Science, 2001.
19. L.D. Landau, E.M. Lifschitz. *Statistical physics, part 1*. Reading (MA): Addison–Wesley Publishing Co., 1955.
20. P. Glansdorff, I. Prigogine. *Thermodynamic theory of structure, stability and fluctuations.* London, 1971.
21. G. Nicolis, I. Prigogine. *Self-organization in nonequilibrium systems: from dissipative structures to order through fluctuation.* New York: John Willey and Sons, 1977.
22. A.M. Krot. The equations of movement of rotating and gravitating spheroidal body. In: *Proceedings of the 54th international astronautical congress (IAC)*, Bremen, Germany, September 29-October 3, 2003 [Preprint IAC-03-J.1.08].
23. L.D. Landau, E.M. Lifschitz. *Fluid mechanics*. Oxford: Pergamon, 1959.
24. E. Schrödinger. An undulatory theory of the mechanics of atoms and molecules. *Phys Rev* 28(6):1049-1070, 1926.
25. A.S. Davydov. *Quantum mechanics.* Moscow: Nauka, 1973 [in Russian].
26. S. Brandt, H.D. Dahmen. *The picture book of quantum mechanics.* New York: Springer-Verlag, 1994.
27. A.G.W. Cameron. Origin of the solar system. *Annu Rev Astron Astrophys* 26: 441-472, 1988.
28. W. Ebeling. *Origin of structures at irreversible processes: introduction in the theory of dissipative structures.* Rostock, 1977.
29. A.M. Krot. Self-organization processes in a slow-flowing gravitational compressible cosmological body. In: *Selected papers of the CHAOS-2008 international conference in the book "Topics on Chaotic Systems"* /Edited by Skiadas C.H., Dimotikalis I., Skiadas C. Singapore, New Jersey, London, HongKong: World Scientific, p. 190-198, 2009.
30. L. Nottale, G. Schumacher, J. Gay. Scale relativity and quantization of the solar system. *Astron* & *Astrophys* 322: 1018-1025, 1997.
31. L. Nottale, G. Schumacher, E.T. Lef`evre. Scale-relativity and quantization of exoplanet orbital semi-major axes. *Astron* & *Astrophys* 361: 379–387, 2000.
32. G.N. Ord. Fractal space-time and the statistical mechanics of random walks. *Chaos, Solitons & Fractals* 7(6): 821-43, 1996.

Chaotic Modeling and Simulation (CMSIM) 1: 81-90, 2012

Simulating annealing and neural networks for chaotic time series forecasting

George Atsalakis and Katerina Tsakalaki

Technical University of Crete, Greece
atsalak@otenet.gr ; kattsak_89@hotmail.com

Abstract: This paper examines how neural networks that use simulating annealing for training is relative to linear and polynomial approximations to forecast a time series that is generated by the chaotic Mackey-Glass differential delay equation. The forecasting horizon is one step ahead. A series of regressions with polynomial approximators and neural networks that use genetic algorithms and simulating annealing for training are taking place and compare the multiple correlation coefficients. The experimental results confirm that neural networks using simulating annealing algorithm perform well as a global search algorithm. Furthermore, it is shown that using the genetic algorithms to determine their values can improve the forecasting effectiveness of the resulting model when applied to a chaotic time series problem.

Keywords: simulating annealing forecasting, chaos forecasting, Mackey-Glass forecasting, time series forecasting, neural network forecasting.

1 Introduction

Chaotic theory is developing in a new way that influences the world around us and consequently also influences our ways of approaching, analyzing and solving problems. It is not surprising that one of the central models in the chaos literature, the Hénon-Heiles model, is presented in a paper with the title "The applicability of the third integral of motion: Some numerical experiments." Numerical experiments in 1964 were the basis for many significant changes in astronomy in the decades that followed. In 1963 Edwin Lorenz, in his pioneering work on "Deterministic Nonperiodic Flow", proposed a more prominent title for chaotic modelling, by including the term "deterministic". His work spearheaded numerous studies on chaotic phenomena (Skiadas, 2009). On the one hand, according to Wikipedia, simulated annealing (SA) is a generic probabilistic metaheuristic for the global optimization problem of locating a good approximation to the global optimum of a given function in a large search space. It is often used when the search space is discrete (e.g., all tours that visit a given set of cities). For certain problems, simulated annealing may be more efficient than exhaustive enumeration— provided that the goal is merely to find

Received: 25July 2011 / Accepted 20 December 2011

ISSN 2241-0503

an acceptably good solution in a fixed amount of time, rather than the best possible solution. On the other hand, time series prediction is a very important practical problem with a wide variety of applications ranging from economic and business planning to weather forecasting and signal processing and control. A difficulty that characterizes a chaotic time series is that if the data is not generated by a high dimensional process, it should have short-term predictability and so the use of linear forecasting models is not appropriate. This led to the development of several mathematical tools, such as neural networks and neuro-fuzzy systems which deal with nonlinearity and nowadays they are widely used by many researchers. More specific, artificial neural networks (ANNs) have received more and more attention in financial time series forecasting in recent years. This popularity springs from their capability of performing highly complex mappings on nonlinear data. Nonetheless, they have some significant drawbacks such as the lack of any restrictive assumptions about the functional relationships between the predictor variables and the predicated variable, the difficulty to deal with qualitative information and the 'black box' syndrome. On the other hand, fuzzy inference systems incorporate human knowledge by using the if-then rules and expertise for inference and decision making. However, the disadvantage of fuzzy logic is the lack of self learning capability. This is the reason why the integration of these two approaches is preferred in order to overcome the disadvantages not only of the neural networks but also of the fuzzy systems and results in neuro-fuzzy system models. Moreover, many forecasting algorithms have also been developed in order to approximate initially, general continuous functions, such as polynomial approximation, local linear approximation, radial basis functions and neural networks. However, these algorithms still present some limitations as far as the power of prediction is concerned and this is due to the irregularity of chaotic behaviour related to the complication of geometric structures that chaotic attractors possess and the sensitive dependence on initial conditions in chaotic systems. This study is examining the predictability of a simulated annealing algorithm that is used to training an neural network, as far as a time series generated by the chaotic Mackey-Glass differential delay equation. The results are compared with linear and polynomial approximations. The rest of the paper is organized as follows: Section 2 reviews related research and Section 3 discusses the proposed methodology of simulated annealing. Section 4 presents the models and Section 5 reports the empirical findings, while Section 6 includes the conclusions and some further discussions about the future research in this sector.

2 Related research

Many researchers have worked on the chaotic Mackey-Glass differential delay equation and have forecasted time series using different methods including artificial neural networks, fuzzy logic, stochastic models, simulated annealing and even integration of two or more methods. Related researches are the

following: Skiadas C. Rompogianakis G. Atsalakis G., (2001) with the paper titled "Chaotic Aspects of a Generalized Rational Model and Application in Innovation Management" , Atsalakis, G., Skiadas C. and Braimis I., (2007) with the paper titled "Probability of trend prediction of exchange rate by neuro-fuzzy techniques", L.P. Maguire, B. Roche, T.M. McGinnity and L.J. McDaid (1998) have forecasted a chaotic time series using a fuzzy neural network, Atsalakis G., Skiadas C. and Nezis D., (2008) have forecasted chaotic time series using a neural network, J. Doyne Farmer and John J. Sidorowich (1987) have forecasted chaotic time series using a forecasting technique, George G. Szpiro (1997) has forecasted chaotic time series using genetic algorithms, L. Studer and F. Masulli (1996) have forecasted chaotic time series using a neuro-fuzzy system, Ajoy Kumar Palit and D. Popovic (1999) have forecasted chaotic time series using neuro-fuzzy approach, Liang Zhao and Yupu Yang (2009) have used PSO-based single multiplicative neuron model for time series prediction, Hirotaka Inoue, Yoshinobu Fukunaga and Hiroyuki Narihisa (2001) have used efficient hybrid neural network for chaotic time series prediction, Rahib H. Abiyev (2006) has forecasted time series using a fuzzy wavelet neural network model, Junhong Nie (1994) has forecasted time series using a fuzzy-neural approach, M.R. Hassan, B. Nath and M. Kirley (2006) have forecasted time series using HMM based fuzzy model, Mohammad Assaad, Romuald Bone and Hubert Cardot (2006) have forecasted chaotic time series using boosted recurrent neural networks, Ding Gang, Zhong Shi-Sheng and Li Yang (2008) have forecasted time series using a wavelet process neural network, Catherine Vairappan, Hiroki Tamura, Shangce Gao and Zheng Tang (2009) have forecasted time series using batch type local search-based adaptive neuro-fuzzy inference system (ANFIS) with self-feedbacks, Xieping Gao and Fen Xiao (2004) have forecasted chaotic time series using multiwavelet networks, Cui Wan, Zhao Zhu, Chang Chun, Bao Wen, Xing Liu and Jun Hua (2005) have forecasted chaotic time series using support vector machines for fuzzy rule-based modeling, W.K. Wong, Min Xia and W.C. Chu (2010) have forecasted time series using an adaptive neural network model, Hong-Wei Wang, Hong Gu and Zhe-Long Wang (2005) have forecasted chaotic time series based on SVD matrix decomposition, Muhammad Ardalani-Farsa and Saeed Zolfaghari (2010) have forecasted chaotic time series with residual analysis method using hybrid Elman-NARX neural networks, Ping Liu and Jian Yao (2009) have forecasted chaotic time series using least square support vector machine based on particle swarm optimization, H.J. Song, C.Y. Miao, Z.Q. Shen, W. Roel, D.H. Maja and C. Francky (2010) have forecasted chaotic time series using neural networks, Hongwei Wang and Hong Gu (2009) have forecasted chaotic time series based on neural network with Legendre polynomials, Yuehui Chen, Feng Chen and Qiang Wu (2007) have forecasted time series using an artificial neural networks based dynamic decision model, F. Pan, H. Zhang and M. Xia (2009) have forecasted time series using a hybrid forecasting model and Meiying Ye (2007) has forecasted chaotic time series using LS-SVM with simulated annealing algorithms.

3 Simulated Annealing

This paper considers the development of neural network that uses a simulated annealing algorithm in order to forecast a time series generated by the chaotic Mackey-Glass differential delay equation. Simulated annealing is a stochastic search method, which does not rely on the use of first- and second-order derivatives, but starts with an initial guess Ω_0 and proceeds with random updating of the initial coefficients until a "cooling temperature" or stopping criterion is reached. This method starts with a candidate solution vector, Ω_0, and the associated error criterion, Ψ_0. A shock to the solution vector is then randomly generated, Ω_1 , and the associated error metric , Ψ_1 is calculated. If the error metric decreases the new solution vector is always accepted. However, since the initial guess Ω_0 may not be very good, there is a small chance that the new vector, even if it does not reduce the error metric, may be moving in the right direction to a more global solution. So with a probability $P_{(j)}$ conditioned by the Metropolis ratio $M_{(j)}$ the new vector may be accepted, even though the error metric actually increases. The rationale for accepting a new vector Ω_i even if the error Ψi is greater than Ψ_{i-1} , is to avoid the pitfall of being trapped in a local minimum point. According to Robinson (1995), simulated annealing consists of running the accept/reject algorithm between the temperature extremes. As the temperature $T_{(j)}$ cools, changes are more and more likely to be accepted only if the error metric decreases and with gradually decreasing temperature, the algorithm becomes "greedy". Simulated annealing is a random search that moves to a better minimum point, escaping from a likely local minimum rather than a global search and this is the reason why the best one has to do after the convergence to a given point is to see if there are better minimum points in the neighbourhood of the initial minimum. Moreover, the current state of the system or coefficient vector $\hat{\Omega}_j$, depends only on the previous state $\hat{\Omega}_{j-1}$, and a transition problem $P_{(j-1)}$ and is thus independent of all previous outcomes. This system has the Markov chain property and as Haykin points out, an important property of this system is asymptotic convergence, even though resort to finite-time approximation of the asymptotic convergence properties does not guarantee the finding of the global optimum with probability one (McNelis, 2005).

4 Models Presentation

This paper proposes a chaotic time series model, which predicts a time series one step ahead and is generated by the following Mackey-Glass time-delay differential equation.

$$\dot{x}(t) = \frac{0.2x(t-\tau)}{1+x^{10}(t-\tau)} - 0.1x(t)$$

The time series value was obtained by applying the conventional fourth-order Runge-Kutta algorithm. This model shows how efficient simulated annealing is relative to linear and polynomial approximations. Figure 1 depicts the Mackey-Glass chaotic time series.

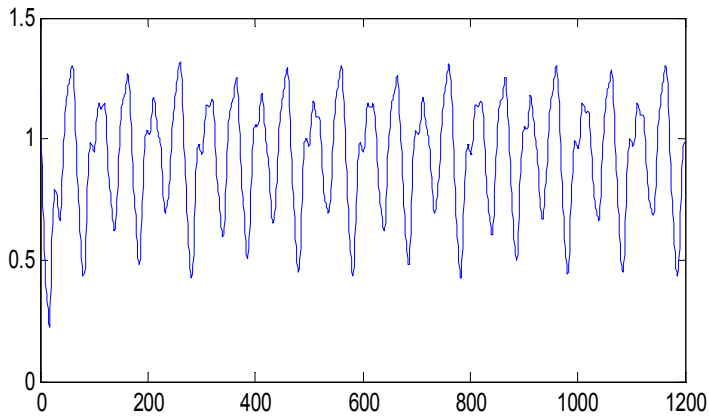

Figure 1. Mackey-Glass chaotic time series

Due to the fact that the time series is chaotic, there is no clearly defined period. Additionally, in time series prediction known values of the time series up to the point in time are used to predict the value at some point in the future. A series of regressions with polynomial approximators and neural networks combined by simulating annealing model is taking place and the multiple correlation coefficients are compared. In this paper, the neural network that is selected uses simulated annealing for training.

Apart from a neural network that uses simulated annealing for training, which was analyzed in section 2, this paper includes the use of linear regression model, power polynomial-order 2 approximation, orthogonal-order 2 approximation (Tchebeycheff, Hermite, Legendre and Laguerre polynomials) and a simple neural network with two neurons and one layer, which uses genetic algorithms for training. Specifically, the linear regression model seeks for a set of

parameters for the regression model to minimize the sum of squared differences between the actual observations y and the observations predicted by the linear model, $\hat{y}$. In contrast to the linear regression model, a polynomial expansion around a set of inputs x with a progressively larger power P is capable of approximating to a given degree of precision any unknown but continuous function $y = g(x)$.[5] and the parameters here are neither limited in number, nor do they have a straightforward interpretation, as the parameters do in linear models. The orthogonal polynomials, such as the Tchebeycheff, Hermite, Legendre and Laguerre polynomials, unlike the typical polynomial based on raising the variable x to powers of higher order, they are based on sine, cosine or alternative exponential transformations of the variable x and they have proven to be more efficient approximators than the power polynomial. Finally, the genetic algorithm is an evolutionary search process, which reduces the likelihood of landing in a local minimum by starting with a population N^* (an even number) of random vectors. The next step is to select two pairs of coefficients from the population at random, with replacement and evaluate the fitness of these four coefficient vectors, in two pair-wise combinations, according to the sum of squared error function. Coefficient vectors that come closer to minimizing the sum of squared errors receive better fitness values and are retained for "breeding" purposes. Then, crossover takes place in which the two parents "breed" two children and following this operation, each pair of parent vectors is associated with two children coefficient vectors. If crossover has been applied to the pair of parents, the children vectors will generally differ from the parent vectors. The fifth step is mutation of the children where with some small probability, which decreases over time, each coefficient of the two children's vectors is subjected to a mutation. The last step is the election tournament, in which the four members of the "family" engage in a fitness tournament with the children being evaluated by the same fitness criterion used to evaluate the parents. The two vectors with the best fitness, whether parents or children, survive and pass to the next generation, while the two with the worst fitness value are extinguished. The above process is repeated, with parents i and j returning to the population pool for possible selection again, until the next generation is populated by N^* vectors and the convergence is evaluated by the fitness value of the best member of each generation. Once the next generation is populated, elitism can be introduced where all the members of the new generation and the past generation are evaluated according to the fitness criterion. If the best member of the older generation dominates the best member of the new generation, then this member displaces the worst member of the new generation and is thus eligible for selection in the coming generation (McNelis, 2005).

5 Results

Table 1 summarizes the results for the goodness of fit or R^2 statistics for this base set of realizations. Linear model, second-order polynomials are compared with simple neural networks with two neurons and one layer trained by genetic algorithms and simulating annealing.

Table 1: Goodness of fit or R^2

Approximation	R^2
Linear	0.65
Polynomial-Order 2	0.89
Tchebeycheff Polynomial-Order 2	0.89
Hermite-Order 2	0.89
Legendre-Order 2	0.89
Lagueree-Order 2	0.89
Neural Network: FF, 2 neurons, 1 layer-genetic algorithm	0.98
Neural Network: FF, 2 neurons, 1 layer-simulated annealing	0.99

This table shows several important results as far as the prediction of a chaotic time series is concerned. First, there are definite improvements in abandoning pure linear approximation. Second, the power polynomial and the orthogonal polynomials give the same prediction results and so there is no basis for preferring one over the other. Third, the neural network, a very simple neural network genetically evolved, is superior to the polynomial expansions and delivers a very good result. However, this section clearly demonstrates the effectiveness of the proposed neural network, a very simple neural network using simulated annealing for training for the prediction of the Mackey-Glass time series. This neural network prevails among all polynomial expansions and the genetically evolved neural network and delivers an excellent result, indicating that this neural network is much more precise relative to the other methods across a wide set of realizations.

6 Conclusion

This paper presents a neural network with two neurons and one layer, which uses simulated annealing to forecast the chaotic Mackey-Glass time series. The model is developed using Matlab software and it is compared with polynomial expansions and a genetically evolved neural network with two neurons and one layer. The results of the prediction are very satisfactory, indicating that this model can predict well as far as chaotic time series modeling is concerned. This research shows that neural networks in general are designed to mimic very well the ability of the human brain to process data and information and comprehend

patterns and have the ability to analyze and solve business problems and implement those solutions, resulting in being a really helpful tool for forecast purposes. Moreover, according to Paul Coddington from Northeast Parallel Architectures Center at Syracuse University, simulated annealing and its use to predict the chaotic Mackey-Glass time series have the following advantages, which make it an attractive option for optimization problems where heuristic methods are not available:

a) It is relatively easy to code, even for complex problems.

b) It can deal with arbitrary systems and cost functions.

c) It statistically guarantees finding an optimal solution.

d) It generally gives a 'good' solution.

Yet, further research is recommended by using various time series data in order to reduce the long training times and improve the forecast results.

References

1. Atsalakis G., Skiadas C. and Nezis D., (2008), Forecasting Chaotic time series by a Neural Network, XIIIth International conference on Applied Stochastic Models and Data Analysis, Greece.
2. Skiadas C., Rompogianakis G. Atsalakis G., (2001), Chaotic Aspects of a Generalized Rational Model and Application in Innovation Management, Accounting, Management, Marketing, The Works of Scientific Session of Petru Maior University, Publishing House of Petru Maior University, Tîrgu-Mureş, volume II, pg. 398-405.
3. Atsalakis G., Skiadas C. and Braimis I., (2007), Probability of trend prediction of exchange rate by neuro-fuzzy techniques, XIIth International conference on Applied Stochastic Models and Data Analysis, Greece.
4. L.P. Maguire, B. Roche, T.M. McGinnity, L.J. McDaid, (1998), Predicting a chaotic time series using a fuzzy neural network, Information Sciences 112, 125-136.
5. Christos H. Skiadas, Charilaos Skiadas, (2009), Chaotic Modelling and Simulation Analysis of Chaotic Models, Attractors and Forms, CRC Press Taylor & Francis Group, New York.
6. Paul D. McNelis, (2005), Neural Networks in Finance: Gaining Predictive Edge in the Market, Elsevier Academic Press, New York.
7. Robinson, Guy (1995), "Simulated Annealing" Webpage: www.npac.syr.edu/copywrite/pcw/node252.
8. J. Doyne Farmer and John J. Sidorowich (1987), Predicting chaotic time series, Physical Review Letters, Vol. 59, No. 8, 845-848
9. George G. Szpiro (1997), Forecasting chaotic time series with genetic algorithms, Physical Review Letters, Vol. 55, No. 3, 2557-2568
10. L. Studer and F. Masulli (1996), On the structure of a neuro-fuzzy system to forecast chaotic time series, Neuro-Fuzzy Systems, 1st International Symposium on Neuro-Fuzzy Systems, AT'96, 103-110

11.Ajoy Kumar Palit and D. Popovic (1999), Forecasting chaotic time series using neuro-fuzzy approach, International Joint Conference on Neural Networks, IJCNN'99, 1538-1543, Vol. 3
12.Liang Zhao and Yupu Yang (2009), PSO-based single multiplicative neuron model for time series prediction, Expert Systems with Applications, Vol. 36, Issue 2, Part 2, Pages 2805-2812
13.Yoshinobu Fukunaga and Hiroyuki Narihisa (2001), Efficient hybrid neural network for chaotic time series prediction, Lecture Notes in Computer Science, Vol. 2130, 712-718
14.Rahib H. Abiyev (2006), Time series prediction using fuzzy wavelet neural network model, Lecture Notes in Computer Science, Vol. 4132, 191-200
15. Junhong Nie (1994), A fuzzy-neural approach to time series prediction, Neural networks, IEEE World Congress on Computational Intelligence, 3164-3169, Vol.5
16.M.R. Hassan, B. Nath and M. Kirley (2006), HMM based fuzzy model for time series prediction, IEEE International Conference on Fuzzy Systems, 2120-2126
17.Mohammad Assaad, Romuald Bone and Hubert Cardot (2006), Predicting chaotic time series by boosted recurrent neural networks, Lecture Notes in Computer Science, Vol. 4233, 831-840
18.Gang, Zhong Shi-Sheng and Li Yang (2008), Time series prediction using wavelet process neural network, Chinese Physics B, Vol. 17, No. 6, 1674-1056
19.Catherine Vairappan, Hiroki Tamura, Shangce Gao and Zheng Tang (2009), Batch type local search-based adaptive neuro-fuzzy inference system (ANFIS) with self-feedbacks for time-series prediction, Neurocomputing, Vol. 72, Issues 7-9, Pages 1870-1877
20.Xieping Gao and Fen Xiao (2004), Multiwavelet networks for prediction of chaotic time series, IEEE International Conference on Systems, Man and Cybernetics, 3328-3332, Vol. 4
21.Cui Wan, Zhao Zhu, Chang Chun, Bao Wen, Xing Liu and Jun Hua (2005), Prediction of the chaotic time series using support vector machines for fuzzy rule-based modeling, http://en.cnki.com.cn/Article_en/CJFDTOTAL-WLXB200507008.htm
22.W.K. Wong, Min Xia and W.C. Chu (2010), Adaptive neural network model for time-series forecasting, European Journal of Operational Research, Vol. 207, Issue 2, Pages 807-816
23.Hong-Wei Wang, Hong Gu and Zhe-Long Wang (2005), Fuzzy prediction of chaotic time series based on SVD matrix decomposition, Proceedings of the Fourth International Conference on Machine Learning and Cybernetics, 2493-2498, Vol. 4
24.Muhammad Ardalani-Farsa and Saeed Zolfaghari (2010), Chaotic time series prediction with residual analysis method using hybrid Elman-NARX neural networks, Neurocomputing, Vol. 73, Issues 13-15, Pages 2540-2553
25.Ping Liu and Jian Yao (2009), Application of least square support vector machine based on particle swarm optimization to chaotic time series prediction, IEEE International Conference on Intelligent Computing and Intelligent Systems, 458-462
26.H.J. Song, C.Y. Miao, Z.Q. Shen, W. Roel, D.H. Maja and C. Francky (2010), Design of fuzzy cognitive maps using neural networks for predicting chaotic time series, Neural Networks, Vol. 23, Issue 10, Pages 1264-1275
27.Hongwei Wang and Hong Gu (2009), Prediction of chaotic time series based on neural network with Legendre polynomials, Lecture Notes in Computer Science, Vol. 5551, 836-843

28. Yuehui Chen, Feng Chen and Qiang Wu (2007), An artificial neural networks based dynamic decision model for time-series forecasting, International Joint Conference on Neural Networks, IJCNN 2007, 696-699
29. F. Pan, H. Zhang and M. Xia (2009), A hybrid time-series forecasting model using extreme learning machines, Second International Conference on Intelligent Computation Technology and Automation, ICICTA'09, 933-936
30. Meiying Ye (2007), Prediction of chaotic time series using LS-SVM with simulated annealing algorithms, Lecture Notes in Computer Science, Vol. 4492, 127-134

Chaotic Modeling and Simulation (CMSIM) 1: 91–99, 2012

Lindenmayer Systems and the Harmony of Fractals

Pedro Pestana

CEAUL — Centro de Estatística e Aplicações da Universidade de Lisboa
Portuguese Catholic University – School of the Arts, CITAR, Porto, and Lusíada University, Lisboa, Portugal
(E-mail: pedro.duarte.pestana@gmail.com)

Abstract. An interactive musical application is developed for realtime improvisation with a machine based on Lindenmayer-systems. This has been used on an installation whose goal is to draw the attention of unexperienced users to the wealth of realtime applications in computer music. Issues on human computer interaction and improvisation grammars had to be dealt with, as well as probabilistic strategies for musical variation. The choice of L-systems as a basis for machine composition is a consequence of their ability to create results that easily have aesthetic appeal, both in the realms of sound and image.

Keywords: human-computer interaction, L-systems, fractals in algorithmic music composition, interactive composition, improvisation, computer music.

1 Introduction

Musical variation, and composition rules defined by Schönberg, exploit to a certain extent the self-similarity of fractals, and Lindenmayer (cf. Rozenberg[11]) created algorithms (in biological research) that can be exploited fully using iteration in algorithmic music composition. But can fractals create harmony of sound and *cantabile* music as well as they create beauty for the eyes in graphical arts?

We present examples of an interactive algorithmic music composition system exploiting Lindenmayer's technique, generating some forms of minimalist music based on user input, and further developments using the interaction of probability models, fractals and chaos.

Lindenmayer systems, or L-systems, are parallel formal grammars introduced in 1968 by the botanist Aristid Lindenmayer[3] as "a theoretical framework for studying the development of simple multicellular organisms" (Prusinkiewicz and Lindenmayer[10]). As such, in essence an L-system is a rule-based generative system that, drawing from a finite set of symbols, applies substitution schemes starting with an initial subset, called in Prusinkiewicz[9] an axiom. In

Received: 20 July 2011 / Accepted: 30 December 2011

ISSN 2241-0503

Chomsky grammars, substitutions are made in series, with each pass focusing exclusively on a sole symbol, while L-systems are parallel, in the sense that all symbols are replaced within each iteration.

Extending the initial application of L-systems, developments were made in order to generate realistic computer images of plants and trees (Smith[15]), fractal curves (Prusinkiewicz[8]), and musical scores (Prusinkiewicz[9]).

Given words with a fair amount of complexity, an L-system will exhibit a noticeable degree of self-similarity over iterations, which makes its results memorable and pleasing when interpreted as musical height or visual branching, in the sense that there is an equilibrium of expected and unexpected developments. In other words, as Schröder[12], p. 109, boldly presents the key ideas of Birkhoff's *theory of aesthetic value*, the results are pleasing and interesting since they are neither too regular and predictable like a boring brown noise with a frequency dependence f^{-2}, nor a pack of too many surprises like an unpredictable white noise with a frequency dependence f^{-0}.

The remainder of this paper is organized as follows. In Section 2 we describe implementations of L-systems for the automatic generation of music. In Section 3 the focus is on the analysis of musical parameters from user input, such as pitch velocity and duration, and their mapping to L-systems. Section 4 deals with possible extensions of this work to polyphonic input and output, and Section 5 deals with the specific implementation of this project. Finally, in Section 6, we briefly discuss further issues and possible developments.

2 Construction of an *L*-system

L-systems come in several categories: context-free (OL-systems) or context-sensitive (IL-systems); deterministic or non-deterministic; propagative or non-propagative, and so on. The interested reader is referred to Manousakis[4] and to Rozenberg[11] for an extensive review of different types of L-systems. The present work uses non-deterministic OL-systems, as described below.

Let $\mathcal{A}$ denote an alphabet of letters ℓ, $\mathcal{V}$ the vocabulary, i.e. the set of words $w = \ell_1\ell_2\cdots\ell_n$ (strings of letters from this alphabet); $\emptyset$, the empty set, is considered a word.

A production $P:\ \mathcal{A} \longrightarrow \mathcal{V}$ is described by random variables associated with each $\ell \in \mathcal{A}$, i.e.

$$\ell \quad \overset{P}{\mapsto} \quad P(\ell) = X_\ell = \begin{cases} w_k \\ \\ p_k = \mathrm{P}[X_\ell = w_k] \end{cases},$$

and *j-letter* $\mathcal{L}_j:\ \mathcal{V} \longrightarrow \mathcal{A}$ selects the j-letter of any given word,

$$w = \ell_1\ell_2\cdots\ell_k \quad \overset{\mathcal{L}_j}{\mapsto} \quad \mathcal{L}_j(w) = \ell_j.$$

We assume that if $\ell_i \neq \ell_j$, then X_{ℓ_i} and X_{ℓ_j} are independent. If the actual result of $P(\ell)$ is w, we write $\ell \mapsto w$, and say that ℓ is the predecessor of w, or alternatively that w is the successor of ℓ.

If $w = \ell_1\ell_2\cdots\ell_k$, $\mathbf{P}(w) = P(\mathcal{L}_1(w))P(\mathcal{L}_2(w))\cdots P(\mathcal{L}_k(w))$. A *production* of size k with root w_0, $\mathcal{P}_{w_0,k}$ is

$$\mathcal{P}_{w_0,k}(\cdot) = \mathbf{P}(\mathbf{P}(\mathbf{P}(\cdots\mathbf{P}(\cdot)\cdots))),$$

and $\mathcal{P}_{w_0}(\cdot) = \bigcup_{k\in\mathrm{N}} \mathcal{P}_{w_0,k}(\cdot)$.

An OL-system is an ordered triplet $G = \{\mathcal{A}, w_0, P_{w_0}\}$, with $w_0 \in \mathcal{A}$ the starting point for the successive iterations, and P_{w_0} is a production of finite size with root w_0. In an OL-system the predecessor is a one-letter word whereas the successor can be of arbitrary length (it can even be an empty word). In a non-deterministic system, different successor words may occur according to a probabilistic distribution. Hence the production may be described in terms of a branching process, whose many possible trajectories are tied to the possibilities that actually do occur.

A very easy construction of a musical grammar (McCormack[5]) could be built by taking an alphabet $\mathcal{A} = \{C, D, E, F, G, A, B\}$ corresponding to the notes of a C major scale (or an even larger musical scale alphabet), an axiom that would be given by user input and a set of productions that may be arbitrary or may follow rules from common practice of harmony. Alternative constructions have been given by Soddell and Soddell[16], who map branching angles to changes in pitch, Prusinkiewicz[9] where a deterministic OL-system is used to generate a graphical turtle interpretation of the production, and then the resulting curve is traversed and the height of each line segment is interpreted as pitch among others. Most of the studied constructions have seamlessly resulted in pleasing musical results and in our approach we opted for the former, more literal one.

As an example, consider the alphabet $\{C, D, E_b, F, G, A_b, B\}$, the root $w_0 = DE_bCB$ (the celebrated Shostakovich signature, used in many of his mature works), and the stochastic transition matrix — a sparse matrix, so that the equilibrium of expected and unexpected generates aesthetic value — describing the probabilities governing the productions P:

	A_b	A_bE_b	A_bG	B	C	CFD	CFG	DC	E_b	F	G	GA_b	GF
C	0	0	0	0.7	0	0	0	0	0	0	0.2	0	0.1
D	0	0	0.8	0	0	0	0	0	0	0	0.2	0	0
E_b	0	0	0	0.8	0.2	0	0	0	0	0	0	0	0
F	0	0	0	0	0.2	0	0.7	0	0	0	0	0.1	0
G	0	0.2	0	0	0.7	0.1	0	0	0	0	0	0	0
A_b	0	0	0	0	0.2	0	0	0.8	0	0	0	0	0
B	0.2	0	0	0	0	0	0	0	0.7	0.1	0	0	0

Assume that we get the sequence

$w_0 = DE_bCB$	1
$w_1 = A_bGBGE_b$	0.0896
$w_2 = DCCFDE_bA_bE_bB$	0.00896
$w_3 = A_bGBBCFGA_bGBDCBE_b$	0.078675968
$w_4 = DCCE_bE_bBCFGCDCCE_bGBE_bB$	0.004934557

with the probabilities indicated in the right column.

So, in this example, with probability 3.11678×10^{-7} we get

$$\mathcal{P}_{DE_bCB,4} = DCCE_bE_bBCFGCDCCE_bGBE_bB.$$

Observe that the rich theory of Markov chains, and concepts such as communicating events, cyclicity, stationarity, can therefore be imported to analyse productions.

3 Analyzing user input

In the proposed interaction model, a user inputs a musical phrase which serves as the root (axiom), and given a significant pause the system reacts branching into the successive iterations given by the production set. At any point the user could feel inspired by the results and step in with a new musical phrase as a new root, stopping the automatic production, from which the computer draws new material according to the same set of productions or a revised version of it. The focus of this work is on the user-satisfaction with the musical results, and as such it was decided that the interface should not be a tried and tested one such as the music keyboard. This is also helpful in that it allows us to use a very robust MIDI communication, leading to a clear interpretation of pitch, velocity and duration.

The possibility of having the computer analyzing the intention of the musical input and generating different productions would be the first step towards a musical and engaging result. A first approach should consist on scale detection, and Chai and Vercoe's strategy based on hidden Markov models (see Chai and Vercoe[1]) was used in order to extrapolate the global outline of the production set, cf. also Noland and Sandler[6]. The set itself was constructed in strict adherences to classic common practice as described by authors such as Piston[7], as it was deemed that the musical results should be satisfying to a wide non-expert "random" audience.

An additional concern has been how to map user-inputted velocity and duration into the productions of the model. Three approaches have been considered and tested for note duration:

- Having an additional algorithm for tempo detection and building a parallel fixed set of productions for note duration.
- Keeping the duration that was given by user-input across successive generations of productions.
- Cycling through the set of user-inputted durations.

The first approach has been abandoned. Without further constraints forcing the user to adhere to a tempo it would have been unmusical to let the computer-generated productions have a strictly quantized feel as a result of the original input being free from adequate rules. The second approach has also been discarded, since after a few generations a pattern of unnatural repetitiveness would begin to emerge, creating unmusical productions. The third approach has been, surprisingly, musically rewarding, as it potentiated the natural feel that resulted from the self-similarity of successive iterations. Consequently, it has been our choice to govern this parameter. The last member of the set needs to be automatically generated, as there is no way to infer the duration of the user's last note. For this we simply repeat the previous duration value.

It was also not clear from the start which solution would be better for velocity mapping and again different paths were evaluated:

- Quantizing the velocity to a set value given by the average value of the user input.
- Giving a fixed velocity to each of the words in the vocabulary, again averaging the user-inputted value for that word.
- Keeping the velocity that was given by user-input across successive generations of productions
- Cycling through the set of user-inputted velocities.

In fact, any of those solutions proved to be too mechanical, and we had to create a new rule that would allow for musical variety. We choose to create a set of user-inputted velocities, and to discard at random one value from the set in each iteration. The result is immediately more natural, since now there is a much longer period before any pattern of duration-velocity pairs can repeat.

4 Extending the system towards polyphony

The above discussion on analysis is straightforward for monophonic input and output, but the possibility of using multiple voices poses a string of new issues that are not so easily solvable. On the input side, making the distinction between harmonic movement and melodic movement is fraught with ambiguity and the allocation of each melodic movement to a unique voice is also a tremendous challenge. On the output side, decisions had to be made as to adherence to melodic rules and voice independence. Each problem has to be addressed in turn.

The distinction between harmonic and melodic movement cannot depend on simultaneity, when human input is considered. Users never perform with infinitesimal precision and we must therefore create time windows within which two events can be considered simultaneous. A sensible time window would be in the range of 30-50 ms, according to the Haas principle or precedence effect, that states that the human listener integrates all sound events that occur within that time frame. This is a very bold statement from a musical perspective as musical interpretation and style might at times dictate that events that are technically simultaneous should be performed with enough separation between

them to clearly exceed the above-mentioned interval. One well-known and consistent example is the Flamenco's *rasgueado*, where the harmonic intervals are always performed as a very quick succession. We must therefore agree on an extended interval based not on a Haas-inspired pursuit of simultaneity, but on the opposite idea of what would not be a melodic interval. With this in mind we can safely say that is untypical for a performer to go faster than a eighth-note on a 120 bpm tempo which would point us to a 63 ms window. This is of course ambiguous and might be prone to error on fast ornamentations.

Correctly distributing events between voices in a setting where different voices might have different musical durations and pauses is a subject that has not yet been successfully solved. Indeed, it is not clear whether the rules described in the previous section would work with multiple axioms as a starting point. Due to those yet unsolved questions, for the time being, the input side of polyphony has been dropped and the user would only be allowed to play monophonically.

It was however interesting from a musical standpoint that the output could be done polyphonically with the aid of an automatic accompaniment. A simplification of the model proposed by Schwarz *et al.*[13], based on HMM, has been used in order to extend the system, using a low and sparsely-generated voice.

5 Implementation

The system was implemented in Max/MSP, making use of the in-build Jitter object jit.linden. A first patcher parses the input and does the scale analysis, and feeds the finished list to the patcher responsible for the productions (shown in Fig. 1). The productions are fed to a third patcher that converts them to MIDI and sends them as UDP packages to SuperCollider, where a simple implementation of a quasi-sinusoidal synth that resembles a vibraphone is used as a sound module.

An example we fed the system with Shostakovich's aforementioned signature $DSCH$ (used musically as D, E_b, C, B) played as a pair of quavers followed by a pair of semi-quavers of equal velocity. The input patcher interprets the motif as played in C harmonic minor and constructs the set of productions already presented as a sparse stochastic transition matrix in Section 2, presented below in a more readable condensed form for those not wanting to dive in stochastic processes theory:

$$P = \left\{ \begin{array}{lll} P_{11} : C \xrightarrow{70\%} B & P_{12} : C \xrightarrow{20\%} G & P_{13} : C \xrightarrow{10\%} GF \\ P_{21} : D \xrightarrow{80\%} G & P_{22} : D \xrightarrow{20\%} A_bG & \\ P_{31} : E_b \xrightarrow{80\%} B & P_{32} : E_b \xrightarrow{20\%} C & \\ P_{41} : F \xrightarrow{70\%} CFG & P_{42} : F \xrightarrow{20\%} C & P_{43} : F \xrightarrow{10\%} GA_b \\ P_{51} : G \xrightarrow{70\%} C & P_{52} : G \xrightarrow{20\%} A_bE_b & P_{53} : G \xrightarrow{10\%} CFD \\ P_{61} : A_b \xrightarrow{80\%} DC & P_{62} : A_b \xrightarrow{20\%} C & \\ P_{71} : B \xrightarrow{70\%} E_b & P_{72} : B \xrightarrow{20\%} A_b & P_{73} : B \xrightarrow{10\%} F \end{array} \right\}.$$

The result can be heard at http://www.stereosonic.org/lindenmayer.

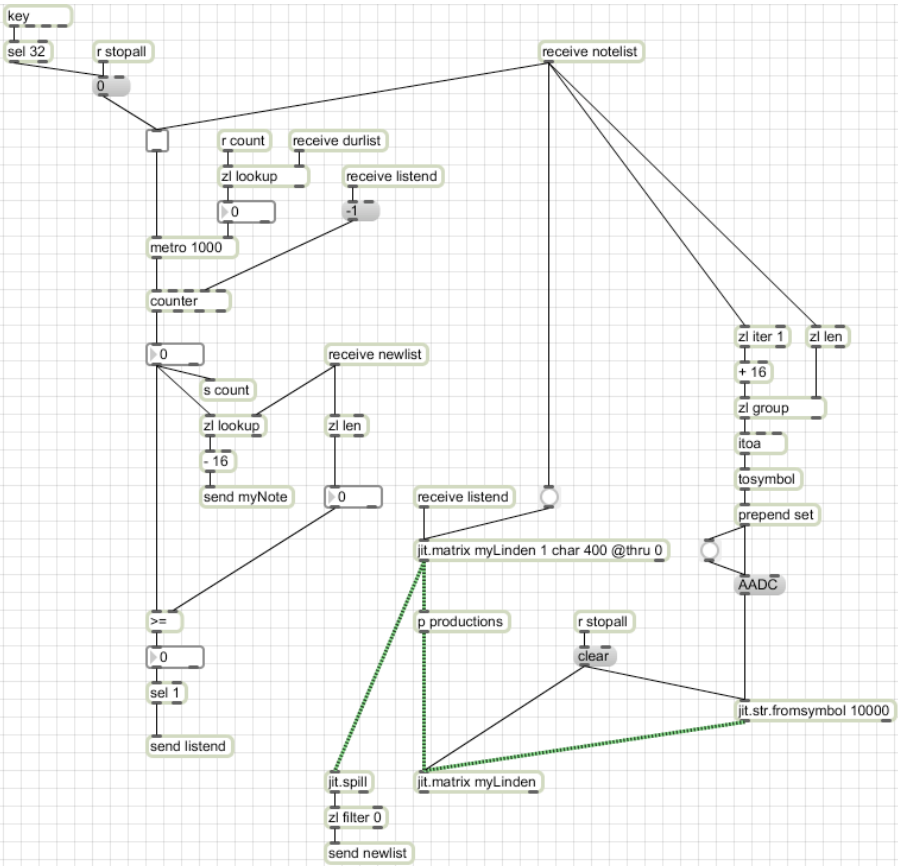

Fig. 1. Max/MSP main patcher

6 Concluding remarks

Many alternative ways do exist of music composition tied to fractals, cf. Johnson[2] and Skiadas[14], for instance. OL-systems as used in our examples generate appealing musical productions as far as letters map onto words of small size.

Otherwise, the system must be interrupted by the user, since a rather small number of iterations generates a musical output that is too clumsy. The organisation of natural languages, and namely of the mating songs of birds and insects, seems to incorporate a strategy of long range dependence axed on a sequence of modulated shortcut Markov-type memories.

Hence, for more elaborated vocabularies and mappings, it would be sensible to use only the r last letters from the (k-1)-th iteration to map onto the k-th iteration, instead of using all the letters as described for OL-systems.

This is easily implemented using an *endletters* application $\mathcal{E}_r : \mathcal{V} \longrightarrow \mathcal{A}$ selecting the r-endletters of any given word,

$$w = \ell_1\ell_2\cdots\ell_k \quad \overset{\mathcal{E}_r}{\mapsto} \quad \mathcal{E}_r(w) = \ell_{k-r+1}\ell_{k-r+2}\cdots\ell_{k-1}\ell_k,$$

so that the memory of the initial $k-r$ letters is erased and the musical composition will flow more naturally.

One of the giants in the early development of Probability, Abraham de Moivre, wrote in his *The Doctrine of Chances*

> "Further, The same Arguments which explode the notion of Luck may, on the other side, be useful in some Cases to establish a due comparison between Chance and Design: We may imagine Chance and Design to be as if it were in Competition with each other, for the production of some sorts of Events, and may calculate what Probability there is, that those Events should be rather owing to one than to the other."

Pure randomness produces "grass" (a term used in some fields of engineering, since the effect of pure noise in a cathodic terminal is similar to a black and white photo of a field of grass). It is necessary to melt randomness with a set of rules to weave a background of order so that the interplay of predictable and surprising events produces a pleasant result. So, among many other things, art is one of the many fields of human activity aiming at taming randomness, to create patterns blending together determinism and randomness.

The examples in http://www.stereosonic.org/lindenmayer reinforce the idea that in music composition L-systems may contribute to this aim, namely creating sketches with minimalist patterns that may serve as source of inspiration for more complex designs.

References

1. W. Chai and B. Vercoe. Detection of key change in classical piano music. Proceedings of the 6th International Conference on Music Information Retrieval, London, 2006.
2. R. S. Johnson. Composing with Fractals. In J. Fauvel, R. Flood and R. Wilson, eds., Music and Mathematics, Oxford University Press, Oxford, 2006
3. A. Lindenmayer. Mathematical models for cellular interaction in development, Journal of Theoretical Biology, vol. 18, pp. 280–315, 1968.
4. S. Manousakis. Musical L-Systems. M.Sc. Thesis in Sonology, The Royal Conservatory, The Hague, 2006.
5. J. McCormack. Grammar-Based Music Composition. In Stocker et al., eds. Complex Systems 96: Fom Local Interactions To Global Phenomena, IOS Press, 1996
6. K. Noland and M. Sandler. Key Estimation Using a Hidden Markov Model. In International Society for Music Information Retrieval, pp. 121–126, Victoria, Canada, 2006.
7. W. Piston. Harmony. W.W. Norton & Company, New York, 1941.

8. P. Prusinkiewicz. Graphical applications of L-systems. Proceedings of Graphics Interface'86, pp. 247-253, 1986a.
9. P. Prusinkiewicz. Score Generation with L-Systems. Proc. Intl. Computer Music Conf '86, pp. 455-457, 1986b.
10. P. Prusinkiewicz and A. Lindenmayer. The Algorithmic Beauty of Plants, Springer, 1990.
11. G. Rozenberg. Lindenmayer Systems: Impacts on Theoretical Computer Science, Computer Graphics, and Developmental Biology, Springer Verlag, 1992.
12. M. Schroeder. Fractals, Chaos, Power Laws: Minutes from an Infinite Paradise. Dover, New York, 2009.
13. D. Schwarz, N. Orio and N. Schnell. Robust Polyphonic MIDI Score Following with Hidden Markov Models, ICMC, 2004.
14. C.H. Skiadas. Exploring and simulating chaotic advection: A difference equations approach. In C. H. Skiadas, ed., Recent Advances in Stochastic Modeling and Data Analysis, pp. 287–294, World Scientific, Singapore, 2007.
15. A.R. Smith. Plants, fractals, and formal languages. Computer Graphics, vol. 18, pp. 1-10, 1984.
16. F. Soddell and J. Soddell. Microbes and Music. In PRICAI 2000 Topics in Artificial Inteligence, pp. 767–777, Springer Verlag, 2000.

FCT *This reseach has been supported by National Funds through FCT — Fundação para a Ciência e a Tecnologia, project PEst-OE/MAT/UI0006/2011. The author is grateful to Professors Álvaro Barbosa (UCP) and Joshua D. Reiss (QMUL) for generous guidance, stimulating discussions and encouragement.*

Chaotic Modeling and Simulation (CMSIM) 1: 101-108, 2012

Modeling and Simulation of a Reactive Packed Distillation Column Using Delayed Neural Networks

Abdulwahab Giwa[1] and Süleyman Karacan[1]

[1]Ankara University, Tandoğan, Ankara, Turkey
(E-mails: agiwa@eng.ankara.edu.tr and karacan@eng.ankara.edu.tr)

Abstract: The complex nature of a reactive packed distillation system due to the occurrence of both reactions and separations in a single unit demanded the need for a very robust tool of representing the process. In view of this, delayed neural networks are considered as one that can handle this problem effectively. As such, in this work, delayed neural networks Nonlinear AutoRegressive, Nonlinear AutoRegressive with eXogenous inputs and Nonlinear Input-Output models are developed and simulated with the aid of MATLAB R2010b to predict the top and bottom sections temperatures of the column. The predicted temperatures of the Input-Output models were found not to be satisfactory. However, the good agreements observed from the plots and the good values of the correlation coefficients and the mean squared errors between the predicted temperatures of NAR and NARX models and the experimental ones showed that these two models can be used to represent the process.
Keywords: Reactive packed distillation, Delayed neural network, Nonlinear AutoRegressive (NAR), Nonlinear AutoRegressive with eXogenous inputs (NARX), Nonlinear Input-Output (NIO), MATLAB/Simulink, Correlation coefficient (R), Mean squared error (MSE).

1 Introduction

In recent years, integrated reactive separation processes have attracted considerable attentions in both academic research and industrial applications, Völker et al., 2007 [1]. One of these processes which is known as reactive distillation is potentially attractive whenever conversion is limited by reaction equilibrium, Balasubramhanya and Doyle III, 2000 [2]. Reactive distillation combines the benefits of equilibrium reaction with a traditional unit operation (in this case, distillation) to achieve a substantial progress in not only promoting the reaction conversion through constant recycling of reactants and removal of products but also reducing the capital and operating costs in one way by reducing the number of equipment units. In addition, another advantage of reactive distillation is its ability to avoid azeotropes. However, the design of reactive distillation processes, especially when a packed column is involved, is still a challenge to chemical engineers because of the difficulties involved in obtaining process models capable of reliably describing the several complexes (such as the exhibition of multiple steady states) and the interrelated phenomena

Received: 20 July 2011 / Accepted 28 December 2011

ISSN 2241-0503

which includes simultaneous reactions and separations in the column. The complicated behavior of the process made the search for a very robust and powerful tool of modeling and simulating the dynamics of the reactive distillation a big task to chemical engineers. One of the strategies proposed for handling this kind of a task are the delayed neural networks because they can be trained to handle complex functions, Beale et al., 2010 [3].

Neural Networks modeling can be viewed as a nonlinear empirical model that are especially useful in representing input–output data, in making predictions in time, and in classifying data, Himmelblau, 2000 [4]. Neural Networks can be highly nonlinear, can learn easily, require little or no a priori knowledge of the structure, are fault-tolerant and can handle complex problems that cannot be satisfactorily handled by the traditional methods, MacMurray and D. M. Himmelblau, 2000 [5].

In this paper, a reactive packed distillation column is modeled and simulated using three different kinds of delayed neural network models and the equilibrium reaction for the production of ethyl acetate from the esterification reaction between acetic acid and ethanol was used as the case study.

2 The Model and Simulations

2.1 Data acquisition

The data used for the delayed neural networks modeling were acquired from the experiments performed in a pilot scale packed reactive distillation plant shown in Figure 1 below. The plant has, excluding the condenser and the reboiler, a height and a diameter of 1.5 and 0.05 m respectively, a cylindrical-shaped condenser having a height and a diameter of 22.5 and 5 cm respectively and a spherical-shaped reboiler with a volume of 3 Litre. The main column was divided into three parts of 0.5 m each. The upper, middle and lower sections were the rectification, reaction and stripping sections respectively. The rectification and stripping sections were packed with rasching rings while the reaction section was filled with Amberlyst 15 catalyst. The column was fed with acetic acid at the top (between the rectification section and the reaction section) whereas ethanol was fed at the bottom (between the reaction section and the stripping section) with the aid of peristaltic pumps which were operated via MATLAB/Simulink program. The top, reaction, stripping and bottom sections temperatures were measured and recorded on-line and in real-time using the thermocouples linked to the computer and also via the MATLAB/Simulink program. The reaction taking place in the column is given as:

$$CH_3COOH + C_2H_5OH \underset{k_b}{\overset{k_f}{\rightleftarrows}} CH_3COOC_2H_5 + H_2O \qquad (1)$$

Two different experiments were carried out using a reboiler duty of 560 W and applying step inputs unto the recycle ratio from total reflux to 5 and acetic acid to ethanol feed ratio from 0 to 1.25 to generate two sets of data. One set was

used for training the models while the other was used to test the developed delayed neural network models.

(a)

(b)

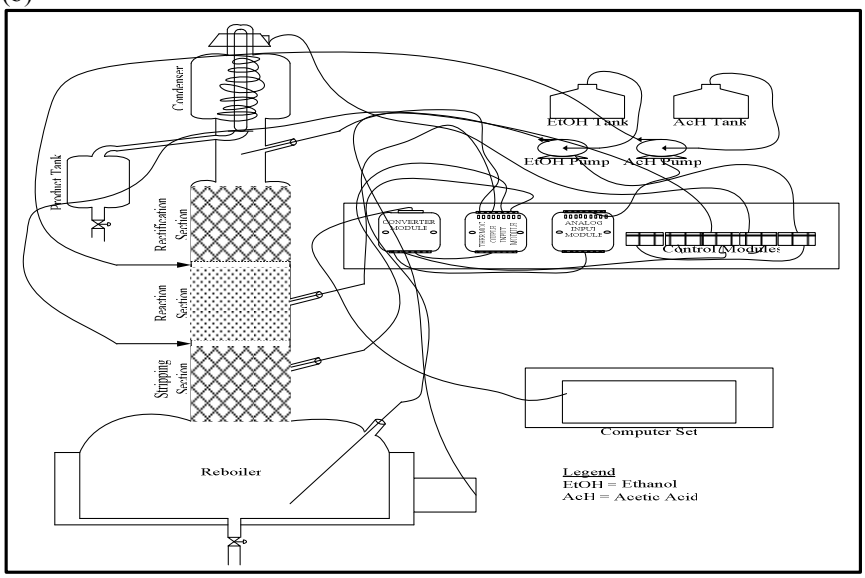

Fig. 1. Reactive Packed Distillation Pilot Plant: (a) Pictorial View; (b) Sketch View

2.2 Model development

In developing the models in the MATLAB environment, the sets of data generated from the experiments were pretreated by converting them to time sequence ones which were represented by a cell array because the delayed neural networks models to be developed required the data to be sequential in nature. The parameters used for the formulation of the models are as shown in Table 1 below:

Table 1. Neural network model formulation parameters

S/N	Parameter	Value/Description
1.	No. of inputs	2
	No. of outputs	2
2.	No. of layers	2
3.	No. of neurons	10
4.	No. of delays	5
5.	Training algorithm	Levenberg-Marquardt

The mathematical expressions for the three kinds of delayed neural networks (Nonlinear Autoregressive, Nonlinear Autoregressive with Exogenous Inputs and Nonlinear Input-Output) models developed for the reactive packed distillation column are:

$$\text{NARX: } y(t) = f\left(u(t-1), u(t-2), ..., u(t-d), y(t-1), y(t-2), ..., y(t-d)\right) \quad (2)$$

$$\text{NAR: } y(t) = f\left(y(t-1), y(t-2), ..., y(t-d)\right) \quad (3)$$

$$\text{NIO: } y(t) = f\left(u(t-1), u(t-2), ..., u(t-d)\right) \quad (4)$$

2.2 Results and discussions

The generated outputs recorded from the experiments carried out as described in Section 2.1 (that is, by applying step changes unto the recycle ratio from infinity to 5 and unto the feed ratio from 0 to 1.25) are as shown in Figure 2 below. Figure 2(a) shows the measurements taken from the pilot plant for the delayed neural networks training while Figure 2(b) contains another set of results taken from the plant for testing the models to be developed. The step changes applied unto the input variables (recycle ratio and feed ratio) are shown in Figure 2(c).

It could be observed from Figure 2 that, even though the responses of the training and testing results are not exactly the same for both the top section and reaction section temperatures, their trends were found to be similar. The discrepancies between them can be attributed to the unmeasured disturbances that normally affect the performances of chemical processes. Of course, these

disturbances have to be taken into considerations when applying the delayed neural networks models in designing controllers for the plant in order to achieve stability and/or improve the performance of the system.

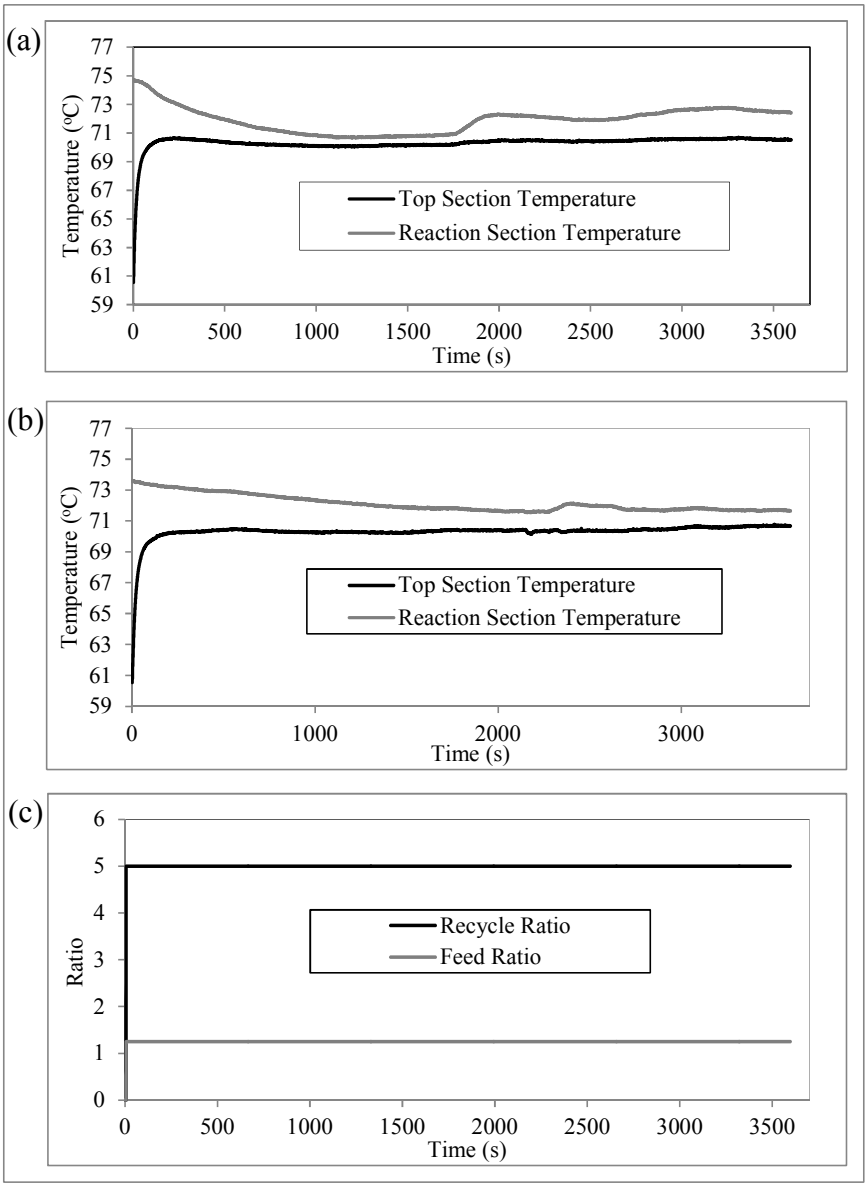

Fig 2. Input-Output Sampled Data: (a) Training Data; (b) Testing Data; (c) Applied Inputs

After using the data in Figure 2 to develop the neural networks models for the reactive packed distillation column, each of them (the models) was tested using the testing data shown in figure 2(b) in order to confirm the accuracy of the model in predicting the top section and the reaction section temperatures. Figure 3, 4 and 5 show the comparisons between the experimental and the predicted results of top section temperatures and the reaction section temperatures for the delayed neural networks NAR, NARX and NIO models respectively.

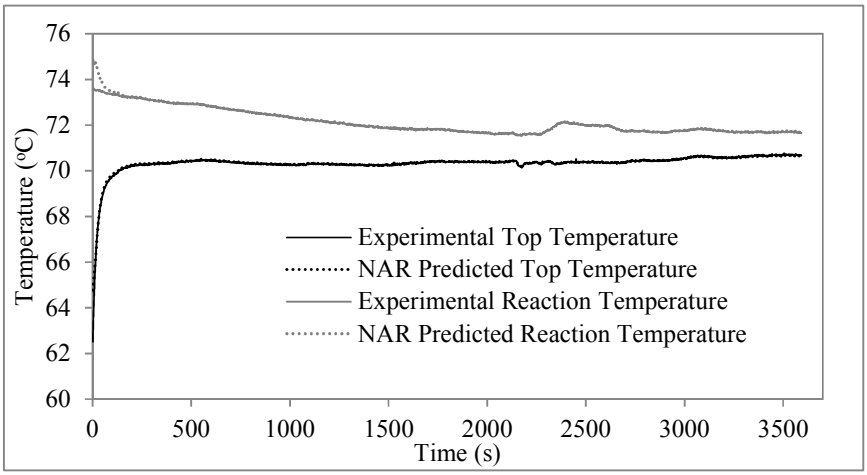

Fig. 3. Comparisons between Experimental Temperatures and Those Predicted Using Delayed Neural Networks NAR Model

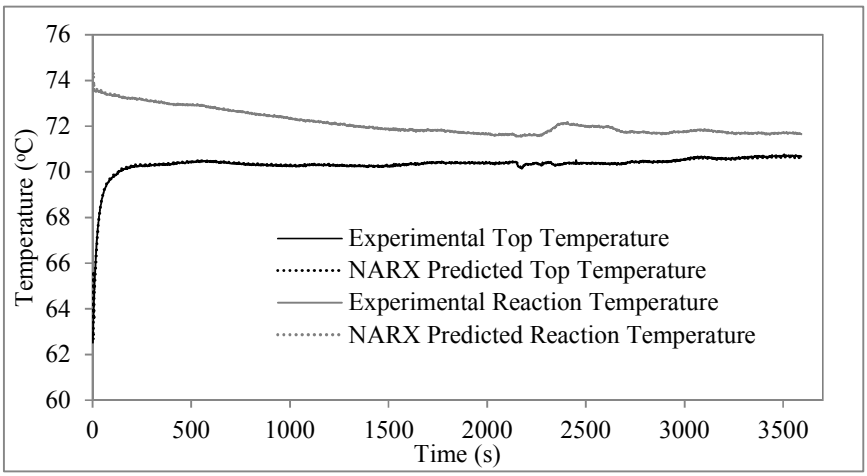

Fig. 4. Comparisons between Experimental Temperatures and Those Predicted using Delayed Neural Networks NARX Model

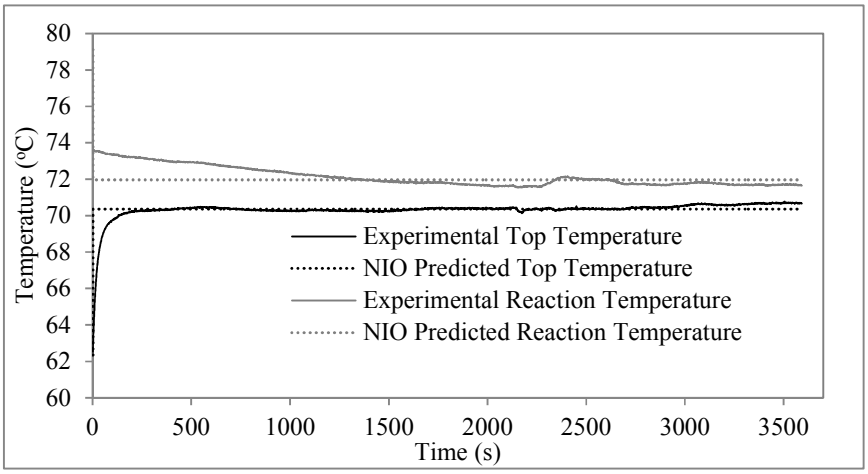

Fig. 5. Comparisons between Experimental Temperatures and Those Predicted Using Delayed Neural Networks NIO Model

From the results shown in Figure 3 and Figure 4, it was observed that there were good agreements between the experimental temperatures and those predicted using the developed delayed neural networks NAR and NARX. However, the predicted temperatures obtained using the Nonlinear Input-Output models were not in good agreements with the experimental ones, as seen in Figure 5.

The validities of the representations of the reactive packed distillation plant using the developed delayed neural networks models were further investigated by calculating the performance indices of the models. The performance indices used in this work are mean squared error (MSE) and correlation coefficient (R) and their calculated values are as tabulated below.

Table 2. Performance indices of the developed models

Model Type	**Top Section Temperature**		**Reaction Section Temperature**	
	MSE	**R**	**MSE**	**R**
NAR	0.0063	0.9927	0.0120	0.9852
NARX	0.0023	0.9952	0.0011	0.9984
NIO	0.2270	0.2642	0.3195	0.0454

From Table 2, it was observed that the correlation coefficients calculated when NAR model was used to predict the top section and reaction section temperatures were 0.9927 and 0.9852 respectively while those of the NARX model were 0.9952 and 0.9984 respectively for the top and reaction sections temperatures. Also, as seen from Table 2, each of the two (NAR and NARX)

models was found to have a very low mean squared error. The low value of the mean squared error is another indication of a good model. The good performances showed by these models can be attributed to the use of some past outputs, as feedbacks, in their structures.

However, in the case of the Nonlinear Input-Output model, the situation was different because, apart from the fact that the curves produced by this model were not in good conformity with those of the experimental ones, its performance values were also bad, as seen from Table 2. For instance, the correlation coefficients obtained when this model was used to predict the top and reaction sections temperatures were 0.2642 and 0.0454 respectively. These values are too low for any model that is to be used to represent a reactive packed distillation plant. The poor performance of this model can be as a result of the fact that its structure does not make use of the past values of the output variables.

3. Conclusions

Three kinds of delayed neural networks models have been developed and simulated. The good closeness of the temperatures predicted using NAR and NARX models to the experimental ones has revealed that both of them can be used to represent the dynamics of the reactive packed distillation column.

Acknowledgements

One of the authors, Abdulwahab GIWA, wishes to acknowledge the support received from The Scientific and Technological Research Council of Turkey (TÜBİTAK) for his PhD Programme. In addition, this research was supported by Ankara University Scientific Research Projects under the Project No. 09B4343007.

References

1. M. Völker, C. Sonntag and S. Engell. Control of Integrated Processes: A Case Study on Reactive Distillation in a Medium-Scale Pilot Plant. *Control Engineering Practice* 15:863–881, 2007.
2. M. H. Beale, M. T. Hagan and H. B. Demuth. *Neural Network Toolbox 7*. The MathWorks Inc., Apple Hill Drive, Natick MA, 2010.
3. L. S. Balasubramhanya and F. J. Doyle III. Nonlinear Model-Based Control of a Batch Reactive Distillation Column. *Journal of Process Control* 10:209-218, 2000.
4. D. M. Himmelblau. Applications of Artificial Neural Networks in Chemical Engineering. *Korean Journal of Chemical Engineering* vol. 17, no. 4, 373–392, 2000.
5. J. C. MacMurray and D. M. Himmelblau. Modeling and Control of a Packed Distillation Column Using Artificial Neural Networks. *Computers and Chemical Engineering* vol. 19, No. 10, 1077–1088, 1995.

Chaotic Modeling and Simulation (CMSIM) 1: 123–145, 2012

Complexity in Theory and Practice: Toward the Unification of Non-equilibrium Physical Processes

Georgios P. Pavlos

Department of Electrical Engineering and Computer Engineering,
Democritus University of Thrace,
Kimmeria University Campus Xanthi, 67100, Greece
(E-mail: gpavlos@ee.duth.gr)

Abstract. During the last two decades our scientific group has developed new nonlinear methods of analysis applied to various physical systems. In this review study we present our scientific contribution to nonlinear science, including also some novel concepts as for the constructive role of complexity in modern physical theory. The experimental verification of chaos existence in physical systems remains one of the most significant problems of non linear science and complexity. The extended chaotic algorithm presented in the following as well as the results concerning its application at different experimental time series reveal the universal character of the complexity theory for the far from equilibrium dynamics of spatially extended physical systems. The developed methodology that was used compromises different types of computational tools as well as theoretical concepts for the physical interpretation of the experimental information. As we present here the strong dispute and criticism of chaos hypothesis in physical systems during the last two decades was fruitful and challenged us to develop a novel composition of experimental and theoretical knowledge of universal character for the far from equilibrium dynamics. The solar and magnetospheric dynamics included in space plasma processes, the environmental and seismic dynamics, the human brain or the on–chip workload are distinct systems which were studied by our group revealing common chaotic characteristics and chaotic phase transition processes. Moreover, the intellectual struggle for the comprehension of the theoretical presuppositions of the experimentally observed universal chaotic character of spatially distributed systems lead us to the fundamentals of complexity theory as manifested at the macroscopic and microscopic level of physical reality. From this point of view, some common characteristics of macroscopic and microscopic complexity included in the scientific knowledge of the recent two or three decades can be used as a road for the physical theory unification. That is complexity, scaling, chaos, quanticity and fractality could be supported as different manifestations of a unified physical law from the microscopic to the macroscopic and cosmological level. As we can argue, determinism and probabilism can also be unified through chaoticity. Moreover, the rising of new physical knowledge reveals that under the macroscopic or the microscopic physical phenomena there exist a fundamental and multilevel acting unit physical process that produces physical reality rather than a fundamental essence or simple

Received: 7 August 2011 / Accepted: 30 December 2011

ISSN 2241-0503

substance from which cosmos can be build.
Keywords: Complexity theory, Intermittent turbulence, Nonlinear time series analysis, Nonextensive Tsallis statistics, Nonequilibrium phase transition, Chaos, SOC, Macroscopic-microscopic complexity, Physical theory unification.

Contents

1 Introduction

After the historical work by Prigogine, Nicolis, Glansdorff and others [43], [78]-[83], [110], [111] the science of Complexity is rapidly growing providing the opportunity, combined with the computational power, for the development of new methods of analysis, modeling and prediction of various processes with intense stochastic or random–chaotic character. This is related to areas of great interest, such as space plasmas, environment, material mechanics, bio–medicine, economy, human society, psychology, urban development, e.t.c. On the other hand, the nonlinear time series analysis as it was developed by Takens, Grassberger & Proccacia, Theiler, Tsonis and others [44], [120], [121], [124], [125] and was systematically used and extended by Pavlos and Athanasiou [6], [7], [90]-[104] is the road for the experimental verification of complex dynamics. The Complexity theory and the experimental time series analysis concerning spatiotemporal and far from equilibrium nonlinear dynamics include significant collective phenomena such as: fractal and multifractal structures, power law distribution and critical scale invariance, nonequilibrium fluctuations causing spontaneous nucleation and evolution of turbulent motion from metastable states, defect mediated turbulence and localized defects changing chaotically in

time and moving randomly in space, spatiotemporal intermittency, chaotic synchronization, anomalous diffusion and directed percolation causing levy-flight spreading processes, turbulent patches and percolation structures, threshold dynamics and avalanches, chaotic itinerancy, or stochastic motion of vortex like objects [10], [11], [29]-[31], [48], [67], [73], [118], [133].

In particular, in the phase space of a complex system various finite dimensional attractors can exist such as: fixed points, limit cycles - torus or more complicated structures as strange attractors. Strange attractors can correspond to chaotic dynamics as self-organized critical dynamics (SOC) or strong chaos. Generally, spatiotemporal chaos includes early turbulence with low effective dimensionality and few coherent spatial patterns or states of fully developed turbulence. These states are out of equilibrium steady states related to bifurcation points of the nonlinear distributed dynamics, as well as to first and second order non-equilibrium phase transition processes. Also, other spatial and temporal patterns as well as spatially localized structures are possible solutions of the nonlinear spatially extended dynamics. With regard the exploration of space plasma complexity by experimental time series analysis, the primary studies by Vassiliadis, Pavlos and other scientists including nonlinear analysis of magnetospheric data [12], [90]-[92], [129], [130], as well as the hypothesis of magnetospheric chaos went through a strong and fruitful criticism [107]-[109]. This criticism was a general dispute about the experimental verification of chaos. In the following we present the main points of the criticism against low dimensional chaos: a) The correlation dimension of experimental time series cannot be distinguished from a stochastic signal with the same power spectrum and amplitude distribution as the original data. b) There is no evidence for the existence of low-dimensionality according to their estimate of correlation dimension obtained using Takens method. c) When there is some evidence of nonlinearity in the experimental time series it is not clear whether it is the result of intrinsic dynamics or nonlinearities in the external pertubations of the system. d) When the system is open and externally largely controlled this alone should provide evidence against the existence of a strange attractor in the observed signals as the system is a randomly driven non-autonomous system.

The refutation of the concept of low dimensional chaos in spatially extended systems as the space plasmas it was further strengthened after the introduction of the concept of self organized criticality (SOC) [10], [25], [64]. Under this circumstantial evidence, Pavlos et al. [95] introduced the term "pseudo–chaos" to discriminate the real low-dimensional chaotic dynamics from the stochastic and nonchaotic colored noise processes. Furthermore, the Thrace group created an extended algorithm for the detection of low dimensional chaos by time series analysis and the discrimination of chaos from stochastic processes which can mimic low dimensional chaos. This algorithm was based on the Wold's decomposition theorem, the theory of input–output dynamics and the embedding theory of Takens, as well as the fruitful contribution of Theiler concerning the method of surrogate data [2]-[7], [44], [95]-[98], [120], [121].

During the last two decades the chaotic algorithm was used to analyse experimental time series corresponding to various physical or technical systems such as: The solar corona and the Earth–Jovian magnetospheres, the solid

outer crust of the earth, the atmospheric system, the human brain and the Network–on–chip Architecture of the mobile technology [53]-[55], [60]-[62], [98]-[101], [126]. The far from equilibrium distributed input–output dynamics is the common character in all these distinct cases of physical systems in which the chaotic analysis of experimental time series revealed significant characteristics such as: multiscale and critical dynamics phase transition processes as well as the noticeable coexistence of intermittent turbulence, high dimensional SOC and low dimensional chaotic processes.

After all, a necessity was raised for a theoretical interpretation of the universal and experimentally observed characteristics that lead us to the fundamentals of complexity theory, according to which phase transition processes or intermittent turbulence phenomena and low dimensional self organized chaos are at the edge of macroscopic and microscopic complexity. Moreover, the universality of Tsallis non-extensive statistics, verified at the macroscopic and the microscopic level, indicates also the universality of complexity theory at both macroscopic and microscopic level [122], [123]. After all the obtained until now practical and theoretical experience makes us to believe that the complexity theory could be the prime motivator towards a global theoretical unification of our understanding of nature from the microscopic to the macroscopic level. However, for such a dream to come true, new physical and mathematical concepts must be used such as, cooperation of local, non–local and long–range correlations in complex systems. A new complementarity is developed fundamental local physical interactions and global ordering physical process including fractal space–time, or fuzzy space and non–communicative geometry or wild topologies [15], [36], [38], [46], [50], [84], [87]. In this direction and in order to remark the new state we can summarize by the following phrase of Castro: *It is reasonable to suggest that there must be a deeper organizing principle, from small to large scales, operating in Nature which might be based in the theories of complexity, non linear dynamics and information theory where dimensions, energy and information are intricately connected* [22].

According to the previous description, this study includes two distinct parts. In the first part (sections 2-4), we present the algorithm of chaotic analysis, as well as significant results by using the chaotic algorithm at experimental signals extracted by complex spatially extended systems. The physical presuppositions of the algorithm and significant applications are presented also. In the second part (sections 5-10), we introduce in a synthetic way significant theoretical concepts aiming at the unifying role of complexity theory from the microscopic to the macroscopic physical level.

2 Theoretical Presuppositions and New Tools for the Time Series Analysis

In general, the spatiotemporal dynamics of spatially extended physical systems is related to irreversible or non–equilibrium thermodynamics, as well as to non–equilibrium statistical physics [25], [58], [123]. According to Nicolis and Prigogine, [78]-[83], [110], [111] the existence of low dimensional order (periodic or chaotic) in an extended system is the central character of physical self

organization and complexity theory. As we present here, different far from equilibrium spatially extended physical systems reveal self organized complexity and chaotic dynamics or other complex dynamics at the edge of chaos as well as non–equilibrium statistical profile according to Tsallis non–extensive statistical theory [123]. These significant characteristics of complexity theory have been revealed by the application of an extended algorithm of nonlinear time series analysis presented in the following.

The experimental study of spatiotemporal complexity includes the question: *"if you have a time signal, what is the kind of information that you hope to get out of it?"*. The physical systems, which we are interested in, are dissipative and spatially extended. The attempt to understand the complex deterministic motion of spatially extended nonlinear dissipative systems, so–called spatiotemporal chaos (STC), is at the forefront of research in nonlinear dynamics. In contrast to simple chaotic systems in the time domain, in which few degrees of freedom are nonlinearly coupled, spatially extended systems include an infinite number of spatially distributed degrees of freedom. For this reason tools and methods developed for low dimensional systems described by non-linear Ordinary Differential Equations (ODE) must be adapted to spatially distributed systems described by nonlinear Partial Differential Equations. The transition to chaos in spatially extended systems is widely investigated in many natural phenomena such as hydrodynamics or magnetohydrodynamics, chemical reactions, pattern formation in biology or brain activity. Spatiotemporal chaos involves intermediate situations between chaos and turbulence or to fully developed turbulence when the system is sufficiently confined. In these states it is possible to characterize the dynamics from a local time series alone estimating fractal dimensions, or Lyapunov exponents in the reconstructed phase space. When the physical extension of the system increases then quantities, measuring the amount of chaos, scale like the system size. When the system size is much larger than the correlation length then the system can be viewed as a collection of essentially independent sub–systems with a size of the order of correlation length, so that the amount of chaos should be proportional to the number of sub–systems. As long as $x_i > L$, where x_i is the correlation length and L the system size, we are dealing with a small system which may be chaotic in time and coherent in space. In the opposite limit $x_i << L$ the dynamical behavior is incoherent in space. This regime occurs for $L >> l_e - l_D$, where l_D is the dissipative length and l_e the excitation length, and it is the regime of spatial chaos or weak turbulence. Weak turbulence is characterized by the chaotic evolution of coherent structures roughly of the size of the correlation length ξ. The dimension of a local attractor can scale linearly with the system volume Ld, where d is the dimensionality of space while the attractor density D_H/L_d can be well defined. When the spatial structure plays an essential role then, according to Chate, Manneville and Wang [29], [30], [133] the spatiotemporal dynamics of the system can be very complex revealing chaotic synchronization, spatiotemporal intermittency or directed percolation, sporadic chaos, localized structures, and defect turbulence as well as phase transition processes. Moreover, defect turbulence and intermittent turbulence, self organized criticality (SOC), avalanche threshold dynamics, spinodal and nucleation phenomena and

far from equilibrium phase transition, Tsallis entropies and non–Gaussian fluctuations as well as diffusion or Levy motion, are some of the different manifestations of spatiotemporal complexity and multiscale–multifractal phenomena that must be studied using nonlinear signal analysis [16], [63], [88], [122].

The chaotic algorithm that can be used to uncover the hidden nonlinear spatiotemporal dynamical characteristics underlying the experimental time series includes different group of tools summarized as follows:

i. Computation Phenomenological Characteristics
   (a) Autocorrelation Coefficient and Power Spectrum (Linear correlations, periodicities, scaling laws
   (b) (Mutual Information (Linear and Nonlinear Correlations)
   (c) Probability Distributions (Power Laws)
   (d) Hurst exponent (Persistence, anti-persistence, white noise)
   (e) Flatness Coefficient F (Intermittent turbulence)
   (f) Structure Functions (Turbulence, anomalous diffusion)
   (g) (Phase portrait (Low Dimensionality)
   (h) Entropy, energy, multifractal structures
   (i) Estimation of q-Tsallis Statistics
   (j) Wavelet analysis (Spatiotemporal structures)

ii. Computation of Geometrical characteristics in the reconstructed state space
   (a) Correlation Dimension (Degrees of freedom)
   (b) Generalized Dimension (Multifractals)
   (c) False Neighbors (Degrees of Freedom)
   (d) Singular values spectrum (SVD components, filtering)

iii. Computation of Dynamical Characteristics in the reconstructed state space
   (a) Maximum Lyapunov Exponent (Sensitivity in initial conditions)
   (b) Power Spectrum of Lyapunov Exponents (Sensitivity in initial conditions in all dimensions in space state)
   (c) Nonlinear modeling and nonlinear prediction algorithms

iv. Testing of Null Hypothesis in order to discriminate between low dimensional chaotic dynamics and linear high dimensional stochastic dynamics
   (a) Surrogate data
   (b) Discriminating statistics

v. Singular Value Analysis in order to
   (a) Estimate Degrees of Freedom
   (b) Filter signals from White or Colored Noise
   (c) Search for input-output dynamics

vi. Recently the above algorithm has been completed by significant new tools such as
   (a) Fuzzy analysis of time series
   (b) Cellular automata, genetic algorithms and neural network modeling (For spatiotemporal modeling and prediction of complexity)

3 Significant Applications of the Chaotic Algorithm

3.1 Solar activity

Solar activity is produced by the emergence of magnetic flux through the photosphere. The magnetic flux forms active regions which include sunspots and solar flares. The physical system underlying the solar activity and the solar cycle is the convection zone of the sun. Convection zone is a strongly turbulent region which occupies the one third of the solar interior. The generation of the magnetic field and its evolution inside the convection zone is one of the most challenging problems for the solar physics, related to the convection zone turbulence, the coronal heating, the solar flares, particle acceleration and transport. The random character of solar activity has been associated theoretically with chaotic behavior and a solar low dimensional strange attractor [106], [113]. For the first time [95] applied chaotic analysis at the sunspot index presenting some evidence for low dimensions solar chaos. Price *et al.* [108] have criticized the chaos hypothesis concerning the solar activity as they reported that applying the chaotic analysis to the wolf sunspot number time series no evidence was found for low dimensional deterministic nonlinear process. Oppositely, the self organized criticality (SOC) theory was introduced for the explanation of solar activity [132]. In a series of studies by Karakatsanis and Pavlos [60], Karakatsanis et al. [61] we have presented strong evidence for the coexistence of two clearly discriminated physical processes in the solar activity. The first process corresponds to the existence of self organized critical state according to the general profile of SOC theory process. The second process corresponds to low dimensional chaotic dynamics. These results were obtained after the nonlinear analysis of the Sunspot Index, according to which, the original signal reveals characteristics of a SOC process, that is, high dimensionality and zero value of the largest Lyapunov exponent. The low dimensional chaotic process was revealed after using high pass filtering of the original Sunspot Index and Solar Flare Index with the methods of first difference or singular value decomposition analysis. The dual character of the solar activity which is hidden in the observed Sunspot Index reveals a double input–output dynamics corresponding to the photospheric and sub-photospheric zones activity of the Solar system. Also, [60], [61] found strong evidence for intermittent solar turbulence as well as for non-extensive statistical processes, according to Tsallis q–statistics.

3.2 Chaos at the Earth and Jovian magnetospheres

The hypothesis of magnetospheric chaos was supported originally by Baker [12], Pavlos [90]-[94] and Vassiliadis [130]. In this direction Tom Chang [24] proposed for the far from equilibrium space plasmas dynamics the generalization of Wilson Renormalization Group theory predicting SOC or chaos states. Strong objection and criticism against the magnetospheric chaos was presented by Price and Prichard [107]-[109]. Pavlos [90], Pavlos et al. [95] paralelly to the nonlinear analysis of magnetospheric signals supported the hypothesis of magnetospheric self organization as basic nonlinear and holistic theory space

plasmas, according to [45], [79]. Moreover, the hypothesis of SOC process was strongly supported as a physical explanation of the magnetospheric dynamics, by Klimas et al. [64], Consolini [31], Uritsky [128], Chapman [28] and others. After this in a series of papers we have shown the existence of two distinct magnetospheric dynamical components: one which is low dimensional and chaotic and a second which is high dimensional of SOC type [95]-[97], [102].

In particular we have shown:

- Change of the plasma sheet state from stochastic and high dimensional (SOC state) to low dimensional and chaotic (chaos state) during the development of a superstorm event.
- Strengthen of the intermittent character during the substorm period as well as development of global self-organization and long-range correlation at the plasma sheet.
- Low dimensional self-organization with long range, intermittent and correlated profile can be developed at regions near the magnetopause and the bow shock.
- High dimensional and stochastic processes and intermittent turbulence during quiet periods inside the plasma sheet
- q-Gaussian statistics and strong evidence for the application of non-extensive statistics, according to Tsallis theory to space plasmas

These results confirm the model of phase transition-like behavior of the magnetosphere during substorms introduced by Sitnov et al.[117]. According to this model the magnetospheric dynamics includes multiscale self organized criticality processes corresponding to second-order phase transition, as well as low dimensional and chaotic processes corresponding to first-order phase transition. The dual character of magnetospheric dynamics observed in situ by the space-craft GEOTAIL by Pavlos et al. [101], [104] is in agreement with our previous results [95], [97] and verify the concept of low dimensional chaos at the magnetospheric dynamics, as well as the intermittent turbulence and SOC in accordance with the general theory of Tom Chang [23], [27] concerning the far from equilibrium self-organization of the magnetospheric system and the far from equilibrium renormalization theory for critical dynamics.

3.3 Low dimensional chaotic seismogenesis

The existence of power law distributions led many scientists to explain earthquakes as a Self Organized Critical (SOC) process, according to Bak theory [10] as well as to consider seismicity as the turbulence of the solid earth crust [10], [11], [18], [40], [59]. These concepts showed that earthquakes can be understood via the general theory of statistical physics for dynamical processes of far from equilibrium phase transitions applied to distributed fault‘s systems. The SOC process has already been connected in the past to the unpredictability of earthquakes since the SOC dynamics is related to the edge of chaos phenomenon characterized by strong randomness and high-dimensionality [119] since SOC models have often been considered as alternatives to the low dimensional chaos

interpretation of the seismic process [98], [100]. On the other hand, chaos includes low dimensional determinism, in contrast with complete unpredictability or randomness, which is lost over long enough time scales, but long-term, intermediate and short term prediction could be related to a chaotic seismic-cycle process [18], [40]. It was for the first time that Pavlos [96] constructed interevent seismic time series according to the dripping faucet dynamical system for testing the hypothesis of seismic chaos. The dripping faucet model is well known for illustrating the appearance of chaotic behavior in nonlinear systems, where time intervals between successive drop detachments are used to reconstruct the dynamics of the system [115]. At low dripping rates the system is periodic, while above a critical dripping rate the system exhibits chaotic behavior characterized by qualitatively different types of strange attractors. Using interevent time intervals between one drop to the next one, the reconstructed dynamics reveals low dimensional deterministic behavior in the reconstructed state space. According to Iliopoulos et al. [53] and Pavlos et al. [96] concerning a seismic process, the loading rate $m(t)$ of mass in the mechanistic dripping faucet model of Shaw corresponds to the transfer of stress in the fault system by the mantle and plate tectonic dynamics (the external driver of the system), while mass unloading corresponds to earthquakes, as releases of the elastic strain energy stored along a fault. The dripping faucet similarly to the earthquake process can be understood as a local, driven, threshold process. In a series of papers by Iliopoulos et al. [53]-[55] and Pavlos et al. [98] the seismic low dimensional chaos was faithfully supported for the case of the Hellenic seismogenesis. These studies showed clearly the existence of a global seismic strange attractor in the Hellenic region with low dimensionality and strong sensitivity to initial conditions concerning the spatiotemporal distribution of earthquakes. Moreover, the chaotic analysis of seismic time series revealed an independent high dimensional SOC dynamics concerning the energy release process. Moreover, [55] applied nonlinear analysis to various seismic time series indicating local low dimensional temporal chaotic character of the seismic process in the North Aegean area and high dimensional SOC process concerning the bursting seismic energy release. The non-extensive q-statistics of Tsallis was observed also by [55].

3.4 Brain activity during health and seizure state

The human brain can be modelled as a driven nonlinear threshold system including interacting spatial networks of statistically identical, nonlinear units or cells. Each cell fires or falls when the electrical potential or current reaches a threshold value. Numerical simulations of these systems reveal spatial and temporal patterns of firing while the dynamics may also be modified by the presence of noise. The spatiotemporal complexity of brain activity can reveal various dynamical states during health or seizure periods [11], [41], [52], [66], [69], [88], [98], [127], [134] applied chaotic analysis for EEG signals as the brain activity changes from health to epilepsy seizure. In this study, we have shown a phase transition process of brain activity from a high dimensional SOC state during the health period to a gradually developed low dimensional chaotic

state. Tsoutsouras *et al.* [126] produced a cellular Automata (CA) model of healthy and epilepsy brain states. In this study, the chaotic clustering of neurons was indicated as a basic mechanism of the phase transition of the brain activity from high-dimensional stochastic dynamics to low-dimensional chaotic dynamics. The CA modeling of brain activity by [126] was found to simulate faithfully the brain dynamics underlying to real data. The brain phase transition process from high-dimensional stochastic to low-dimensional chaotic states supported by CA modeling and by real data chaotic analysis was found to belong to a universal complex spatiotemporal process observed at various physical systems such as the solar activity at the magnetospheric substorms, as well as at the seismic process of the earth lithospheric fault system [54], [60], [61], [101].

3.5 Self Organized Criticality and Chaos at the on-chip workload process

In recent years, the mobile technology was developed so dramatically that has opened new challenges in the embedded system design domain. Different, from the traditional desktop systems, embedded devices demand not only high processor performance but also low power consumption. Thus, the development of proper methods in power consumption management, which will extend the battery life, is without doubt, an imperative need. It was the first time that a SOC–Chaos phase transition process was observed during periods of on-chip workload by [136]. These are results of high significance concerning the design of Network-on-chip Architecture. Dynamic frequency scaling (DFS) is used to adjust the working frequency according to the system workload in order to save the power consumption without degrading the system performance significantly beyond the application tolerance. The main problem of DFS solutions is how to compute the system workload trend. Generally, the workload analysis is an open issue which has occupied the international literature by the beginning of the computer science technology. Recently, [136] used chaotic analysis of workload time series in order to develop novel power aware dynamic frequency scaling technique based on the workload treud of an embedded application. Particular chaotic analysis of workload signals showed the existence of workload critical dynamics and phase transition between states with distinct dynamical dimensionality. This gives the opportunity to handle dynamic data streams with complex behavior. The benefit of this approach based at the real time chaotic analysis of the workload signal is related to the management of the power consumption. The simulation results showed that the methodology based on chaotic analysis can achieve remarkable improvements at the final power consumption. The main idea of our approach is to adjust the processing frequency of our system by analysing the workload fluctuations without degrading the final performance or violating any deadline. The key of our methodology is that we use an abstract model of workload analysis that combines advanced mathematical tools from the Chaos Theory domain. This gives us the opportunity to handle dynamic data streams with complex behavior. The benefit of our approach is that it is a system-level platform independent

technique, which permits us, through the analysis and the prediction of the workload trend, to manage the power consumption of an embedded system calibrating only the processing frequency. The simulation results showed that our methodology can achieve remarkable improvements at the final power consumption, which range between 17% and 38% depending on the restriction of the application deadlines. These results are complementary to previous analysis of system performance degray taking into account the interaction between workload fluctuations and the nonlinearity of the system. Moreover, the phase transition process described by Zompakis [136] can be used for proposing new adaptive techniques related with dynamics power management.

4 Theoretical Documentation of the Results Obtained by Chaotic Analysis

Until now, Chaos or SOC states, intermittent turbulence including multifractal and multiscale characteristics, Tsallis q-statistics, as well as out of equilibrium phase transition processes, were found to be of universal character at distinct physical or technological systems. Also, all the previous systems at which the chaotic analysis was applied belong to the general type of distributed and far from equilibrium input-output threshold nonlinear dynamics. For these systems the general theory of far from equilibrium non linear stochastic dynamics described by generalized Langeving equations can be applied [47]. According to Chang [23]-[25] the stochastic Lagrangian methodology for the solution of the stochastic Langevin equations and the far from equilibrium renormalization group theory can be used for the estimation of the fixed points of the dynamics. From this point of view, various macroscopic states and process can be related to different fixed points in the affine space of the stochastic Lagrangian dynamics. In general, far from equilibrium nonlinear stochastic dynamics can be described by a set of generalized Langevin equations [25]:

$$\frac{\partial \phi_i}{\partial t} = f_i(\phi, x, t) + n_i(x, t) \tag{1}$$

where $f_i (i = 1, 2, \ldots)$ are nonrandom forces corresponding to the functional derivative of the free energy functional, $x_\mu (\mu = 1, \ldots, d)$ are the spatial coordinates, t is the time and $\phi(x, t)$ represents the stochastic variables which describe the fault dynamics and $n_i(x, t)$ are random force fields or noises. According to Chang [24] the behavior of a nonlinear stochastic system far from equilibrium can be described by the density functional P, defined by path integral formulation:

$$P\phi(x, t) = \int D(x) \exp^{-i \int L(\dot{\phi}, \phi, x) dx dt} \tag{2}$$

where $L(\dot{\phi}, \phi, x)$ being the stochastic Lagrangian of the system, which describes the full dynamics of the stochastic system. Moreover, the far from equilibrium renormalization group theory applied to the stochastic Langrangian L gives the singular points (fixed points) in the affine space of the stochastic

distributed system. At the fixed points the system reveals the character of criticality, as near criticality the correlations among the fluctuations of the random dynamic field are extremely long-ranged and there exist many correlation scales. Also, close to dynamic criticality certain linear combinations of the parameters, characterizing the stochastic Lagrangian of the system, correlate with each other in the form of power laws and the stochastic system can be described by a small number of relevant parameters characterizing the truncated system of equations with low or high dimensionality. According to these theoretical results, the stochastic system can exhibit low dimensional chaos or high dimensional SOC like behavior, including spatiotemporal fractal structures with power law profiles. The power laws are connected to the near criticality phase transition process which creates spatial and temporal correlations as well as strong or weak reduction (self-organization) of the infinite dimensionality corresponding to a spatially distributed system. According to Lyra and Tsallis [71], the power laws are not caused by the SOC process, but by the nonextensive statistics observed at far from equilibrium process with long range correlations. From this point of view, a SOC or low dimensional chaos interpretation depends upon the kind of the critical fixed (singular) point in the functional solution space of the system. When the stochastic system is externally driven or perturbed, it can be moved from a particular state of criticality to another characterized by a different fixed point and different dimensionality or scaling laws. Thus, SOC theory could be a special type of critical dynamics of an externally driven stochastic system [70]. Furthermore, according to Chang [26], Chang et al. [27] as well as Vieira [131], SOC and low dimensional chaos can coexist in the same dynamical system as a process manifested by different kinds of fixed (critical) points in its solution space. As the dynamical system evolves in time (autonomously or under external forcing), the state of the system described by the values of the dynamical parameters in the stochastic Lagrangian L, changes as well. The change of the critical state of the system can reveal different dynamical scenarios, as it evolves from one critical state to another, after external tuning. Also, it is possible to reveal local instabilities by creating metastable states which evolve to states of lower energy. This is a local symmetry breaking phenomenon and leads to a local phase transition process. Such local instabilities are connected to avalanche or nucleation dynamics, which can be present in systems that are at mean-field or near-mean-field state, with the possibility of spinodal decomposition process [63], [114]. Moreover, the theory of far from equilibrium critical dynamics can be related to the equilibrium phase transition theory, as both include local metastable states characterized by spinodal lines and spinodal phase transitions.

5 Is Complexity the Road for the Final Unification of the Physical Theory? New Concepts for an Old Problem.

The old problem in physics is the unification of mechanics and thermodynamics. For Albert Einstein, physical theory must correspond objectively to the

physical reality. Thus, the hard core of a final physical theory must be the mathematical determinism. For Heisenberg, Bohr and Born, physical theory has to be related to the phenomenology of reality. Because of this, probabilism is the unavoidable hard core of every physical theory. On the other hand, the hard core of complexity is nonlinearity. Nonlinear dynamics includes determinism in the form of periodic attractors with integer dimension as well as probabilism in the form of chaotic fractal attractors. From this point of view we understand that there exists an internal connection between nonlinear dynamics and thermodynamics since entropy is a propabilistic property of a dynamical system. Nonlinear deterministic dynamics including strong irregularity of chaotic mixing or $f*$ exact type, includes thermodynamical characteristics [72]. Such a type of strongly nonlinear unstable determinism is equivalent also to stochastic or probabilistic dynamics [74], [83], [111].

Moreover determinism and probabilism can be interrelated also through Rochlin theorem [112] according to which every $f*$ exact transformation is the factor of a k automorphism. In this way Boltzmann's (stochastic) dynamics can be proved to be the trace of Liouville's (deterministic) dynamics or the Boltzmann's equation is the trace of Liouville equation [72]. In the same direction quantum probabilism can be related to classical determinism and dissipation according to [32], [49]. Another significant character of nonlinear deterministic dynamics is the bifurcation profile of solutions and the critical point dynamics (near or far from equilibrium) as the pattern formation or morphogenesis character [47]. According to Wilson [135] the critical physical theory related to the dynamics must take into account the entire spectrum of length scales from 10^{-8} cm to 10^{11} cm. However, more than this it seems that complexity and nonlinear dynamics includes the theoretical kernel for a global unification of physical theory, as we argue in a previous study by Pavlos *et al.* [101]. Critical dynamics showed the significance of renormalization group theory, the scale invariance principle related to fractal geometry, as well as the relation of dynamics with topological and dimensional characteristics of space. However, the deep question of complexity theory is how forms are generated in nature and what is the relationship between physical forces and the stable geometries of morphogenesis and pattern formation. According to Kovacs [67] somehow space-time symmetries create the fundamental laws of nature. Moreover, it could be possible to imagine some extended kind of geometrical invariance principle and novel topological characteristics to produce every kind of pattern, according to the dream of Einstein, concerning the geometrical unification of physical theory and physical dynamics. According to El Naschie [36], [39] and Ord [87] noncommutative geometries and fractal space-time can be used for the extension of complexity from the macroscopic to the microscopic level. Scale invariance principles also can be used for the unification of microscopic and macroscopic complexity. Some efficient evidence for such a dream we present indicatively in the following.

6 Complexity as a New Physical Theory

Is Complexity a major revolution in science such as Relativity and Quantum Theory? For many scientists attempts to explain complexity and self-organization by using the basic laws of physics have met with little success. Novel forms of self-organization are generally unexpected for the classic reductionistic point of view. However, while complexity is considered as a new and independent physical theory which was developed after the Relativity Theory and Quantum mechanics, it must be consistent with these theories. It is related to far from equilibrium dynamics and concerns the creation and destruction of spatiotemporal patterns, forms and structures. According to Balescu [8], Nicolis and Prigogine [78], [79], Nicolis [80], [81], and Prigogine [110], [111], complexity theory corresponds to the flow and development of space-time correlations instead of the fundamental local interactions. According to the classical point of view the physical phenomena (macroscopic or microscopic) must be reducible to a few fundamental interactions. However, according to Nicolis [82], since 1960 an increasing amount of experimental data challenging this idea has become available. This impose a new attitude concerning the description of Nature. Moreover, according to Sornette [118], systems with a large number of mutually interacting parts and open to their environment can self-organize their internal structure and their dynamics with novel and sometimes surprising macroscopic emergent properties. These general characteristics make the complexity theory, a fundamentally probabilistic theory of the non-equilibrium dynamics.

7 Complexity as a Form of Macroscopic Quanticity

The central point of complexity theory is the possibility for a physical system, which includes a great number of parts or elements, to develop internal long-range correlations leading to macroscopic ordering and coherent patterns. These long-range correlations can also appear at the quantum level. In particular, according to the general entanglement character of the Quantum theory, the quantum mechanical states of a system with two or more parts cannot be expressed as the conjunction of quantum states of the separate parts. This situation generally reflects the existence of non-local interactions and quantum correlations while the measurements bearing on either part correspond to random variables which are not independent and can be correlated independently with the spatial distance of the parts [116]. This means that the quantum density operator cannot be factored while the quantum state corresponds to the global and undivided system. The macroscopic manifestation of the quantum possibility for the development of long-range correlations is the spontaneous appearance of ordered behavior in a macroscopic system, examples of which are phenomena like superfluidity and superconductivity or lasers [68].

These quantum phenomena display coherent behavior involving the collective cooperation of a huge number of particles or simple elements and a vast number of degrees of freedom. They correspond also to equilibrium or nonequilibrium phase transition processes which constitute the meeting point

of quantum theory and complexity. Here the development of quantum long-range correlations leads to a macroscopic phase transition process and macroscopic ordering. It is not out of logic or physical reality to extend the (unifying) possibility of quantum process to developed long-range correlations, according to the quantum entanglement character, into a macroscopic self-organizing factor causing also the far-from equilibrium symmetry breaking and macroscopic pattern formation. From this point of view we can characterize complexity as a form of a macroscopic quanticity [34], [135].

8 Quantum Theory as a Form of Microscopic Chaoticity and Complexity

Bohm and Hiley [21] imagined that the Quantum theory must be the manifestation of subquantum complex dynamics. During the last years, we observe the productive onset or the impetus invasion of chaos and complexity from macroscopic to the microscopic quantum level. In the following we present some novel concepts in this direction:

- Determinism at the Planck‘s scale [49]-[51].
- Order and deterministic chaos at the quantum level [32]
- Analytical continuation and fractal space-time can convert an ordinary diffusion equation into a Schrodinger‘s equation and a telegraph equation into a Dirac's equation. From this point of view analytical continuation is a short cut of quantization [76], [77].
- Positive Lyapunov exponents of non-abelian gauge fields reveal the significance of chaos for the quantum field theory [20].
- Coupled map lattices with spatiotemporal chaotic profile can be used to simulate quantum field theories in an appropriate scaling limit [17], [22].
- Kaneko‘s coupled map lattices including chaotic strings provide the background for the Parisi-Wu stochastic quantization of ordinary string and quantum field theories [14], [15]. Chaotic strings can be used also to provide a theoretical argument why certain standard model parameters are realized in nature reproducing numerical values of the electroweak and strong coupling constants masses of the known quarks and leptons neutrino, W boson and Higg's mass.
- Renormalization group (RG) flows on the superstring world sheet becomes chaotic and leads to non-Markovian Fokker-Planck equation with solutions describing the transition from order to chaos and revealing the Feigenbaum universal constant [65]. The appearance of this constant reveals the scaling of space-time curvatures at the fixed points of the RG flow which becomes chaotic near singularities where the curvature is very large [75], [105].
- The Parisi-Wu [89] stochastic quantization theory relates the quantum field theory in D-dimensions to a classical Langevin equation in $D+1$-dimensions where the Parisi-Wu fictitious time plays the role of an extra dimension. In this picture there exists a short of classical stochasticity and quantum theory duality [33]. The stochastic quantization can be transformed to chaotic quantization, similar to chaotic deterministic dynamical systems

which can generate Langevin dynamics in an appropriate scaling limit. In this approach, quantum field theories can be simulated by chaotic dynamics

- Non-extensive statistics [123], fractal string and branes, fractal statistics, fractons and anyons particles as well as chaotic M(atrix) theory indicate the establishment of chaos and complexity at the microscopic and the quantum level [22]. In this direction, Gerardus 't Hooft raised the conjecture that quantum theory can be derived as the low-energy limit of a microscopically deterministic but dissipative theory [50]. According to this concept classical Perron-Frobenius operators or deterministic automata can produce quantum states in Hilbert spaces as well as the Schrodinger equation [1], [9], [35], [42].

After all, we can imagine that quantum states are produced by a sub-quantum self-organized process. This sub-quantum self-organization must concern information process rather than simple material or energy self-organization.

9 Universality of Tsallis non-extensive statistical mechanics

According to Tsallis, Boltzmann-Gibbs statistical mechanics and standard thermodynamics do not seem to be universal. Tsallis extended the Boltzmann-Gibbs statistics and Boltzmann-Gibbs entropy to non-extensive statistical mechanics and non-extensive q-entropies. The classical Boltzmann-Gibbs extensive thermostatistics constitutes a powerful tool when microscopic interactions and memory are short ranged and space-time is a continuous and differentiable Euclidean manifold. However, far from equilibrium these characteristics are changed as multiscale coupling and non-locality characteristics can appears. In turbulence for example, the presence of long-range correlations imply non-local interactions between large and small scales as the relation between them is not local in space and time but functional. This indicates that small-scale fluctuations in each time space point depend on the large scale motions in the whole time-space domain and vice versa. Generally, the non-extensive statistical mechanics introduced by Tsallis rather than being just a theoretical construction it is relevant to many complex systems at the macroscopic or the microscopic level with long-range correlations-interactions or multifractal behavior. A crucial property of Tsallis entropy S_q is the pseudo-additivity for given subsystems A and B in the sense of factorizability of the microstate according to the relations $S_q(A+B) = S_q(A) + S_q(B) + (1-q)S_q(A)S_q(B)$ where $S_q = k_B \frac{(1-\sum p_i^q}{q-1}$ and k_B is Boltzmann's constant. The non-local coupling and long-range correlations of complex dynamics corresponds to the multiplicative tern of the previous relation. Also, the non-extensive behavior of macroscopic or microscopic complexity is related to the non-Euclidean and multi-fractal space time [22], [46], [58], the quantum gravity and quantum entanglement [122].

10 The road of Complexity for the Physical Theory Unification

According to previously presented concepts and descriptions, about the nonequilibrium statistical mechanics, the Feynman rules and diagrams become common tool from the estimation of probabilistic processes at the microscopic quantum level or the macroscopic level of continuous media as they are being described by the Ginzburg-Landau model [13], [19], [47]. In this direction, we could imagine Feynman rules and renormalization group theory as the universal characteristics of probabilistic processes at the microscopic and the macroscopic level. The renormalization group equations have many common features with non-linear dynamical systems, so that apart from existence of isolated fixed points, the coupling in a renormalizable field theory may flow also towards more general even fractal attractors. This could lead to Big Mess scenarios in application to multiphase systems, from spin-glasses and neural networks to fundamental string theory [75]. In this direction Cristopher Hill [46] introduced the fractal theory space where the key idea is that the Feynman path integral is invariant under a sequence of renormalization group transformations that map the kth lattice into the $k-1$ lattice. In the continuum limit these models produced quantum field theories in fractal dimensions D. These theories are connected to the scaling behavior of fractal strings (branes), while the couplings oscillate on a limit cycle. Moreover the concept of fractal space-time can be used for the foundation of an extended Einsteins Relativity Principle unifying the micro and macro levels [84], [85].

In this direction, [87] showed that fractal trajectories in space with Hansdorff dimension $D = 2$ exhibit both an uncertainty principle and a De Broglie wave - particle duality relations. Furthermore, Nottale [84], [85] introduced the principle of Scale Relativity according to which the laws of physics are scale invariant. This theory is related also to the concept of fractal space-time. According to Nottale, the consequence of scale invariance principle and space-time fractality opens the door for a grand unification of cosmos, from the microscopic quantum level to the macroscopic and cosmological level. The starting point of the theory is the refusing of the unjustified assumption of the differentiability of the space-time continuum. The non-differentiable space-time continuum is necessarily fractal. The development of the theory starts by making the various physical quantities explicitly dependent on the space-time scale while the fundamental laws become also scale dependent. In this frame of theory the non-differentiability of space-time implies the breaking of time reversibility, and the global unification of microscopical and macroscopical laws, [37], [56], [57], [86], [103].

References

1.Arefëva, I.Ya., Medvedev, P.B., Rytchkov, O.A. & Volovich, I.V. [1999] "Chaos in M(atrix) Theory", *Chaos, Solitons & Fractals* **10**, p. 213.

2.Argyris J., I. Andreadis, G.P. Pavlos, M. Athanasiou [1998] "The influence of noise in the correlation dimension of chaotic attractors", *Chaos, Solitons & Fractals* **9(3)**, p. 343-361.

3.Argyris J., I. Andreadis, G.P. Pavlos, M. Athanasiou [1998] "On the influence of noise on the Largest Lyapunov exponent and on the geometric structure of attractors", *Chaos, Solitons & Fractals* **9(6)**, p. 947-958.
4.Argyris, J., L. Tenek, I. Andreadis, M. Athanasiu, and G.P. Pavlos [1998] "On chaotic oscillations of a laminated composite cylinder subject to periodic application of temperature" *Chaos, Solitons & Fractals* **9(9)**, p. 1529-1554.
5.Argyris J., I. Andreadis, G.P. Pavlos, M. Athanasiou [2000] "On a classification of dynamic systems subject to noise" *Chaos, Solitons & Fractals* **11**, p. 297-302.
6.Athanasiu,M.A. & Pavlos, G.P. [2001] "SVD Analysis of the magnetospheric AE index time series and comparison with low dimensional chaotic dynamics," *Nonlin. Proc. Geophys.* **8**, p. 95-125.
7.Athanasiu M.A., G.P. Pavlos, D.V. Sarafopoulos, and E.T. Sarris [2003] "SVD Analysis of the magnetospheric AE index time series and comparison with low dimensional chaotic dynamics," *Nonlin. Proc. Geophys.* **8**, p. 95-125.
8.Balescu, R. [1975] "Equilibrium and nonequilibrium statistical mechanics", Copyright, Wiley, J., New York.
9.Banks, T., Fischler, W., Shenker, S.H. & Susskind, L. [1997] "M theory as a matrix model: A conjecture", Phys. Rev. D, **55**, p. 5112.
10.Bak, P., Tang, C. & Wiesenfeld, K. [1988] "Self Organized Criticality" *Phys. Rev. A* **38(1)**, p. 364-374.
11.Bak, P. [1996] *How Nature Works*, (Springer-Verlag New York, Inc).
12.Baker, D.N., Klimas, A.J., McPherro, R.L. & Buchner, J. [1990] "The evolution from weak to strong geomagnetic activity: An interpretation in terms of deterministic chaos" *Geophys. Res. Lett.* **17**, p. 41.
13.Bausch, R., Jansshen, H.K. & Wagner, H. [1976] "Renormalized Field Theory of Critical Dynamics", *Z.Physik*, **B24**, p. 113.
14.Beck, C. [1991] "Higher correlation functions of chaotic dynamical systems-a graph theoretical approach", Nonlinearity, **4**, p. 1131.
15.Beck, C. [1995] "Chaotic quantization of field theories", *Nonlinearity*, **8**, p. 423.
16.Beck, C. [2001] "Dynamical Foundations of Nonextensive Statistical Mechanics", *Phys. Rev. Let.*, **87**, p. 180601-1.
17.Beck, C. [2002] "Nonextensive methods in turbulence and particle physics", *Hysica A*, **305**, p. 209.
18.Ben Zion, Y., Eneva, M. & Liy, Y. [2003] "Large earthquake cycles and intermittent criticality on heterogeneous faults due to evolving stress and seismicity", *J. Geophys. Res.*, **108**, p. 2307.
19.binne, J.J., Dowrick, N.J., Fisher, A.J. & Newman, M.E.J. [1993] "Theo theory of critical phenomena", Oxford Universiy Press, New York.
20.Biro, T., Muller, B. & Matinyan, S. [2004] "Chaotic Quantization: Maybe the Lord plays dice, after all?", *Lecture Notes in Physics*, **633**, p. 164.
21.Bohm, D. & Hilley, B. [1993] "The undivided universe", Routledge, London.
22.Castro, C. [2005] "., On non-extensive statistics, chaos and fractal strings", Physica A **347**, p. 184.
23.Chang, T., Nicoll, J.F. & Young, J.E. [1978] "A closed-form differential renormalization group generator for critical dynamics", *Phys. Lett.*, **67A(4)**, p. 287-290.
24.Chang, T. [1992] '"Low-Dimensional Behavior and Symmetry Braking of Stochastic Systems near Criticality Can these Effects be Observed in Space and in the Laboratory", *IEEE* **20(6)**, p. 691-694.
25.Chang, T., Vvedensky, D.D. & Nicoll, J.F [1992] "Differential Renormalization Group Generators for static and dynamic critical phenomena", *Physics Reports*, **217(6)**, p. 279-360.

26.Chang, T. [1999] "Self-organized criticality, multi-fractal spectra, sporadic localized reconnections and intermittent turbulence in the magnetotail", *Physics of Plasmas*, **6(11)**, p. 4137-4145.
27.Chang, T., Tam, S.W.Y., Wu, C-C, & Consolini, G [2003] "Complexity, Forced and/or Self-Organized Criticality, and Topological Phase Transitions in Space Plasmas", *Space Sci. Rev.*, **107**, p. 425-445.
28.Chapman, S.C., Watkins, N.W., Dendy, R.O., Helander, P. & Rowlands, G. [1998] "A simple avalanche model as an analogue for magnetospheric activity", *Geophysical Research Letters*, **25(13)**, p. 2397-2400.
29.Chate, H. & Manneville, P. [1989] "Role of defects in the transition to turbulence via spatiotemporal intermittency", *Physica D*, **37**, p. 33-41.
30.Chate, H. [1995] "On the analysis o spatiotemporally chaotic data", *Physica D*, **86**, p. 238-247.
31.Consolini, G., [1997] "Sandpile cellular automata and magnetospheric dynamics", 8th GIFCO Conference: Cosmic physics in the year 2000, p. 123 - 126.
32.Contopoulos, G., Efthymiopoulos, C. & Harsoula, M. [2008] "Order and chaos in quantum mechanics" *Non. Phenom. Complex Systems*, **11**, p. 107.
33.Damgaard, P. & Huffel, H. [1987] "Stochastic Quantization", *Phys. Rev. Let.*, **152**, p. 227.
34.Davies, P. [1987] "The Cosmic Blueprint", William Heinemann Ltd., Great Britain.
35.De Wit, B. [1988] "On the quantum mechanics of supermembranes", *Nuclear Physics B*, **305**, p. 545.
36.El Naschie, M.S. [1998] "Superstrings, Knots, and Noncommutative Geometry in E(infinity) Space", Int. Journal of Theoretical Physics, **37**, p. 2935.
37.El Naschie, M.S. [2004] "A review of E infinity theory and the mass spectrum of high energy particle physics", Chaos, Solitons & Fractals, **19**, p. 209-236.
38.El Naschie, M.S. [2005] "Einstein's dream and fractal geometry", Chaos, Solitons & Fractals, **24**, p. 1.
39.El Naschie, M.S. [2006] "Elementary prerequisites for E-infinity (Recommended background readings in nonlinear dynamics, geometry and topology)", *Chaos, Solitons & Fractals*, **30**, p. 579.
40.Evison, F.F. [2001] "Long-range synoptic earthquake forecasting: An aim for the millennium," *Tectonophys.*, **338**, p. 207-215.
41.Freeman, W.J. [1987] "Simulation of chaotic EEG patterns with a dynamic model of the olfactory system", *Biol.Cybern.*, **56**, p. 139-150.
42.Frohlich, J. & Hoppe, J. [1998] "On Zero-Mass Ground States in Super-Membrane Matrix Models", *Commun.Math.Phys.*, **191**, p. 613.
43.Glansdorff, P. & Prigogine, I. [1973] "Thermodynamic Theory of Structure, Stability and Fluctuations", *Am. J. Phys.*, **41(1)**, p. 147.
44.Grassberger, P. & Procaccia, I. [1983] "Measuring the strangeness of strange attractors", *Physica D: Nonlinear Pgenomena*, **9**, p. 189.
45.Haken, H. [1983] *Synergetics: Introduction and Advanced Topics*, Springer.
46.Hill, C. "Fractal theory space: Spacetime of noninteger dimensionality", *Phys. Rev. D*, **67**, p. 085004.
47.Hohenberg, P. & Halperin, B. "Theory of dynamic critical phenomena", *Rev. of Mod. Phys.*, **49**, p. 435.
48.Hohenberg, P.C. & Shraiman, B.I. [1989] "Chaotic behavior of an extended system", *Physica D*, **37**, p. 109-115.
49.Hooft, G.T. [1999] "Quantum gravity as a dissipative deterministic system", *Class. Quantum Grav.*, **16**, p. 3263-3279.
50.Hooft, G.T. [2001a] "Determinism and Dissipation in Quantum Gravity", *Basics and highlights in fundamental physics: proceedings of the International School of Subnuclear Physics*, **37**, p. 397.

51.Hooft, G.T. [2001b] "How Does God Play Dice?(Pre) Determinism at the Planck Scale", An Essay in Honor of John S. Bell, arXiv:hep-th/0104219.
52.Iasemidis L.D., & Sackellares, J.C. [1996] "Chaos Theory and Epilepsy", *The Neuroscientist*, **2**, p. 118-126.
53.Iliopoulos, A., Pavlos, G. & Athanasiu, M. [2008] "Spatiotemporal Chaos into the Hellenic Seismogenesis: Evidence for a Global Strange Attractor", *Nonlin. Phenom. Complex Sys.* **11(2)**, p. 274.
54.Iliopoulos, A. & Pavlos, G. [2010] "Global Low Dimensional Seismic Chaos in the Hellenic Region," *Intern. J. Bifurc. Chaos* **20(7)**, p. 2071.
55.Iliopoulos, A.C., Pavlos, G.P., Papadimitriou, E., Sfiris, D. [2011] "Chaos, Self Organized Criticality, Intermittent Turbulence and Nonextensisvity Revealed from Seismogenesis in North Aegean Area" *submitted*.
56.Iovane, G. [2006a] "Cantorian spacetime and Hilbert space: Part I-Foundations", Chaos, Solitons & Fractals, **28**, p. 857-878.
57.Iovane, G. [2006b] "Cantorian space-time and Hilbert space: Part II-Relevant consequences", Chaos, Solitons & Fractals, **29**, p. 1-22.
58.Jizba, P. & Arimitsu, T. [2004] "The world according to Renyi: thermodynamics of multifractal systems", Annals of Physics, **312**, p. 17.
59.Kagan, Y. Y. [1994] "Observational evidence for earthquakes as a nonlinear dynamic process" *Physica D*, **77**, p. 160-192.
60.Karakatsanis, L.P. & Pavlos, G.P. [2008] "Self Organized Criticality and Chaos into the Solar Activity", Nonlinear Phenomena in Complex Systems, **11(2)**, p. 280-284.
61.Karakatsanis, L.P., Pavlos, G.P., Iliopoulos, A.C. & Tsoutsouras, V.G. [2010] "Evidence for Coexistence of SOC and Chaos processes in the Solar Flare Dynamics", Modern Challenges in Nonlinear Plasma Physics, Accepted for publication, *Accepted for publication*, eds. Vassiliadis, D., American Institute of Physics.
62.Karakatsanis, L.P., Pavlos, G.P., Iliopoulos, A.C., Tsoutsouras, V.G. & Pavlos, E.G., "Evidence for Coexistence of SOC, Intermittent Turbulence and Low-Dimensional Chaos Processes in Solar Flare Dynamics, *AIP Conf. Proc.*, **1320**, pp. 55-64.
63.Klein, W., Gould, H., Gulbahce, N., Rundle, J.B. & Tiampo, K. [2007], "Structure of fluctuations near mean-field critical points and spinodals and its implication for physical processes", *Phys. Rev. E*, **75**, p. 031114
64.Klimas, A.J, Valdivia, J.A., Vassiliadis, D., Baker, D.N., Hesse, M. & Takalo, J. [2000] "Self-organized criticality in the substorm phenomenon and its relation to localized reconnection in the magnetospheric plasma sheet", *J. Geophys. Res.*, **105**, p. 18765-18780.
65.Kogan, I. & Polyakov, D. [2003] "Chost-Matter Mixing and Feigenbaum Universality in String Theory", *Physics of Atomic Nuclei*, **66**, p. 2062.
66.Korn, H., & Faure, P. (2003), "Is there chaos in the brain? II. Experimental evidence and related models", *C.R. Biologies*, **326**, p. 787-840.
67.Kovas, A.L. [1994] "Nonlinear Dynamics of Spatio-Temporal Processes in Complex Systems", *Mathl. Comput. Modelling*, **19**, p. 47.
68.Leggett, A. [1989] "Low temperature physics, superconductivity and superfluidity", in Davies, Cambridge University Press
69.Linkenkaer-Hansen K., [2002] "Self-Organized Criticality and Stochastic Resonance in the Human Brain", Helsinki University of Technology, Laboratory of Biomedical Engineering.
70.Lu, E.T. [1995] "Avalanches in continuum driven dissipative systems", *Phys. Rev. Lett.*, **74**, p. 13.

71.Lyra, M. L. & Tsa lis C. [1998] "Nonextensivity and Multifractality in Low-Dimensional Dissipative Systems," *Phys. Rev. Lett.* **80(1)**, p. 53-56.
72.Mackey, G.W. [1989] "The dynamic origin of increasing entropy", *Rev. Mod. Phys.*, **61**, p. 981.
73.Mayer-Kress, G. & Kaneko, K. [1989] "Spatiotemporal Chaos and Noise", *Journal of Statistical Physics*, **54**, p.1489.
74.Misra, B., Prigogine, I. & Courbage, M. [1979] "From deterministic dynamics to probabilistic descriptions", *Physica A*, **98**, p. 1.
75.Morozov, A. & Niemi, J. [2006] "Can Renormalization Group Flow End in a Big Mess?", *Nuclear Physics B*, **666**, p. 311.
76.Nelson, E. [1966] "Derivation of the Schrodinger equation from Newtonian mechanics", *Phys. Rev.*, **150**, p. 1079.
77.Nelson, E. [1985] "Quantum Fluctuations", *Princeton University Press*, New York.
78.Nicolis, G. & Prigogine, I. [1971] "Fluctuations in nonequilibrium systems" *Proc. Nat. Acad. Sci.* **68x**, p. 2102.
79.Nicolis, G. & Prigogine, I. [1977] "Self-organization in nonequilibrium systems: From dissipative structures to order through fluctuations", *Willey, New York.*
80.Nicolis, G. [1979] "Irreversible thermodynamics", Rep. Prog. Phys., **42**, p. 225.
81.Nicolis, G. [1986] "Dissipative Systems", Rep. Prog. Phys., **49**, p. 873.
82.Nicolis, G. [1989] "Physics of Far-From-Equilibrium Systems and Self-organisation", in Davies, Cambridge University Press.
83.Nicolis, G. & Prigogine, I. [1989] "Exploring Complexity: An Introduction", eds. Freeman, W.H., San Francisco.
84.Nottale, L. [1993] "Fractal Space-Time and Micro-physics", Towards a Theory of Scale Relativity, eds. World Scientific.
85.Nottale, L. [1994] "Scale Relativity, Fractal Space-time and Quantum Mechanics", *Chaos, Solitons & Fractals*, **4**, p. 361.
86.Nottale, L. [1996] "Scale Relativity and Fractal Space-Time: Applications to Quantum Physics, Cosmology and Chaotic Systems", *Chaos, Solitons & Fractals*, **7**, p. 877.
87.Ord, G.N. [1983] "Fractal space-time: a geometric analogue of relativistic quantum mechanics", J. Phys. A: Math. Gen., **16**, p. 1869.
88.Paczuski M., Maslov S. & Bak P., "Avalanche dynamics in evolution, growth, and depinning models", *Phys. Rev. E*, **53**, p. 414.
89.Parisi, G. & Wu, Y. [1981] "Perturbation theory without gauge fixing", *Scientia Sinica*, **25(4)**, p. 484.
90.Pavlos, G.P., [1988] "Magnetospheric dynamics", in Proc. Symposium on Solar and Space Physics, eds. Dialetis, D., National Observatory of Athens, p. 1-43.
91.Pavlos, G.P., Trochoutsos, P.C., Liatsis, P., Rigas, A.G & Tsonis, T., [1991] "Evidence of low dimensional chaotic dynamics in solar wind plasma", *XVI EGS, General Assebly*, Wiesbaden.
92.Pavlos, G.P., Rigas, A.G., Dialettis, D., Sarris, E.T., Karakatsanis, L.P. & Tsonis, A.A., [1992a] "Evidence for Chaotic Dynamics in the outer Solar Plasma and the Earth Magnetosphere", *Chaotic Dynamics: Theory and Practice, NATO ASI Series B:Physics*, Plenum Press, New York, **298**, p. 327-339.
93.Pavlos G.P., Dialettis, D., Kyriakou, G.A. & Sarris, E.T. "A Preliminary low-dimensional Chaotic Analysis of the solar Cycle", *Ann. Geophysicae*, **10**, p. 759-762.
94.Pavlos G.P., Kyriakou, G.A., Rigas, A.G., Liatsis, P., Trochoutsos, P.C. & Tsonis, A.A. [1992c] "Evidence for Strange Attractor Structures in Space Plasmas", *Ann. Geophysicae*, **10,**, p. 309-322.

95.Pavlos, G.P., Diamantidis, D., Adamopoulos, A., Rigas, A.G., Daglis, I.A. & Sarris, E.T. [1994a] "Chaos and Magnetospheric Dynamics", *Nonlinear Processes in Geophysics*, **1**, p. 124-135.
96.Pavlos, G. P., Latousakis, I., Dialettis, D., Karakatsanis, L.P. & Papaioannou, G. [1994b] "Chaotic analysis of a time series composed of seismic events recorded in Japan", *Int. J. Bifurcation and Chaos*, **4**, p. 87-98.
97.Pavlos, G.P., Athanasiou, M., Diamantidis, D., Rigas, A.G. & Sarris, E.T. [1999] "Comments and new results about the magnetospheric chaos hypothesis", *Nonlin. Proc. Geophys.*, **6**, p. 99-127.
98.Pavlos, G.P., Iliopoulos, A.C. & Athanasiu, M. [2007] "Self Organized Criticality or / and Low Dimensional Chaos in Earthquake Processes. Theory and Practice in Hellenic Region", *Nonlinear Dynamics in Geosciences*, eds. Tsonis A. & Elsner J. , (Springer), p. 235-259.
99.Pavlos, G.P., Tsoutsouras, V.G., Iliopoulos, L.P. & Athanasiou, M. [2008a] "Self Organized Criticality (SOC) and Chaos Behavior in the Brain Activity" *10th volume of the series Order and Chaos*, eds. Boundis A. & Pnevmatikos S, (University of Patras Press), p. 145.
100.Pavlos, G.P., Iliopoulos, A.C., Karakatsanis, L.P. & Athanasiou, M.A. [2008b] "The Broad Universality of the Stochastic Unification of SOC, Chaos and other Nonlinear Processes" *10th volume of the series Order and Chaos*, eds. Boundis A. & Pnevmatikos S, (University of Patras Press), p. 157-167.
101.Pavlos, G.P., Iliopoulos, A.C., Tsoutsouras, V.G., Karakatsanis, L.P. & Pavlos, E.G. [2010a] "Spatiotemporal Chaos in Distributed Systems: Theory and Practice" *Chaotic Systems: Theory and applications*, eds. Skiadas C. H. & Dimotikalis I., (World Scientific), p. 268-283.
102.Pavlos, G.P., Iliopoulos, A.C., Athanasiou, M.A., Karakatsalis, L.P. & Tsoutsouras, V.G. [2010b] "Complexity in Space Plasmas: Universality of Non-equilibrium physical Processes", Modern Challenges in Nonlinear Plasma Physics, *Accepted for publication*, eds. Vassiliadis, D., American Insittute of Physics.
103.Pavlos, G.P., Iliopoulos, A.C., Karakatsanis, L.P., Tsoutsouras, V.G. & Pavlos, E.G. [2010c] "Complexity Theory and Physical Unification: From Microscopic to Macroscopic level", *Submitted for Publication.*
104.Pavlos, G.P., Iliopoulos, A.C, Tsoutsouras, V.G., Sarafopoulos, D.V., Sphiris, D.S., Karakatsanis, L.P. & Pavlos, E.G. [2011] "First and Second Order Non-equilibrium Phase Transition and Evidence for Non-extensive Tsallis Statistics in Earth's Magnetosphere", *Submitted for Publication.*
105.Polyakov, D. [2001] "Ads / CFT correspondence, critical strings and stochastic quantization", *Class. Quantum Grav.*, **18**, p. 1979.
106.Polygiannakis J., Preka-Papadema, P., Moussas, X. [2003], "On signalnoise decomposition of timeseries using the continuous wavelet transform: application to sunspot index", *Mon. not. R. Astron. Soc.*, **343**, p. 725-734.
107.Price, C.P. & Prichard, D.J. [1993] "The non-linear response of the magnetosphere: 30 October 1978", *Geophys. Res. Lett.*, **20**, p. 771-774.
108.Price, C.P., Prichard, D.J. & Bischoff, J.E. [1994] "Nonlinear Input/Output Analysis of the Auroral Electrojet Index", *J. Geophys. Res.*, **99**, p. 13227-13238.
109.Prichard, D.J. [1995] "Short comment for magnetospheric chaos", *Nonlinear Proc. Geophysics*, **20**, p. 771-774.
110.Prigogine, I. [1977] "Time, structure and fluctuations", Nobel Lecture.
111.Prigogine, I. [1996] "La Fin des Certitudes", Editions Odile Jacob.
112.Rochlin, V.A. [1964] "Exact endomorphisms of Lebesque spaces", *Am. Math. Soc. Tansl.*, **39**, p. 1.

113.Ruzmaikin, A.A. [1985] "The solar Dynamo", *Solar Physics*, **100**, p. 125-140.
114.Schweiger, A.O., Baros, K. & Klein, W. [2007] "Transient nucleation near the mean-field spinodal", *Phys. Rev. E*, **75**, p. 031102.
115.Shaw, R. [1984] "The dripping faucet as a model chaotic system," The Science Frontier Express Series (Aerial Press, Santa Cruz).
116.Shimony, A. [1989] "Conceptual foundations of quantum mechanics", in Davies, Cambridge University Press.
117.Sitnov, M.I., Sharma, A.S., Papadopoulos, K., & Vassiliadis, D. [2001] "Modeling substorm dynamics of the magnetosphere: From self-organization and self-organized criticality to nonequilibrium phase transitions", *Phys. Rev. E*, **65**, p. 016116.
118.Sornette, Didier [2006] " Probability Distributions in Complex Systems," *Encyclopedia of Complexity and Systems Science*, ed. Meyer, R.A., (Springer), p. 7009-7024.
119.Sykes, L.R. *et al.* [1999] "Rethinking Earthquake Prediction" *Pure Apll. Geophys.* **155**, p. 207-232.
120.Takens, F. [1981] "Detecting strange attractors in turbulence", *Lecture Notes in Mathematics, eds. D.A. Rand and L.S. Young*, **898**, p. 366.
121.Theiler, J., Galdikian, B., Longtin, A., Eubank, S., Farmer, J.D. [1992a] "Using surrogate data to detect nonlinearity in time series", *Nonlinear Modeling and Forecasting, vol. XII of SFI studies in the Sciences of Complexity*, eds. M. Casdagli and S. Eubank, p.163.
122.Tsallis, C. [1988] "Possible Generalization of Boltzmann-Gibbs Statistics", J. Stat. Phys., **52**, p. 479.
123.Tsallis, C. [2009] "Introduction to Nonextensive Statistical Mechanics", Springer.
124.Tsonis A. [1992] "Chaos: From Theory to Applications", Kluwer Academic Publications.
125.Tsonis A. [2008] "Randomnicity: rules and randomness in the realm of the infinite", Imperial College Press.
126.Tsoutsouras, V., Sirakoulis, G.,Pavlos, G., Iliopoulos, A. [2011] "Simulation of healthy and epileptiform brain activity using cellular automata", *submitted*.
127.Tsuda I., [2001] "Toward an interpretation of dynamic neural activity in terms of chaotic dynamical systems", *Behav. Brain. Sci.*, **24**, p. 793-810.
128.Uritsky, V.M. & Pudovnik, M.I. [1998] "Low frequency 1/f-like fluctuations of the AE-index as a possible manifestation of self-organized criticality in the magnetosphere", *Ann. Geophysicae*, **16**, p. 1580.
129.Vassiliadi, D., Sharma, A.S. & PApadopoulos, K. [1991] "Lyapunov exponent of magnetospheric activity from AL time series", *Geophys. Res. Let.*, **18**, p. 1643.
130.Vassiliadis, D., Sharma, A.S., Papadopoulos, K. [1992] "Time series analysis of magnetospheric activity using nonlinear dynamical methods", *Chaotic Dyanmics: Theory and Practise"*, ed. Bountis, T., Plenum, (New York).
131.Vieira, M.S. [1999] "Chaos and synchronized chaos in an earthquake model", *Phys. Rev. Lett.*, **82**, p. 201-204.
132.Vlahos, L. *ESA Publications*, **505**, p. 105.
133.Wang, J-X. [1995] "Sporadic chaos in space-time dynamical processes", *Physical Review E* **52**, p. 1318.
134.West B.J., [1990] "Fractal Physiology and Chaos in Medicine", World Scientific Publishing Co. Pte. Ltd.
135.Wilson, K. [1983] "The renormalization group and critical phenomena", *Rev. Mod. Phys.*, **55**, p.583.

136.Zompakis, N., Bartzas, A., Tsoutsouras, V., Soudris, D. & Pavlos, G. [2010] "Dynamic Frequency Scaling for MPSoCs based on Chaotic Workload Analysis", *ARCS '10 - 23th International Conference on Architecture of Computing Systens 2010 - 23th International Conference on Architecture of Computing Systems*, Hannover, Germany

Chaotic Modeling and Simulation (CMSIM) 1: 147–155, 2012

Informational Technologies for Quasilinear Research of Combined Stochastic and Chaotic Systems

Igor N. Sinitsyn[1] and Vasily V. Belousov[2]

[1] Institute for Informatics Problems, RAS, Moscow, Russia
(E-mail: sinitsin@dol.ru)
[2] Institute for Informatics Problems, RAS, Moscow, Russia
(E-mail: vbelousov@ipiran.ru)

Abstract. This article is dedicated to the problems of modeling and simulation of combined stochastic and chaotic systems. Modern informational technologies for nonlinear stochastic systems are used to solve these problems. Discussed methods are based on the off-line information of stochastic systems. They use equivalent linearization and normal approximating techniques for solving equations for mathematical expectations and covariances. Two results for Duffing equation are given in this paper. This example contains the solution for harmonically and stochastically forced Duffing equation. Second example contains the solution for quasiharmonically forced Duffing equation.
Keywords: Combined stochastic and chaotic systems, Equivalent linearization techniques (ELT), Informational technologies, Analytical modeling, Duffing equation, Ito stochastic differential equation, Gaussian (normal) process, Wiener process, Poisson process, Mathematical expectation, Covariance matrix, Matrix of covariance functions, One-dimensional distribution, Two-dimensional distribution, MATLAB.

1 Introduction

It is known [5], [6] modern modeling (analytical, statistical and combined) and estimation (filtering, extrapolation, interpolation, parameters identification) informational technologies (IT) for nonlinear stochastic systems (StS) are based on off-line and on-line information. For engineering applications there are successfully used quasilinear methods based on equivalent linearization techniques (ELT) for solving equations (Eqs) for mathematical expectations and covariances. Experimental results received in [6],[7] for combined StS and chaotic systems (ChS) research IT show that these ELT may be used also.

The article is devoted to ELT for the combined stochastic and chaotic systems based on the off-line information. Problems of modeling and simulation based on the on-line information will be discussed in next articles.

Received: 20 July 2011 / Accepted: 30 December 2011

ISSN 2241-0503

2 Eqs of combined stochastic and chaotic systems

For off-line analytical modeling of ChS with Gaussian perturbations based on Fokker-Plank- Kolmogorov Eq, Feller-Kolmogorov Eq for Poisson perturbations and Pugachev-Sinitsyn Eq for perturbations being the derivative of stochastic process with independent increments need to solve singular Eqs. The solution of these Eqs is very difficult for nowadays computers as for the on-line and the off-line information.

According to ELT one linearize the right hand of given stochastic differential Eq (in Ito sense) and implement known Pugachev-Dunkan ordinary deterministic Eqs for mathematical expectation, covariance matrix and matrix of covariance functions at corresponding initial conditions. The coefficients of these Eqs due to nonlinearity depend on mathematical expectation and covariance matrix. So these deterministic Eqs are interconnected and need joint solution.

For robust ELT it is quite enough to suppose the normal law for density of input signal for nonlinear element and use known formulae of statistical linearization for typical scalar and vector nonlinear functions [5],[6].

Following [5] let us consider differential combined StS and ChS described by the vector Ito Eq:

$$dY = a(Y,t)dt + b(Y,t)dW_0 + \int\limits_{R_0^q} c(Y,t,u)\, P^0(t,du), \quad Y(t_0) = Y_0. \qquad (1)$$

Here $Y = [Y_1 \dots Y_p]^T$ is the state vector; $a = a(Y,t)$ and $b(Y,t)$ are known $(p\times 1)$ — dimensional and $(p\times m)$ — dimensional functions of Y, t; $W_0 = W_0(t)$ is the m — dimensional Wiener random process of the intensity $\nu_0 = \nu_0(t)$; $c = c(Y,t,u)$ is $(p \times 1)$ — dimensional function of Y, t and of the auxiliary $(q \times 1)$ — dimensional parameter u;

$$\mu = \int\limits_{\triangle} dP(t,A) - \int\limits_{\triangle} \nu_P(t,A)\, dt \qquad (2)$$

is a centred Poisson measure, where the second integral term in (2) is a number of the jumps of a Poisson process $P(t,A)$ at time interval $\triangle$; $\nu_P = \nu_P(t,A)$ is the intensity of $P(t,A)$; A is the Borel set of the space R_0^q with the pricked origin of the coordinates.

The integral in Eq (1) is extended on R_0^q. The initial value Y_0 represents a random variable which does not depend on the increments of $W_0(t)$ and $P(t,A)$, $\triangle = (t_1, t_2]$ which follows t_0, $t_0 \le t_1 \le t_2$ for any set A.

At practice when the integrand $c(Y,t,u)$ admits presentation: $c(Y,t,u) = b(Y,t)c'(u)$ we need to assume the formulae for stochastic process with independent increments:

$$W(t) = W_0(t) + \int\limits_{R_0^q} c'(u)\, P^0(t,du). \qquad (3)$$

In this case we get instead of Eq (1) the following Eq:

$$\dot{Y} = a(Y,t) + b(Y,t)V, \quad Y(t_0) = Y_0. \tag{4}$$

Here $V = \dot{W}$ is the white noise with one-dimensional characteristic function $h_1 = h_1(\rho;t)$ and its logarithmic time derivative

$$\Psi(\rho;t) = \frac{1}{h_1(\rho;t)}\frac{\partial h_1(\rho;t)}{\partial t} = -\frac{1}{2}\rho^T\nu_0(t)\rho + \int\limits_{R_0^q}\left[e^{i\rho^T c'(u)} - 1 - i\rho^T c'(u)\right]\nu_P(t,u)\,du, \tag{5}$$

where $\nu_0(t)$ id the intensity of $W_0(t)$ and $\nu_P(t,u)\,du$ is the intensity of the Poisson stream of the jumps equal to $c'(u)$.

3 Basic Eqs for ELT

Approximating the one-dimensional distribution Y (characteristic function and probability density) by normal (Gaussian) one we shall have

$$\begin{aligned} g_1(\lambda;t) &\approx \exp\{i\lambda^T m_y - \frac{1}{2}\lambda^T K_y\lambda\}, \\ f_1(\lambda;t) &\approx \left[(2\pi)^p|K_y|\right]^{-1/2}\exp\{-\frac{1}{2}(y-m_y)^T K_y^{-1}(y-m_y)\} \end{aligned} \tag{6}$$

In Eqs (6) m_y and K_y are the expectation and covariance matrix of the state vector defined by the ordinary differential Eqs:

$$\dot{m}_y = \varphi_1(m_y, K_y, t), \quad m_y(t_0) = m_0, \tag{7}$$

$$\dot{K}_y = \varphi_2(m_y, K_y, t), \quad K_y(t_0) = K_0. \tag{8}$$

Here

$$\begin{aligned} \varphi_1(m_y,K_y,t) &= E_N a(Y,t), \\ \varphi_2(m_y,K_y,t) &= \varphi_{21}(m_y,K_y,t) + \varphi_{21}^T(m_y,K_y,t) + \varphi_{22}(m_y,K_y,t), \\ \varphi_{21}(m_y,K_y,t) &= E_N\left\{a(Y,t)(Y-m_y)^T\right\}, \\ \varphi_{22}(m_y,K_y,t) &= E_N\overline{\sigma}(Y,t)^T, \end{aligned} \tag{9}$$

$$\begin{aligned} \overline{\sigma}(Y,t) &= \overline{\sigma_0}(Y,t) + \int\limits_{R_0^q} c'(u)b(Y,t)b(Y,t)^T c'^T(u)\,\nu_P(t,du), \\ \overline{\sigma_0}(Y,t) &= E_N b(Y,t)\nu_0(t)b(Y,t)^T \end{aligned} \tag{10}$$

and the subscript N denotes that the expectation E_N is calculated for normal distribution $N(m_y, K_y)$. The number of Eqs for normal approximation method (NAM) is equal to $Q_{NAM} = p(p+3)/2$.

NAM for approximate determination of stationary m_y^* and K_y^* gives Eqs:

$$\varphi_1(m_y^*, K_y^*) = 0, \quad \varphi_2(m_y^*, K_y^*) = 0. \tag{11}$$

For two-dimensional distributions in addition to Eqs (7)–(11) we have

$$\begin{aligned} g_{t_1 t_2}(\lambda_1, \lambda_2) &\approx \exp\{i\overline{\lambda}^T \overline{m}_2 - \frac{1}{2}\overline{\lambda}^T \overline{K}_n \overline{\lambda}\}, \\ f_2(y_1, y_2; t_1, t_2) &\approx \left[2\pi^{2p}|\overline{K}_2|\right]^{-1/2} \exp\{-\frac{1}{2}(\overline{y_2} - \overline{m}_2)^T \overline{K}_n^{-1}(\overline{y_2} - \overline{m}_2)\}, \end{aligned} \tag{12}$$

and p^2 ordinary differential Eqs:

$$\begin{aligned} \frac{\partial K_y(t_1, t_2)}{\partial t_2} &= K_y(t_1, t_2) K_y(t_2)^{-1} \varphi_{21}(m_y(t_2), K_y(t_2), t_2)^{-1}, \\ K_y(t_1, t_2) &= K_y(t_2, t_1)^T, K_y(t_1, t_1) = K_y(t_1) \text{ at } t_1 = t_2, \end{aligned} \tag{13}$$

$$\begin{aligned} \frac{dk_y(\tau)}{d\tau} &= \varphi_{21}(m_y^*, K_y^*) K_y^{*-1} k_y(\tau), \\ k_y(\tau) &= K_y(t_1, t_1 + \tau) = k_y(-\tau)^T, k(0) = K_y^*, \end{aligned} \tag{14}$$

where

$$\lambda = [\lambda_1^T \ \lambda_2^T]^T, \quad \overline{m}_2 = \left[m_y(t_1)^T \ m_y(t_2)^T\right]^T,$$

$$\overline{K}_2 = \begin{bmatrix} K_y(t_1, t_1) & K_y(t_1, t_2) \\ K_y(t_2, t_1) & K_y(t_2, t_2) \end{bmatrix}, \quad \overline{y}_2 = [y_1^T \ y_2^T]^T.$$

For stationary systems in Eqs (11), (14) one use the spectral density instead of covariance matrix and amplitude-frequency characteristic.

ELT Eqs (6), (7), (8), (12), (13) for the combined StS and ChS described by Eq (4) at $b(Y,t) = b_0(t)$

$$\dot{Y} = a(Y,t) + b_0(t)V, \quad Y(t_0) = Y_0 \tag{15}$$

after statistical linearization by known formulae [5]:

$$a(Y,t) = a_0(m_y, K_y) + a_1(m_y, K_y)Y^0, \quad (Y^0 = (Y - m)) \tag{16}$$

may be presented in the form:

$$\dot{m}_y = a_0(m_y, K_y, t) = E_N a(Y,t), \quad m_y(t_0) = m_{y_0}, \tag{17}$$

$$\dot{K}_y = a_1(m_y, K_y, t)K_y + K_y a_1(m_y, K_y, t)^T + b_0(t)\nu(t)b_0(t)^T, \quad K_y(t_0) = K_{y_0}, \quad (18)$$

$$\frac{\partial K_y(t_1, t_2)}{\partial t_2} = K_y(t_1, t_2)a_1(t_1, t_2)^T \text{ at } t_2 > t_1$$
$$K_y(t_1, t_2) = K_y(t_2, t_1)^T \text{ at } t_2 < t_1. \quad (19)$$

Putting $\dot{m}_y = 0$, $\dot{K}_y = 0$, $K_y(t_1, t_1 + \tau) = k_y(\tau)$ we get Eqs for stationary processes. Eqs (17)–(19) are the basic Eqs for ELT analytical modeling of Combined StS and ChS.

It is evident that in combined StS and ChS chaotic properties will prevail when corresponding amplitude-frequency characteristic for Eq (17) parametrically dependent on m_y and K_y is not simple.

When the stochastic input signal contains the harmonic component one use combined harmonic and statistical linearization [6].

For input signal given by canonical expansion (CE) we develop corresponding ELT based on [6] and symbolic calculations [7], [8]. IT based on CE ELT are effective as for analytical, statistical and combined modeling (simulation).

For the on-line information optimal nonlinear estimation in ChS with small stochastic perturbations is based on Kushner-Stratonovich Eq for conditional density or corresponding Eq for conditional characteristic function. These Eqs are very difficult for solution on nowadays computers even for simple models [5], [6].

According to robust ELT based on normal density one may use Kalman, Kalman-Bucy or Pugachev Eqs with coefficients depending on mathematical expectation and covariance matrix.

The discussed ELT was realized by modern software tools developed in MATLAB.

Applications: statistical and chaotical vibromechanics, fluctuations of the Earth Pole and irregular rotation of the Earth.

4 Examples

4.1 Harmonically and stochastically forced Duffing Eq

Let us consider harmonically and stochastically forced Duffing Eq:

$$\ddot{X} + \alpha\dot{X} + \beta X + \gamma X^3 = A_0 + A\cos(\omega t) + V,\ X(t_0) = X_0, \dot{X}(t_0) = \dot{X}_0, \quad (20)$$

where α, β, γ, A_0, A, ω being constant values; $V = \dot{W}$ is the white noise of the intensity $\nu = \nu(t)$; W being the process with independent increments. After putting $X_1 = X$, $X_2 = \dot{X}$ and X^3 statistical linearization performing by the formulae [5]:

$$X_1^3 \approx K_0(m_1, D_1)m_1 + K_1(m_1, D_1)X_1^0,$$
$$K_0(m_1, D_1) = (m_1^2 + 3D_1), \quad K_1(m_1, D_1) = 3(m_1^2 + D_1) \tag{21}$$

we get Eqs for mathematical expectations:

$$\dot{m}_1 = m_2,\ \dot{m}_2 = -\alpha m_2 - \beta m_1 - \gamma(m_1^2 + 3D_1)m_1 + A_0 + A\cos(\omega t),$$
$$m_1(t_0) = m_{1_0}, \quad m_2(t_0) = m_{2_0} \tag{22}$$

and centered variables:

$$\dot{X}_1^0 = X_2^0,\ \dot{X}_2^0 = -\alpha X_2^0 - \beta X_1^0 - 3\gamma(m_1^2 + D_1)X_1^0 + V,$$
$$X_1^0(t_0) = X_{1_0}^0, \quad X_2^0(t_0) = X_{2_0}^0. \tag{23}$$

Ordinary differential Eqs for $K_{11}(t) = D_1 = MX_2^{02}$, $K_{12}(t) = K_{X\dot{X}}$, $K_{22}(t) = D_2 = MX_2^{02}$ may be presented in the form

$$\begin{cases} \dot{K}_{11} = 2K_{12},\ \dot{K}_{22} = -2\alpha K_{22} - 2\big[\beta + 3\gamma(m_1^2 + D_1)\big]K_{12} + \nu, \\ \dot{K}_{12} = K_{22} - \alpha K_{12} - \big[\beta + 3\gamma(m_1^2 + D_1)\big]K_{11} \end{cases} \tag{24}$$

at corresponding initial conditions. Eqs (22) and (24) are interconnected due to dependence of coefficients at m_i, D_i $(i = 1, 2)$ on m_1 and D_1.

Eqs (22) and (24) permit to detect the following effects.

1. At $A_0 = 0$ and given D_1 the chaos structure described by Eqs (22) coincides with the structure of chaos in Eqs (22) at $V = 0$ for $\beta_\xi = \beta + 3\gamma D_1$ [4].
2. At $A_0 = 0$ and given $\nu = const$ the chaos structure described by Eqs (22) coincides with the structure of chaos in Eqs (22) at $V = 0$ for m_1 and D_1 described by joint set of Eqs (22) and (24) for $\beta = \beta + \triangle\beta(\nu)$, $\triangle\beta(\nu) = 3\gamma D_1(t, \nu)$.
3. At given periodical intensity $\nu = \nu(\Omega t)$ we find the bias detecting effect due to parametric term $\langle D_1 m_1\rangle$ at $n_1\omega + n_2\Omega = 0$. Such structure of chaos corresponds to bias chaos structure [4] at $A_{\xi 0} = A_0 - 3\gamma\langle m_1 D_1\rangle$.

4.2 Quasiharmonically forced Duffing Eq

Let us consider quasiharmonically forced Duffing Eq:

$$\ddot{X} + \alpha\dot{X} + \beta X + \gamma X^3 = A_0 + A\cos(\psi),$$
$$X(t_0) = X_0, \quad \dot{X}(t_0) = \dot{X}_0, \tag{25}$$

$$\dot{\psi} = \omega + Y, \tag{26}$$

$$\dot{Y} = -\alpha_1 Y + V, \quad Y(t_0) = Y_0 \tag{27}$$

where α, β,γ, A_0, A, ω, being constants; $\nu = \nu(t)$ being the intensity of the white noise V. Putting

$$\begin{gathered} X_1 = X,\, X_2 = \dot{X}_1,\, X_3 = Y, \\ X_1^3 \approx (m_1^2 + 3D_1)m_1 + 3(m_1^2 + D_1)X_1^0, \\ \cos(\psi) \approx e^{-D_3/2}\cos(\omega t + m_3) + \left[-e^{-D_3/2}\sin(\omega t + m_3)\right]X_3^0, \end{gathered} \tag{28}$$

we get the joint set of Eqs for m_i, $K_{ii} = D_i$ and $K_{ij}\,(i, j = 1, 2, 3)$:

$$\begin{cases} \dot{m}_1 = m_2,\, \dot{m}_2 = -\alpha m_2 - \beta m_1 - \gamma(m_1^2 + 3D_1)m_1 + \\ \qquad A_0 + Ae^{-D_3/2}\cos(\omega t + m_3), \\ \dot{m}_3 = -\alpha_1 m_3, \end{cases} \tag{29}$$

$$\begin{cases} \dot{X}_1^0 = X_2^0 \\ \dot{X}_2^0 = -\alpha X_2^0 - \beta X_1^0 - 3\gamma(m_1^2 + D_1)X_1^0 - Ae^{-D_3/2}\sin(\omega t + m_3)X_3^0, \\ \dot{X}_3^0 = -\alpha_1 X_3^0 + V; \end{cases} \tag{30}$$

$$\begin{aligned} &\dot{K}_{11} = 2K_{12},\, \dot{K}_{33} = \nu - 2\alpha_1 K_{33}, \\ &\dot{K}_{22} = -2\left[\beta + 3\gamma(m_1^2 + D_1)\right]K_{12} + 2\alpha K_{22} - 2Ae^{-D_3/2}\sin(\omega t + m_3)K_{23}, \\ &\dot{K}_{12} = K_{22} - \left[\beta + 3\gamma(m_1^2 + D_1)\right]K_{11} - \alpha K_{12} + Ae^{-D_3/2}\sin(\omega t + m_3)K_{13}, \\ &\dot{K}_{13} = K_{23} - \alpha_1 K_{13}, \\ &\dot{K}_{23} = -\left[\beta + 3\gamma(m_1^2 + D_1)\right]K_{13} + Ae^{-D_3/2}\sin(\omega t + m_3)K_{33} - (\alpha + \alpha_1)K_{23}. \end{aligned}$$

5 Conclusions

1. At given $m_3^* = 0$, $D_1 = D_1^*$, $D_3 = D_3^*$, Eqs (25) have chaos structure for Eq (25) at $Y \equiv 0$ [4] if we put $\beta_\xi = \beta + 3\gamma D_1^*$, $A_\xi = Ae^{-D_3^*/2}$.
2. At given $\nu = const$ the chaos structure for Eq (25) is described by known formulae [4] at $\beta_\xi = \beta + \triangle\beta(\nu)$, $\triangle\beta(\nu) = 3\gamma D_1(t, \nu)$, $A_\xi = Ae^{-D_3(t,\nu)/2}$. More then that due to the dependence of $D_1(t)$ on $\sin(n\omega t)$ and $\cos(n\omega t)$ $(n = 2, 3, \dots)$ we find the parametric effect of pulsation.
3. At given periodical intensity $\nu(\Omega t)$ we may find bias effect on frequencies $n\Omega$ and $n\omega$ in chaos structure.

The derived results of modeling of the chaos structure coincides with the results from [4], [3], [1], [2].

In Figure 1 presented the secant plane $t = [mod 2\pi/\omega]$ for the case of rigid elastic characteristic: $\alpha = 0.2$, $\beta = 1$, $\gamma = 1$, $A_0 = 0$, $A = 50$, $\omega = 1.9$.

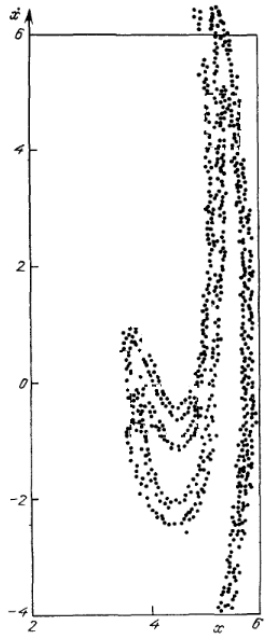

Fig. 1. Chaos structure for rigid elastic characteristic.

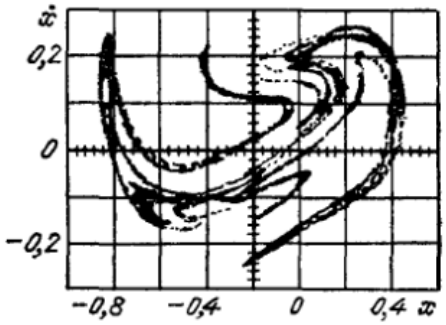

Fig. 2. Chaos structure for asymmetrical external influence.

In Figure 2 presented the secant plane $t = [mod 2\pi/\omega]$ for the case of asymmetrical external influence: $\alpha = 0.05$, $\beta = 0$, $\gamma = 1$, $A_0 = 0.04$, $A = 0.14$, $\omega = 1$.

The work is supported by Russian Foundation for Basic Research (Project 10-07-00021).

References

1.Hayashi C., Abe M., Oshima K., Kawakami H. The Method of Mapping as Applied to the Solution for Certain Types of Nonlinear Differential Equations // Pro-

ceedings of IX International conference on nonlinear fluctuations, Kiev, Ukraine, pp 40-44, 1981.

2.Kawakami H. The Bifurcation Pattern of Periodic Solutions Observed in Duffings Equation // Proceedings of IX International conference on nonlinear fluctuations, Kiev, Ukraine, pp 162-165, 1981.

3.Kryukov, B.I. and G.I. Seredovich. About strange behavior of decisions of the Duffing equation. Reports of AS USSR, vol.258, no.2, pp 311-314, 1981 (In Russian).

4.Neymark Ju.I., Landa P.S. Stochastic and Chaotic Oscillations. 2nd Ed. Moscow, Librocom, 2009 (In Russian).

5.Pugachev, V.S. and I.N. Sinitsyn. Stochastic Systems. Theory and Applications. World Scientific, Singapore, 2001.

6.Sinitsyn I.N. Canonical Expansions of Random Functions and Its Application to Scientific Computer-Aided Support. TORUS PRESS, Moscow, 2009 (In Russian).

7.Sinitsyn I.N., Korepanov E.R., Belousov V.V., Shorgin V.S., Makarenkova I.V., Konashenkova T.D., Agafonov E.S., Semendyaev N.N. Development of computer-aided statistical scientific support for high precision and with high availability systems // Systems and Means of Informatics, Institute for Informatics Problems, Moscow, Russia, vol. 20, no. 1, pp 5-42, 2011 (In Russian).

8.Sinitsyn, I.N., E.R. Korepanov, V.V. Belousov and A.V. Kucenko. Methodological and software support for stochastic systems quality analysis development using symbolic equations // Proceedings of VI International Conference System Identification and Control Problems (SICPRO '07), Moscow, pp 1447-1462, 2007 (In Russian).

9.Sinitsyn, I.N., V.I. Sinitsyn, E.R. Korepanov, V.V. Belousov and E.S. Agafonov. Symbolic mathematical support for stochastic systems analysis and modeling based on canonical expansions of random functions. // Proceedings of VIII International Conference System Identification and Control Problems (SICPRO '09), Moscow, pp 1059-1072, 2009 (In Russian).

Chaotic Modeling and Simulation (CMSIM) 1: 169-175, 2012

Biological Growth in the Fractal Space-time with Temporal Fractal Dimension

Marcin Molski[1]

[1] Theoretical Chemistry Department, Adam Mickiewicz University of Poznań, Poland
(E-mail: mamolski@amu.edu.pl)

Abstract: It has been found/ proposed/ that the growth curves representing neuronal differentiation or malignant tumor progression can be successfully fitted by the temporal fractal function y(t), which describes the time-evolution of the system, characterized by the temporal fractal dimension b_t and scaling factor a_t. It can be proved that for biological systems whose growth is described by the Gompertz function, the temporal fractal dimension and scaling factor are time-dependent functions $b_t(t)$ and $a_t(t)$, which permits calculation of their values at an arbitrary moment of time or their mean values at an arbitrary time-interval. The model proposed has been applied to determine the temporal fractal dimension of the tumor growth and synapse formation as qualitatively these processes are described by the same Gompertz function. The results obtained permit formulation of two interesting rules: (i) a system of interacting cells within a growing biological system has its own, local intrasystemic fractal time, which differs from the linear (b_t=1) scalar time of the extrasystemic observer; (ii) the fractal structure of time, characterizing biological growth, is lost during progression. The possibility of mapping the Gompertz growth function onto the temporal fractal one, confirms the thesis that biological growth is a self-similar, alometric and coherent process of a holistic nature

Keywords: Fractal space-time, Temporal fractals, Mapping procedure, Biological growth, Tumorigenesis, Synapse formation.

1 Introduction

The morphometric computer-aided image analysis reveals that the growth of biological systems occurs in the space-time with the spatial fractal dimension (also called Haussdorff dimension) defined by

$$b_s = \lim_{\varepsilon \to 0} \frac{\ln n(\varepsilon)}{\ln(1/\varepsilon)}$$

Here, n(ε) is the minimum number of hypercubes of dimension ε required to completely cover the biological, physical or mathematical object under

Received: 29 June 2011 / Accepted 30 December 2011

ISSN 2241-0503

consideration. The fractal dimension can be defined also by the self-similar power law scaling function

$$y(x) = a_s x^{b_s} \qquad x > 0$$

in which y(x) denotes the number of self-similar objects in the sphere or circle of a radius x; b_s and a_s stand for the spatial fractal dimension and the scaling factor, respectively. In biological systems the fractal structure of space in which cells interact and differentiate is essential for their self-organization and emergence of the hierarchical network of multiple cross-interacting cells, sensitive to external and internal conditions. Hence, the biological phenomena take place in the space whose dimensions are not represented only by integer numbers (1,2,3 etc.) of Euclidean space. In particular, tumors and synapses grow in a space with non-integer fractal dimension. Cellular systems grow not only in space but also in time. Recently, an idea has been developed that the curves describing the growth of biological systems can be successfully fitted by the temporal counterpart of the space fractal function [1,2]

$$y(t) = a_t t^{b_t} \qquad t > 0$$

in which y(t) characterizes the time-evolution of the system, b_t is its temporal fractal dimension whereas a_t - a scaling factor. In this work we present the results of mapping of the Gompertz function [3]

$$G(t) = G_0 e^{\frac{b}{a}\left(1-e^{-at}\right)}$$

widely applied to fit the demographic, biological and medical data, onto the fractal function y(t). As a result one obtains the time-dependent expressions for $b_t(t)$ and $a_t(t)$, which permit calculation of their values at an arbitrary moment of time or their mean values at an arbitrary time-interval. In the Gompertz function G_0 stands for the initial mass, volume, diameter or number of proliferating cells, a is retardation constant whereas b denotes the initial growth or regression rate constant.

2 The Model

To obtain the explicit form of $b_t(t)$ and $a_t(t)$ by the mapping procedure, we employ the generalized spline interpolation method [4], which permits interpolating the Gompertz function by a family of power law curves

$$\left\{ y_i(t) = a_t(t_i) t^{b_t(t_i)} \quad i = 1,2,....N \right\}$$

determined at the points $\{t_i, y_i(t_i)\}$. Defining the sets of parameters $b_t = \{b_t(t_i), i=1,2\ldots\}$, $a_t = \{a_t(t_i), i=1,2\ldots\}$, one may derive the fractal function y(t) assuming that the Gompertz and interpolating functions are isovalued and isosloped for the each momentum t. Then the equality of the functions y(t), G(t) and their first derivatives provides the set of nonlinear equations

$$a_t t^{b_t} = e^{\frac{b}{a}\left(1-e^{-at}\right)} - 1 \qquad b_t a_t t^{b_t - 1} = b e^{-at} e^{\frac{b}{a}\left(1-e^{-at}\right)}$$

whose solutions are the analytical expressions

$$b_t(t) = bte^{-at} \frac{e^{\frac{b}{a}\left(1-e^{-at}\right)}}{e^{\frac{b}{a}\left(1-e^{-at}\right)} - 1} \qquad a_t(t) = t^{-b_t} \left[e^{\frac{b}{a}\left(1-e^{-at}\right)} - 1 \right]$$

defining the fractal function

$$y(t) = a_t(t) t^{b_t(t)}$$

characterizing the Gompertzian growth. The above specified formulae satisfy the proper boundary conditions for $t \to 0$ and $G_0=1$ (one cell). From their plots it can be easily proved that function y(t) is indistinguishable from G(t), hence the mapping procedure is successful.

3 The results

The synapse formation can be characterized by the Gompertz growth curve obtained by the fitting the experimental data obtained by Jones-Villeneuve et al. [5]. The fit provided [2] the parameters: a=0.0739(89) [hour], b=0.3395(378) [hour] for constrained $G_0=1$ evaluated with the nonlinear regression coefficient R=0.9737. In the next step the parameters a and b were used to calculate the time-dependent fractal dimension $b_t(t)$ and scaling factor $a_t(t)$ using the above specified formulae. Their plots are presented in Fig. 1.

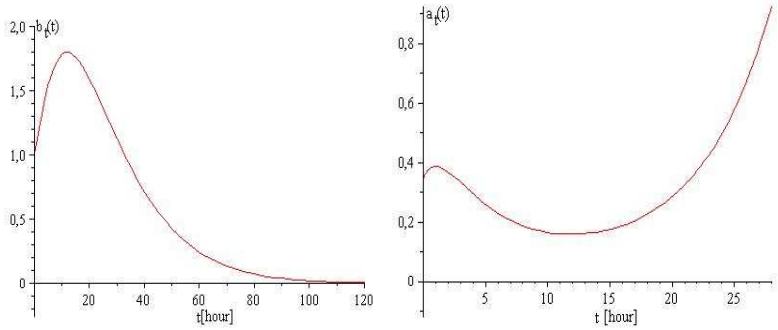

Fig. 1. Plots of the time-dependent temporal fractal dimension $b_t(t)$ and scaling factor $a_t(t)$ for neuronal cells growth characterized by the Gompertz parameters a=0.0739(89) [hour] and b=0.3395(378) [hour] [2].

In the case of tumorigenesis, we consider as an example the Flexner-Jobling rat's tumor whose growth is described by the Gompertz function with the parameters: a=0.0490(63) [day], b=0.394(66) [day] determined by Laird [6]. They were used to generate plots of $b_t(t)$ and $a_t(t)$ presented in Fig. 2.

Analysis of the results obtained reveal that during neuronal differentiation and synapse formation, the temporal fractal dimension $b_t(t)$ increases from 1 for t=0 to a maximal value 1.80 for t=11.97 [day] and then decreases to zero. We find here an interesting correlation with the spatial fractal dimension calculated *in vivo* for retinal neurons; it takes value 1.68(15), whereas the diffusion-limited-aggregation model predicts 1.70(10) [7]. These spatial dimensions are equal in the range specified standard errors to the temporal fractal dimension 1.80 determined in this work. In the case of brain's neurons of two teleost species *Pholidapus dybowskii* and *Oncorhynchus keta*, the application of the box-counting method provided the fractal dimension equal to 1.72 for less specialized neurons, whereas highly specialized neurons displayed a relatively low dimension [8]. We conclude that the temporal fractal dimension can be applied as a numerical measure of the neuronal complexity emerging in the process of differentiation, which is correlated with the morphofunctional cell organization. In particular, the change from the maximal value of the fractal dimension $b_t(t=11.97)=1.80$ to the dimension attained at the plateau $b_t(t=50)=0.43$ reflects the appearance of the highly specialized neurons evolving from the less specialized ones. The temporal fractal dimension of the Flexner-Jobling's tumor growth increases from 1 for t=0 to a maximal value of 2.98 for t=20 [day] and then decreases to zero. Both $b_t(t)$ and $a_t(t)$ determined for neuronal differentiation and tumour progression behave in the identical manner. We conclude that tumorigenesis has a lot in common with the neuronal differentiation and synapse formation, although the dynamics of these processes

are different: the maximal values of the temporal fractal dimension are equal to 1.8 and 2.98, respectively.

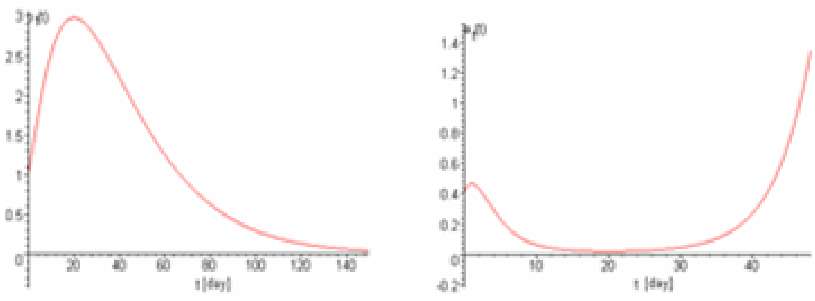

Fig. 2. Plots of the temporal fractal dimension $b_t(t)$ and the scaling factor $a_t(t)$ for Flexner-Jobling rat's tumor whose growth is characterized by the parameters a=0.0490(63) [day], b=0.394(66) [day] [6].

4 Conclusions

The results obtained permit formulation of two interesting rules governing the biological growth in the fractal space-time:

(i) A system of interacting cells within a growing biological system, has its own, local intrasystemic fractal time, which differs from the linear (b_t=1) scalar time of the extrasystemic observer;
(ii) The fractal structure of time characterizing biological growth, is lost during progression.

The point (i) admits that intrasystemic time has more than one dimension. This conclusion is consistent with the results of theoretical investigation proving that the best manifold for description of physical phenomena is a six-dimensional space-time with the same number of temporal and spatial dimensions [9-12]. The point (ii) can be interpreted in the framework of the noise theory [13,14]. The temporal fractal dimension $b_t(t)$ characterizing the tumorigenesis and synapse formation, takes values from the range <1,0>. The formal replacement of time by the reciprocal frequency in $b_t(t)$

$$b_t(t) \xrightarrow{t \to 1/f} b_t(1/f)$$

enables interpretation of different phases of the biological growth in terms of noise characteristics. By analogy to the frequency of signals of the spatial or temporal fractal characteristics, the limit $b_t(t=0)=1$ corresponds to the pink noise

($1/f^1$ noise), $b_t(t=\infty)=0$ – white noise ($1/f^0$ noise), whereas deviation of $b_t(t)$ from unity reveals fractality [13,14] of the biological processes. So, the loss of the fractal structure of time during progression can be interpreter as a transition to the stage of white noise.

Following Bajzer and Vuk-Pavlovic [15,16] one may prove that the Gompertz function satisfies the self-similar relationship

$$G(t+s)=\alpha(s)G(t)^{\beta(s)} \quad \beta(\mathrm{s})=\exp(-as) \qquad \alpha(s)=G_{\infty}^{1-\beta(s)}$$

which links also the scaled fractal function

$$y(t+s)+G_0=\alpha(s)\left[y(t)+G_0\right]^{\beta(s)}$$

The possibility of mapping of the Gompertz growth function onto the temporal fractal one, confirms the thesis that biological growth is a self-similar, alometric and coherent process of a holistic nature [17]. It means that all spatially separated subelements (cells) of the whole system, are interrelated via long-range (slowly decaying) interactions, which seem to be an essential ingredients of the self-organized systems. Such interactions can be mediated e.g. through diffusive substances (growth factors), which interact with specific receptors on the surface of the cells, affecting and controlling proliferation. It has been proved [17] that the Gompertz function represents the coherent state of growth, which is a macroscopic analogue of the quantal minimum-uncertainty coherent state of the Morse oscillator. Such states are space-like (nonlocal) and propagate along the well-defined time trajectory being coherent in space. The mapping procedure transfers this peculiar property of the Gompertz function onto the fractal y(t) one. Hence, the biological growth in the fractal space-time with temporal fractal dimension is predicted to be coherent in space.

References

1. M. Molski, J. Konarski, Tumor growth in the space-time with temporal fractal dimension. *Chaos, Solitons & Fractals* 36: 811-818, 2008.
2. M. Molski, J. Konarski, Neuronal differentiation and synapse formation in the fractal space-time with temporal fractal dimension. *Synapse* 60: 567, 2006.
3. B. Gompertz, On the nature of the function expressive of the law of human mortality, and on a new mode of determining the value of life contingencies. *Phil Trans Roy Soc London* 115: 513-585, 1825.
4. B.D.Bojanov, H.A.Hakopian, A.A. Sahakian. Spline functions and multivariate interpolations. Springer-Verlag Gmbh 1993.

5. E.M. Jones-Villeneuve, M.W. McBurney, K.A. Rogers, V.I. Kalnins. Retinoic acid induces embryonal carcinoma cells to differentiate into neurons and glial cells. *J Cell Biol* 94: 253-262, 1982.

6. A.K. Laird, Dynamics of tumor growth. *Brit J Canc* 18: 490-502 (1964); A.K.Laird. Dynamics of tumor growth: comparison of growth rates and extrapolation of growth curves to one cells. *Brit J Canc* 19:278-291, 1965.

7. F. Caserta F, H.E. Stanley, W.D. Eldred, G. Daccord, R.E. Hausman, J. Nittmann. Physical mechanisms underlying neurite outgrowth: a quantitative analysis of neuronal shape. *Phys Rev Lett* 64:95-98, 1990.

8. V.V Isaeva, E.V. Puschina, Y.A. Karetin. The quasi-fractal structure of fish brain neurons. *Russ J Marine Biol* 30: 127-134, 2004.

9. E.A..B. Cole Particle decay in six-dimensional relativity. *J. Phys. A: Math. Gen.* 113: 109, 1980.

10. E.A.B Cole and S.A. Buchanan. Space-time transformations in six-dimensional special relativity. *J. Phys. A: Math. Gen.* 15: L255, 1982.

11. M. Pavsic. Unifies kinematics of bradyons and tachyons in six-dimensional space-time. *J. Phys. A: Math. Gen.* 14: 3217, 1981.

12. M.T. Teli. General Lorentz transformations in six-dimensional space-time. *Physics Letters A* 122: 447, 1987.

13. P. Bak, C. Tang, K. Wiesenfeld. Self-Organized criticality: an explanation of $1/f$ noise. *Phys Rev Lett*. 59: 381–384, 1987.

14. P. Szendro, G. Vincze, A. Szasz. Pink-noise behavior of biosystems. *Eur Biophys J.* 30: 227-231, 2001.

15. Z. Bajzer. Gompertzian growth as a self-similar and allometric process. *Growth Dev Aging* 63: 3-11, 1999.

16. Z. Bajzer. S. Vuk-Pavlovic. New dimensions in Gompertzian growth. *Journal of Theoretical Medicine* 2: 307-315, 2000.

17. M. Molski, J. Konarski. Coherent states of Gompertzian growth. *Phys Rev E* 68: 021916(1-7), 2003

Chaotic Modeling and Simulation (CMSIM) 1: 177-184, 2012

Chaotic Dynamics of Coupled Nonlinear Circuits in Ring Connection

Maria S. Papadopoulou[1], Ioannis M. Kyprianidis[2], Ioannis N. Stouboulos [3]

[1, 2, 3] Physics Department, Aristotle University of Thessaloniki, Greece
(E-mails: [1] mpapa@physics.auth.gr, [2]imkypr@auth.gr, [3]stouboulos@physics.auth.gr)

Abstract: It is generally difficult to synchronize a ring network that features chaotic behaviour, especially if the system's order is too large. In this paper, we consider a ring network of three identical nonlinear and non-autonomous circuits of fourth order, which are bidirectionally coupled through three coupling linear resistances R_C. We present simulation and experimental results for synchronization of such a network in low frequency area, and derive a sufficient condition for chaotic synchronization of this type of network.
Keywords: Ring connection, Nonlinear circuit, Low frequency area, Chaotic synchronization.

1 Introduction

Synchronization is an important property of chaotic dynamical systems. In the past decades the synchronization in large scale complex networks has attracted lots of attention in various fields of science and engineering [2, 3, 5, 14, 15, 16]. In general, a complex network is a large set of interconnected nodes, where a node is a fundamental unit-joint with detailed contents, which lines intersect or branch.
The nonlinear electric circuits are veritable tools to study the fundamental mechanisms underlying the onset of chaos. A variety of autonomous [7, 8, 12] and non-autonomous [6, 10] circuits have been reported in the literature in recent times. A plethora of bifurcation and chaos phenomena, such as period doubling routes to chaos, intermittency, quasi periodicity, chaotic synchronization and so on, have been studied extensively.
In this paper, theoretical and experimental results of chaos synchronization of three identical non-autonomous circuits, bidirectionally coupled in ring connection network are presented. The system's evolution from non synchronized oscillations to synchronized ones, when its individual circuit exhibits chaotic behaviour, is studied.

2 The Nonlinear, Non-Autonomous Circuit

Chaotic performance of the fundamental non-autonomous circuit has been investigated in the past [4]. It is based on a third order autonomous piecewise

Received: 29 June 2011 / Accepted 10 January 2012

ISSN 2241-0503

linear circuit, which introduced by Chua and Lin [1], and is capable of realizing every member of Chua's circuit family. A second inductor L_2 has been added in the branch of the voltage source $v_s(t)$, in order to enrich circuit's dynamics. The circuit also consists of two active elements, a nonlinear resistor R_N, which has a v-i characteristic of N-type with G_a=-0.35mS, G_b=5.0mS and B_p=0.8V, and a negative conductance G_n=-0.50mS. In recent papers, circuit's dynamics in low frequency area has been studied extensively [10, 11, 13]. The circuit's parameters are considered unchangeable during our study. More particularly: L_1=L_2=100mH, C_1=33nF, C_2=75nF and R_1=1KΩ. We use sinusoidal input signal $v_s(t)$ with amplitude V_o equal to 0.60V or 0.75V, while the frequency f ranges from 30Hz to 50Hz. Using the above parameters circuit exhibits chaotic behaviour. In Figures 1a) and b) theoretical and experimental phase portraits v_{C2} vs. v_{C1} for V_o=0.75V and f=35Hz are presented, respectively. The maximum Lyapunov exponent for the above parameters is positive (LEmax=0.0156), which indicates that the system exhibits chaotic behavior.

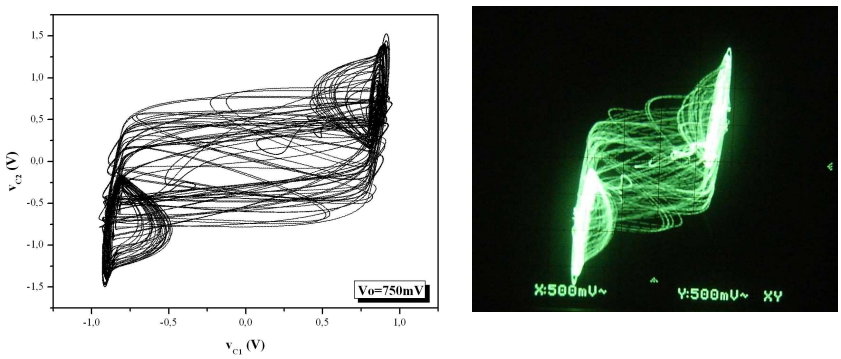

a) theoretical b) experimental

Fig. 1. Phase portrait v_{C2} vs. v_{C1} for V_o=0.75V and f=35Hz.

3 Dynamics of Ring Connection Topology

In a recent paper [9] we have seen that chaotic synchronization of two identical non-autonomous, unidirectionally coupled, nonlinear, fourth order circuits is possible. In this work, chaotic synchronization of three bidirectionally coupled circuits in ring connection, as seen in Figure 2, is studied.

More particularly, as illustrated in Figure 2, circuits NA1C1, NA1C2 and NA1C3 are bidirectionally coupled through three identical linear resistances R_C. The connection points are in capacitances C_{2i}, where i=1, 2 and 3 denotes circuit NA1C1, NA1C2 and NA1C3, respectively.

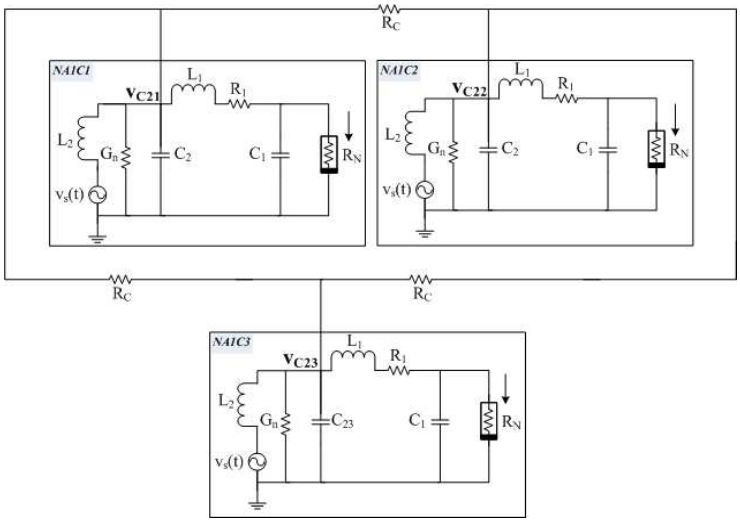

Fig. 2. Three non-autonomous, nonlinear fourth order circuits in ring connection.

The resulting set of system's differential equations is derived using Kirchhoff's circuit laws.

$$\frac{dv_{C11}}{dt} = \frac{1}{C_1}\left(i_{L11} - i_{RN1}\right)$$

$$\frac{dv_{C21}}{dt} = -\frac{1}{C_2}\left(G_n \cdot v_{C21} + i_{L11} + i_{L21} - \frac{v_{C23} - v_{C21}}{R_C} + \frac{v_{C21} - v_{C22}}{R_C}\right)$$

$$\frac{di_{L11}}{dt} = \frac{1}{L_1}\left(v_{C21} - v_{C11} - R_1 \cdot i_{L11}\right)$$

$$\frac{di_{L21}}{dt} = \frac{1}{L_2}\left[v_{C21} - R_2 \cdot i_{L21} - v_s(t)\right]$$

$$\frac{dv_{C12}}{dt} = \frac{1}{C_1}\left(i_{L12} - i_{RN2}\right)$$

$$\frac{dv_{C22}}{dt} = -\frac{1}{C_2}\left(G_n \cdot v_{C22} + i_{L12} + i_{L22} - \frac{v_{C21} - v_{C22}}{R_C} + \frac{v_{C22} - v_{C23}}{R_C}\right)$$

$$\frac{di_{L12}}{dt} = \frac{1}{L_1}\left(v_{C22} - v_{C12} - R_1 \cdot i_{L12}\right)$$

$$\frac{di_{L22}}{dt} = \frac{1}{L_2}\left[v_{C22} - R_2 \cdot i_{L22} - v_s(t)\right]$$

$$\frac{dv_{C13}}{dt} = \frac{1}{C_1}\left(i_{L13} - i_{RN3}\right)$$

$$\frac{dv_{C23}}{dt} = -\frac{1}{C_2}\left(G_n \cdot v_{C23} + i_{L13} + i_{L23} - \frac{v_{C22} - v_{C23}}{R_C} + \frac{v_{C23} - v_{C21}}{R_C}\right)$$

$$\frac{di_{L13}}{dt} = \frac{1}{L_1}\left(v_{C23} - v_{C13} - R_1 \cdot i_{L13}\right)$$

$$\frac{di_{L23}}{dt} = \frac{1}{L_2}\left[v_{C23} - R_2 \cdot i_{L23} - v_s(t)\right]$$

Where the current i_{RNi} through the nonlinear element i, with i=1, 2, 3 for circuit 1, 2 and 3 respectively, and input signal $v_s(t)$ are given by equations:

$$i_{RNi} = G_b v_{C1i} + 0.5\left(G_a - G_b\right)\left(\left|v_{C1i} + B_p\right| - \left|v_{C1i} - B_p\right|\right)$$

$$v_s(t) = V_o \cos(2\pi f t)$$

In figures 3a) and b) bifurcation diagrams $v_{C21}(t)$-$v_{C22}(t)$ vs. e_C and $v_{C22}(t)$-$v_{C23}(t)$ vs. e_C are presented, where e_C is the coupling parameter and is given by equation.

$$e_C = R_1 / R_C$$

where R_C is the coupling resistance.

We can see that chaotic synchronization of the three identical circuits in ring connection is observed for coupling parameter e_C>0.568, or for coupling resistance R_C<1.8kΩ

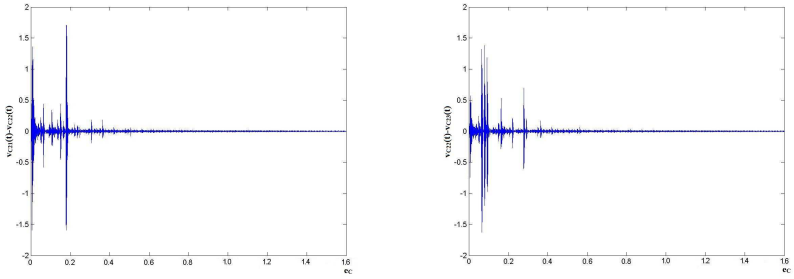

a) $v_{C21}(t)$-$v_{C22}(t)$ vs. e_C b) $v_{C22}(t)$-$v_{C23}(t)$ vs. e_C

Fig. 3. Bifurcation diagrams for V_o=0.75V and f=35Hz.

In figure 4 simulation and experimental results of waveforms $v_{C21}(t)$-$v_{C22}(t)$ for various values of coupling resistance R_C are presented. More particularly, in figures 4a), c) and e) simulation $v_{C21}(t)$-$v_{C22}(t)$ for R_C=1.0MΩ ($e_C \rightarrow 0$), R_C=10.0kΩ (e_C=0.1) and R_C=1.8kΩ (e_C=0.568) are shown, while in figures 4b), d) and f) experimental $v_{C21}(t)$-$v_{C22}(t)$ for the same parameters are illustrated.

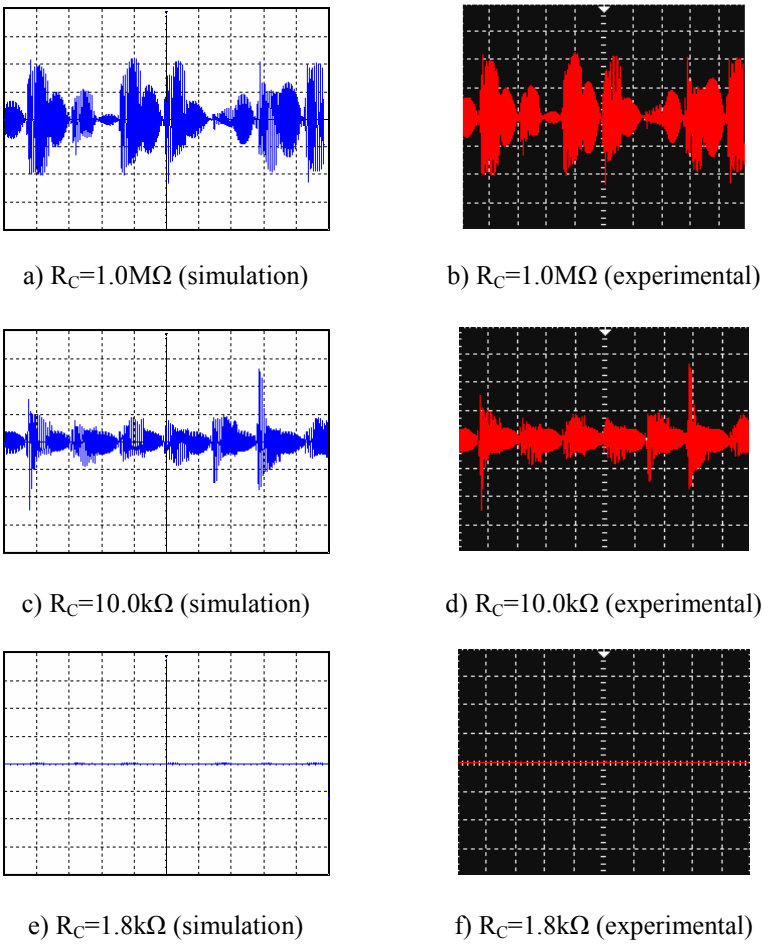

a) R_C=1.0MΩ (simulation) b) R_C=1.0MΩ (experimental)

c) R_C=10.0kΩ (simulation) d) R_C=10.0kΩ (experimental)

e) R_C=1.8kΩ (simulation) f) R_C=1.8kΩ (experimental)

Fig. 4. a), c), e) Simulation and b), d), f) Experimental waveforms $v_{C21}(t)$-$v_{C22}(t)$ (x: 1ms/ div, y: 1V/ div).

In figures 4e) and f) we can see that chaotic synchronization occurs for coupling resistance R_C=1.8kΩ (e_C=0.568). This threshold synchronization value of R_C is

lower than in the case of chaotic synchronization of two bidirectionally coupled identical circuits, with the same circuit's settings, which is R_C=2.28 (e_C=0.479) [9].
In figures 5 and 6 a collection of results are displayed. Specifically, in figure 5 we can see the threshold synchronization value of coupling parameter e_C versus frequency f, for amplitude of the input sinusoidal signal V_o=0.60V and V_o=0.75V. We can see that the values of e_C in the case of V_o=0.60V are lower than in the case of V_o=0.75V. In figure 6 the threshold synchronization value of coupling resistance R_C versus frequency f for the same parameters as in figure 5 is presented.

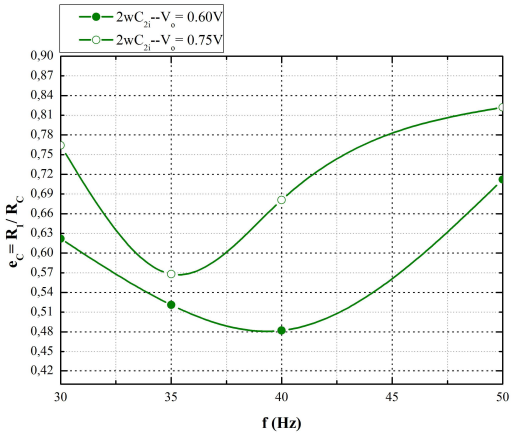

Fig. 5. Threshold synchronization value of coupling parameter e_C vs. f.

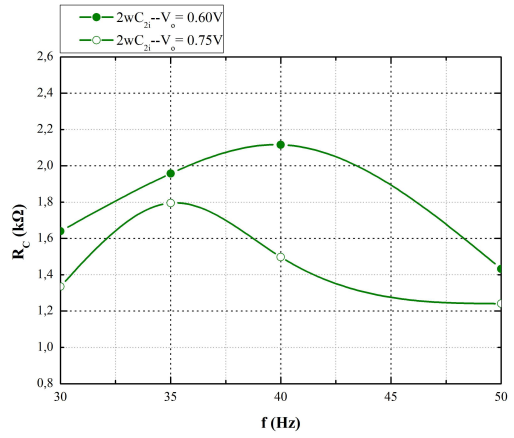

Fig. 6. Threshold synchronization value of coupling resistance R_C vs. f.

4 Conclusions

In this paper, we have studied chaos synchronization of three identical non-autonomous circuits, bidirectionally coupled in ring connection network, in low frequency area. Simulation and experimental results of the system's evolution from non synchronized oscillations to synchronized ones, when its individual circuit exhibits chaotic behaviour, were presented. Both, theoretical calculations and experimental results appear to be in complete agreement. We have seen that the values of threshold synchronization coupling parameter e_C in the case of V_o=0.60V are lower than in the case of V_o=0.75V, for various values of input frequency f, but higher than in the case of two bidirectionally coupled identical circuits with the same setup.

References

1. L.O. Chua and G.N. Lin. Canonical Realization of Chua's Circuit Family, *IEEE Trans. on Circuits and Systems*, vol. 37, no. 7, 885–902, 1990.
2. 2. O. Gaci and S. Balev. A General Model for Amino Acid Interaction Networks, *World Academy of Science Engineering and Technology* 44: 401–405, 2008.
3. H. Jeong, B. Tombor, R. Albert, Z.N. Oltvai and A.-L. Barabási. The Large-Scale Organization of Metabolic Networks, *Nature 407*: 651–654, 2000.
4. I.M. Kyprianidis and I. N. Stouboulos. Chaotic and Hyperchaotic Synchronization of Two Nonautonomous and Nonlinear Electric Circuits, *IEEE 8th Int. Conf. on Electronics, Circuits and Systems* 3: 1351–1354, 2001.
5. I.M. Kyprianidis and I.N. Stouboulos. Chaotic Synchronization of Three Coupled Oscillators with Ring Connection, *Chaos Solitons and Fractals*, vol. 17, no. 2-3, 327–336, 2003.
6. E. Lindberg, L. Member, K. Murali and A. Tamasevicius. The Smallest Transistor-Based Nonautonomous Chaotic Circuit, *IEEE Trans. on Circuits and Systems—II: Express Briefs*, vol. 52, no. 10, 661–664, 2005.
7. E. Lindberg, E. Tamaseviciute, G. Mykolaitis, S. Bumeliene, T. Pyragiene, A. Tamasevicius and R. Kirvaitis. Autonomous Third−Order Duffing−Holmes Type Chaotic Oscillator, *European Conference on Circuit Theory and Design*, 663–666, 2009.
8. H. Nakano and T. Saito. Basic Dynamics from a Pulse-Coupled Network of Autonomous Integrate-and-Fire Chaotic Circuits, *IEEE Trans. on Neural Networks*, vol. 13, no. 1, 92–100, 2002.
9. M.S. Papadopoulou, I.M. Kyprianidis and I.N. Stouboulos. Chaos Synchronization and its Application to Secure Communication, *Journal of Concrete and Applicable Mathematics*, vol. 9, no. 3, 205–212, 2011.
10. M.S. Papadopoulou, I.M. Kyprianidis and I.N. Stouboulos. Complex Chaotic Dynamics of the Double-Bell Attractor, *WSEAS Trans. on Circuits and Systems*, vol. 7, no. 1, 12–21, 2008.
11. M.S. Papadopoulou, I.N. Stouboulos and I.M. Kyprianidis. Study of the Behaviour of a Fourth Order Non-Autonomous Circuit in Low Frequency Area, *Nonlinear Phenomena in Complex Systems*, vol. 11, no. 2, 193–197, 2008.

12. I.N. Stouboulos, I.M. Kyprianidis and M.S. Papadopoulou, Antimonotonicity and Bubbles in a 4th Order Non Driven Circuit, *Proc. of the 5th WSEAS Int. Conf. on Non-Linear Analysis Non-Linear Systems and Chaos*, 81–86, 2006.
13. I.N. Stouboulos, I.M. Kyprianidis and M.S. Papadopoulou. Genesis and Catastrophe of the Chaotic Double-Bell Attractor, *Proc. of the 7th WSEAS Int. Conference on Systems Theory and Scientific Computation*, 139–144, 2007.
14. S.H. Strogatz. Exploring Complex Networks, *Nature* 410: 268–276, 2001.
15. X. Wang and G. Chen. Synchronization in Small-World Dynamical Networks, *Int. J. Bifur. Chaos*, vol. 12, no. 1, 187–192, 2002.
16. W. Yu, J. Cao, G. Chen, J. Lü, J. Han and W. Wei. Local Synchronization of a Complex Network Model, *IEEE Trans. on Systems Man and Cybernetics*, vol. 39, no. 1, 230–241, 2009.

Chaotic Modeling and Simulation (CMSIM) 1: 185–194, 2012

Improvement Performance of TH-UWB System Using Spatiotemporal Chaotic Sequences

Anis Naanaa and Safya Belghith

Sys'com laboratory, Ecole Nationale d'Ingénieurs de Tunis (ENIT), Tunisia
(E-mail: anis_naanaa@yahoo.com, safya.belghith@enit.rnu.tn)

Abstract. The residential environments are an important scenario for Ultra Wide Band (UWB) communication systems. In this paper, the performance of correlating receivers operating in a Line-Of-Sight (LOS) scenario in these environments is evaluated. In such channel the interference between users is an additional source of noise, that may deteriorate the performance of the system. In this research axis; it aims to exploit the richness of chaotic and spatiotemporal sequences with respect to topologic properties. We check through simulations, that chaotic sequences are shown to have improved performance compared to the Gold sequences in terms of Bit Error Rate (BER).
Keywords: Time hopping Utra wide band, Chaotic sequences, Multi-path channel, Spatiotemporal..

1 Introduction

Ultra-wideband (UWB) systems [1] use ultrashort impulses to transmit information which spreads the signal energy over a very wide frequency spectrum of several GHz. The sucess of UWB systems for short-range wireless communications [1,4] is due to the fact that they potentially combine reduced complexity with low power consumption, low probability-of-intercept (LPI) and immunity to multipath fading. In 2004, the IEEE 802.15.4a group presented a comprehensive study of the UWB channel over the frequency range 2-10 GHz for indoor residential, indoor office, industrial, outdoor and open outdoor environments [5]. In this work we are concerned with the indoor residential environment channel.
In time-hopping format (TH-UWB) TH codes are used as multiple user diversity and pulse position modulation (PPM) as data transmission [1,4]. As any wireless communication system, the interference between users is an additional source of noise, that may degrade the performance of the system. Thus the choice of the modulation type, the multiple access techniques, the codes allowing multiple access is important in the determination of the system performance. Different works have tackled the statistical characteristics of the

Received: 28 June 2011 / Accepted: 28 December 2011

ISSN 2241-0503

Multi-User Interference (MUI). Many of them have modeled the MUI as a random Gaussian process [1,4,6]. Due to this assumption, no code optimization has been considered.
Other works have dealt with the optimization of the performance by code selection [2,3]. In [3], the authors considered the asynchronous case, multi channel propagation such IEEE 802.15.3a channel model and rake receiver; they derived a criterion to find optimal codes that minimizes the variance of the MUI of a reference user. The proposed criterion appears as a significant measure to design TH-codes that optimize the performance of a reference user.

In [7] a criterion named Average Collision Number (ACN) that minimize the MUI variance has been defined then the average BER of active users was computed to confirm the relevance of this criterion, it has been shown that sequences having smaller ACN allow better BER. As we show later this criterion is unsuitable in some cases for selecting codes. In this contribution, instead of the ACN criterion we will use the new criterion called Average of Squared Collision Number (ASCN). Based on this criterion we will analyse how much chaoticity of the chaotic codes affects the performance of the considered TH-UWB system. To validate our criterion, the performance in terms of BER is computed by simulating the TH-UWB system with line-of-sight (LOS) multipath and AWGN channel in a residential environment IEEE 802.15.4a.

This paper is organized as follows. Section 2 gives a detailed description of the TH-UWB system; after introducing the TH-UWB-PPM system model, we give the format of the channel model IEEE 802.15.4a and the statistics of correlation receiver. In Section 3 the ASCN criterion is defined and compared to ACN [7]. In section 4 we define the different considered sequences; for chaotic sequences, the ASCN is computed versus bifurcation parameter and compared to Lyapunov exponent. In section 5, we validate our method by reporting simulation results showing the advantage of using ASCN. Finally we conclude in section 6.

2 System description

In this section, we begin by reminding the TH-UWB system model and the expression of the received signal in a synchronous TH-UWB system using the PPM modulation. Then we compute the variance of the MUI versus TH-codes when a correlation receiver is used.

2.1 System model

A typical expression of the TH-UWB transmitted signal for a user j is given by equation 1.

$$s^{(j)}(t) = \sum_{k=-\infty}^{\infty} \sum_{l=0}^{N_f-1} w(t - kT_s - lT_f - \widetilde{c}_l^{(j)} T_c - d_k^{(j)} \delta) \tag{1}$$

Where $w(t)$ is the transmitted UWB pulse shape, T_s is the period of one bit.Every bit is conveyed by N_f frames. Each frame has a duration of T_f and

is divided into N_c time slots. Each time slot has a duration of T_c. $\widetilde{c}_l^{(j)}$ is the TH code sequence assigned to the user j, where $\widetilde{c}_l^{(j)} \in \{0, 1, \ldots, N_c - 1\}$. The location of each pulse in each frame is defined by the code $\widetilde{c}_l^{(j)}$. $d_k^{(j)} \in \{0\,, 1\}$ is the binary transmitted symbol at time k by user j, δ is the time shift associated with binary PPM, the pulses corresponding to bit 1 are sent δ seconds later than the pulses corresponding to bit 0. $N = N_c N_f$ presents the total processing gain of the system.

2.2 IEEE 802.15.4a Channel Model (CM1)

The IEEE 802.15.4a has recently proposed a channel model [5] propagation in residential area [5]. According to this model the impulse response is [5,8],

$$h^{(j)}(t) = \sum_{m=0}^{M-1} \sum_{r=0}^{R-1} \alpha_{r,m}^{(j)} \delta(t - T_m^{(j)} - \tau_{r,m}^{(j)}) \tag{2}$$

where $\alpha_{r,m}$ is the tap weight of the r-th ray (path) in the m-th cluster, T_m is the arrival time of the m-th cluster and $\tau_{r,m}$ is the arrival time of the r-th ray in the m-th cluster. The distribution of the cluster arrival times is given by a Poisson process and the distribution of the ray arrival times is given by a mixed Poisson process [5]. The small scale fading statistics are modeled as Nakagami-m distributed with different m-factors for different multipath components. The probability density function of Nakagami-m distribution is given in [5]. The ray amplitudes are lognormal distributed. The channel model which is used in the paper is for LOS scenarios in residential environments, referred to as CM1 [5]. The parameters of the channel are modeled as a function of the transmitter-receiver distance and the line-of-sight (LOS) availability.

If N_u is the number of active users transmitting asynchronously; the received signal is

$$r(t) = \sum_{j=1}^{N_u} \sum_{m=0}^{M-1} \sum_{r=0}^{R-1} \alpha_{r,m}^{(j)} s^{(j)}(t - T_m^{(j)} - \tau_{r,m}^{(j)}) + n(t) \tag{3}$$

2.3 Statistics of the correlation receiver

The output of the correlation receiver of the i^{th} user at time h is given by:

$$s_h^{(i)} = \sum_{p=0}^{N_f-1} \int_{hT_s + pT_f + \widetilde{c}_p^{(i)} T_c + \tau_{0,0}^{(i)} + T_0^{(i)}}^{hT_s + pT_f + \widetilde{c}_p^{(i)} T_c + T_c + \tau_{0,0}^{(i)} + T_0^{(i)}} r(t) v(t - hT_s - pT_f - \widetilde{c}_p^{(i)} T_c - \tau_{0,0}^{(i)} - T_0^{(i)}) dt \tag{4}$$

where $v(t)$ is the receiver's template signal defined by $v(t) = w(t + \delta) - w(t)$. An accurate value of $\tau_{0,0}^{(i)}$ can be obtained by UWB acquisition techniques such as [13]. From the previous equations and after variable changes, we obtain

$$s_h^{(i)} = T_U(i) + T_{ISI}(i) + T_I(i) + T_N(i) \tag{5}$$

with

T_U is the useful signal, T_{ISI} is inter-symbol interference signal, T_I is the MUI and T_N is the term corresponding to the noise.

In [7], we defined a criterion named ACN for selecting codes in synchronous and single-path TH-UWB system. Also we have shown numerically, that this criterion is adequate even in the multi path channel.
Indeed in the synchronous case, it has been shown that

$$T_I(i) = E_w \sum_{j=1, j\neq i}^{N_u} \alpha^{(j)}(2d_h^{(j)} - 1)cn(i,j) \tag{6}$$

where E_w is the amplitude which controls the transmitted power, $\alpha^{(j)}$ is the tap weight of the user j, $d_h^{(j)}$ is the binary sequence, $cn(i,j)$ is the number of collision between codes $\widetilde{c}^{(i)}$ and $\widetilde{c}^{(j)}$. $\widetilde{c}^{(j)}$ can be computed by taking into account the developed Time-Hopping Codes (DTHC) [9] corresponding to TH codes as follows, for a given code $\widetilde{c}^{(j)}$, the DTHC is a binary code of length $N_c N_f$ and is defined by

$$c_r^{(j)} = \begin{cases} 1 \; if \; r = \widetilde{c}_l^{(j)} + lN_c, r = 0 \ldots, N_c N_f - 1. \\ 0 \; otherwise. \end{cases} \tag{7}$$

$$cn(i,j) = \sum_{l=0}^{N_f N_c - 1} c_l^{(i)} c_l^{(j)} \tag{8}$$

The Average Collision Number ACN of the sequence set $(\widetilde{c}^{(j)})$, $j = 1, \ldots N_u$ is therefore defined by [7]:

$$ACN = \frac{1}{N_u(N_u - 1)} \sum_{i=1}^{N_u} \sum_{j=1, j\neq i}^{N_u} cn(i,j) \tag{9}$$

3 ASCN criterion

In [7] we have defined the ACN criterion, and we have showed that the experimental results validate the relevance of the ACN as an 'off-line' performance evaluation criterion for codes sequences. These results motivated us to use the ACN as a tool to predict the performance of code sequences.
However, we found intuitively that this criterion may in some cases be unsuitable for code selection. For example we take three users ($N_u = 3$). For scenario A, the THC are respectively $\widetilde{c}_l^{(1)} = [\,0\,0\,1\,1\,]$, $\widetilde{c}_l^{(2)} = [\,1\,1\,1\,1\,]$ and $\widetilde{c}_l^{(3)} = [\,0\,0\,2\,2\,]$. We find that the total number of collisions is equal to 4. For scenario B, the THC are respectively $\widetilde{c}_l^{(1)} = [\,0\,0\,1\,1\,]$, $\widetilde{c}_l^{(2)} = [\,0\,0\,1\,1\,]$ and $\widetilde{c}_l^{(3)} = [\,2\,2\,2\,2\,]$. Also the total number of collisions is equal to 4. In both scenarios, $ACN = \frac{4}{6}$.
To remedy to this drawback, we defined a new criterion called Average of

Squared Collision Number ASCN which is defined as:

$$ASCN = \frac{1}{N_u(N_u-1)} \sum_{i=1}^{N_u} \sum_{j=1, j\neq i}^{N_u} cn^2(i,j) \tag{10}$$

This is motivated by the observation that when the collisions are regrouped on few positions the performance are significantly degraded.
Now if we consider this new criterion; for scenario A, $ASCN = \frac{8}{6}$. For scenario B, $ASCN = \frac{16}{6}$. In this work, we propose to use the ASCN criterion to examine the performance of the TH-UWB system.
This is confirmed by Table 1 where we represented the BER for the two scenarios with $N_u = 3$ and $N_c = 4$. We can see that the BER of scenario A is almost the half of the BER of scenario B.

Table 1. ACN vs ASCN with BER simulation.

	ACN	ASCN	BER
Scenario A	4/6	8/6	0.0728
Scenario B	4/6	16/6	0.1662

4 ASCN optimization using chaotic sequences

Chaotic sequences have some properties that motivate researchers to use them in various applications: determinism, long term unpredictability and high sensitivity to initial conditions. Especially chaotic sequences generated by one dimensional non linear transformation have been used in cryptography, watermarking, spectrum spreading systems [10].

We begin by defining Gold and chaotic sequences that will be considered in this work; then we define the ASCN for chaotic sequences versus their bifurcation parameter, and analyse how chaoticity measured by Lyapunov exponent is correlated with the ASCN.

Gold sequences

The Gold sequence based TH codes are generated as shown in [11], where we illustrate how is generated a sequence taking values in $\{0, 1, \cdots, N_c - 1 = 7\}$ and with a length $N_f \leq 29$.

Sequences generated by Skew tent map

Chaotic sequences are generated by the Skew tent map defined by:

$$x_{n+1} = \begin{cases} \frac{x_n}{r}, & 0 \leq x_n \leq r \\ \frac{1-x_n}{1-r}, & r < x_n \leq 1 \end{cases} \tag{11}$$

The skew tent map exhibits chaotic behavior for every value of the bifurcation parameter $r \in [0\ 1]$.

Sequences generated by Logistic map

The logistic map is given by the following equation:

$$x_{n+1} = rx_n(1 - x_n) \tag{12}$$

The logistic map exhibit alternatively regular and chaotic behavior when r belongs to [3 4].

Figures 1 and 2 show the Lyapunov exponent and ASCN versus the bifurcation parameter r for different chaotic sequences. We can see that the curves of the ASCN follow the one of Lyapunov exponent and that the greater the exponent is the smaller the ASCN. For logistic map $r = 4$ gives the best value of Lyapunov exponent and ASCN. For skew tent map $r = 0.5$, have the best ASCN and Lyapuonv exponent. According to these two examples, we showed

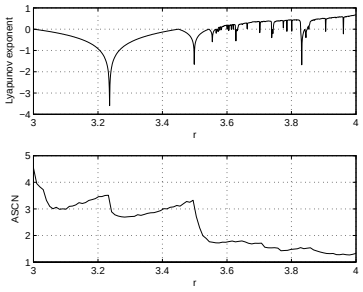

Fig. 1. Lyapunov exponent and ASCN for logistic.

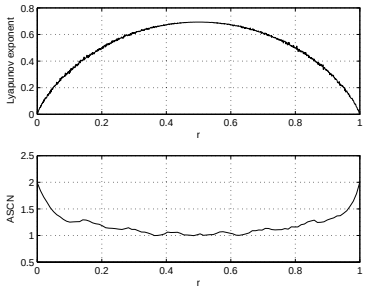

Fig. 2. Lyapunov exponent and ASCN for skew tent map.

numerically that the ASCN of a quantized chaotic sequence depends on the chaoticity of these sequences measured by their Lyapunov exponent.

In Figure 3, we represent the ASCN versus user number for $N_c = 8$; for Gold sequences considered here as a reference and the two quantized chaotic sequences defined above; the ASCN of chaotic sequences are averaged over 100 realizations. For both logistic and skew tent maps we considered the bifurcation parameter that gives the best ASCN, i.e. $r = 4$ for logistic map and $r = 0.5$ for skew tent.
The results show that skew tent map chaotic sequences, have a better ASCN than Gold sequences. We can notice likewise that Gold sequences show better performance compared to the chaotic sequence when $N_u < 6$, this is because of the orthogonality of this sequences.

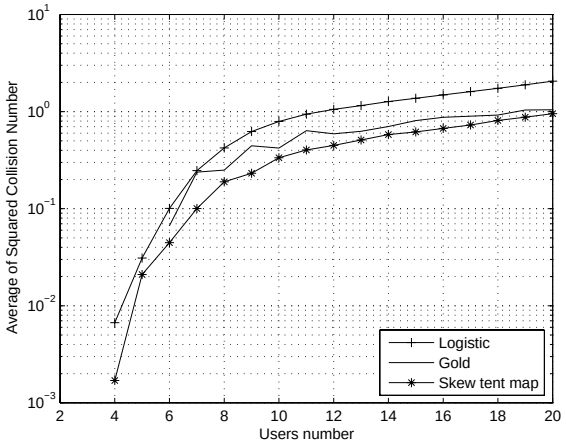

Fig. 3. ASCN versus user number for different types of codes. $N_c = 8$.

Sequences generated by spatiotemporal chaotic systems

Spatiotemporal chaotic systems have been the subject of intensive research in physics in the 80's to model and study some physical phenomena exhibiting chaotic behavior in time and space at once, such as turbulence, convection in chemical reactions and engineering. They have generally been modeled by networks of coupled lattice or CML (Coupled Map Lattices). Different models of CML have been proposed in the literature [12]. In our work we are interested only to the family of CML given by:

$$x_{i+1}(k+1) = (1-\epsilon) f\left[x_{i+1}(k)\right] + \epsilon f\left[x_i(k)\right] \tag{13}$$

Where:

- i is the space index, $i = 1, \cdots, M$, M the system dimension
- k is the time index, $k = 1, \cdots, N$
- f is a one dimensional chaotic map defined in the interval [0 1].
- ϵ is the coupling coefficient.

Spatiotemporal systems exhibit greater complexity compared to classical chaotic systems. They also provide more chaotic sequences, this increases the chaoticity of the system is a property of great importance in the use of CML to generate code sequences.

5 Performance comparaison of classical and chaotic codes sequences

In this section, we present the performance of MA-TH-UWB system in a residential environment CM1 channel by simulating the system and computing the

BER; we consider the correlation receiver and the Gaussian pulse defined by:

$$w(t) = (1 - 4\pi(\frac{t}{\tau})^2)\exp(-2\pi(\frac{t}{\tau})^2) \tag{14}$$

The simulation parameters are listed in table 2. For simplicity, we assume that

Table 2. Simulations parameters of TH-UWB system

Simulation parameters	Acronym	Value
Pulse duration	τ	0.2ns
Sampling frequency	F_s	8GHz
Chip duration	T_c	1ns
Number of sampling	N_e	50
Number of chip	N_c	8
Number of frame	N_f	4
Number of bits for each user	Nb	10^5
Factor for spread spectrum Gold	N	31
Number of path	L	10
Signal to Noise Ratio	SNR	10dB

the number of paths L is the same for all users.
For chaos based TH-codes we used logistic and skew tent maps with parameters $r = 4$ and $r = 0.5$ respectively. These values correspond to the minimal of ASCN (the maximal of Lyapunov exponent) in the two cases. The simulation results are shown in Fig. 4 where we presented the BER of the system versus user number for Gold and the two chaos based sequences. We can see that skew tent map based sequences allow the best performance however logistic map based ones allow the worst performance. These results compared to the results shown in Fig. 3 prove that the ASCN is a suitable criterion to select TH-codes.

The ASCN of the used skew tent map is equal to 1 however it is equal to

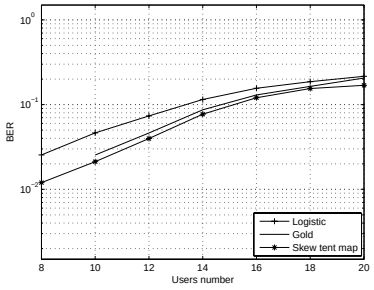

Fig. 4. BER performance of asynchronous TH-UWB system for different TH codes.

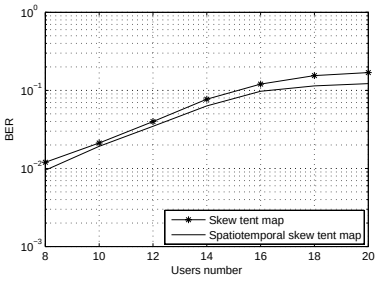

Fig. 5. BER performance of asynchronous TH-UWB system: Skew tent map vs. spatiotemporal.

almost 1.3 for the used logistic map. This explains the superiority of skew tent map based sequences with respect to the logistic map based ones. In Fig.

5 we represent the BER versus user number for the skew tent map and the spatiotemporal system (13) based on skew tent map, for a coupling coefficient $\epsilon = 0.97$, the spatiotemporal are averaged over 100 realizations and the bifurcation parameter is set to the value that gives the best ASCN, i.e. $r = 0.5$. We can see clearly that the THC generated by the CML can get better performance than THC generated by the skew tent map. Thus, the proposed spatiotemporal chaotic system considered is not only advantageous in terms of synchronization, but can also generate THC outperform the conventional chaotic system.

6 Conclusion

In this contribution we considered code selection problem for MA-TH-UWB systems. We defined the ASCN criterion to choose codes and we showed that the lower the ASCN the better the performance. Based on this result, we chose to look for codes with low ASCN by using the features of chaotic transformation; we found that the ASCN of chaotic map based sequences depends on the chaoticity of the map measured by Lyapunov exponent; we showed specifically that the higher the Lyapunov exponent the lower the ASCN; and subsequently the better the performance.
On the other hand, the use of THC generated by spatiotemporal chaotic system has shown better performance in term of BER that other sequences used in this article. This improves the quality and the security of the transmission, and shows the significance of using chaos specifically spatiotemporal chaotic system in communication.

References

1.R. A. Scholtz, "Multiple Access with Time-Hopping Impulse Modulation," in *Proc. MILCOM 1993*, Bedford, MA, October 1993, pp. 447–450.
2.I. Guvenc, and H. Arslan, "Design and performance analysis of TH-sequences for UWB-IR systems," in *Proc. IEEE Wireless Comm. and Networking Conf*, Atlanta, Georgia, USA, Mar. 2004, pp. 914–919.
3.C. J. Le Martret, A. L. Deleuze and P. Ciblat, Optimal TH Codes for Multi-User Interference Mitigation in UWB Impulse Radio, *IEEE Trans On Comm*, vol. 5, No. 6, Jun. 2006.
4.M. Z. Win and R. A. Scholtz, Ultra-Wide Bandwidth Time Hopping Spread-Spectrum Impulse Radio for Wireless Multiple Access Comm, *IEEE Trans. On Comm.*, vol. 48, pp. 679–691, Apr. 2000.
5.A. F. Molisch, and al. *IEEE 802.15.4a channel modelfinal report,*, November 2004.
6.F. Ramirez Mireles, "Error probability of ultra wideband ssma in a dense multipath environment," in *Proc. Milcom Conf*, Anaheim, CA, USA, Oct. 2002, vol. 2, pp. 1081–1084.
7.A. Naanaa, Z. B. Jemaa and S. Belghith, "Average Collision Number Criterion for TH-UWB Code Selection," in *Fifth ICWMC 2009*, Cannes, France, August 2009, pp. 122–127.
8.A. Saleh and R. Valenzuela, *A statistical model for indoor multipath propagation,*. IEEE Journal on Select. Areas Commun., vol. SAC-5, no. 2, pp. 128-137, Feb. 1987.

9.C. J. Le Martret and G. B. Giannakis, "All-Digital impulse radio for wireless cellular systems," *IEEE Trans On Comm*, vol. 50, No. 9, pp. 1440–1450, Sep. 2002.
10.G.M. Maggio, N. RulLov and L. Rggiani, Pseudo chaotic time hopping for UWB impulse radio, *IEEE Trans. Circuits and Systems-I*, vol. 48, No. 12, pp. 1424–1435, Dec. 2001.
11.D. J. E. Clabaugh, *Characterization of Ultra Wide Band Multiple Access Performance Using Time Hopped-Biorthogonal Pulse Position Modulation*. Ph.D. March 2004.
12.P. Almers, J. Karedal, S. Wyne, and al. *Uwb channel measurements in an industrial environment*. In IEEE Global Telecommunications Conference, volume 6, Nov. 2004.
13.W. Suwansantisuk, M. Z. Win, "Multipath Aided Rapid Acquisition: Optimal Search Strategies," *IEEE Trans On Information Theory*, vol. 53, No. 1, Jan. 2007.

Chaotic Modeling and Simulation (CMSIM) 1: 195–204, 2012

Chaotic Oscillations of Nonideal Plane Pendulum Systems

Aleksandr Yu. Shvets[1] and Alexander M. Makaseyev[2]

[1] National Technical University of Ukraine "Kyiv Polytechnic Institute", Kyiv, Ukraine (E-mail: alex.shvets@bigmir.net)
[2] National Technical University of Ukraine "Kyiv Polytechnic Institute", Kyiv, Ukraine (E-mail: makaseyev@ukr.net)

Abstract. The atlas of maps of dynamic regimes of system "pendulum–electric motor" is constructed. It is established that the deterministic chaos is a typical steady-state regime of the given system. Its class of Feigenbaum universality is defined. The analytical approximation of a Poincare map in a chaotic regime is discovered.
Keywords: nonideal systems, chaotic attractors, Feigenbaum constant, Poincare maps.

1 Introduction

In the majority of investigations of the dynamics of pendulum systems are being conducted without taking into account the limitations of excitation source power, so it is assumed that the power of excitation source considerably exceeds the power that the vibrating system consumes. Such systems are called ideal in sense of Sommerfeld–Kononenko [2]. In many cases such idealization leads to qualitative and quantitative errors in describing dynamical regimes of pendulum systems [4]–[6].

Therefore, in most practical problems an object "the oscillating system – the source of oscillation" should be principally treated as a nonideal in sense of Sommerfeld–Kononenko dynamical system [2]. In such systems, the oscillation source power is always assumed comparable to the power consumed by the oscillating system. This requires taking into account interactions between oscillating loading and the energy source of oscillations.

2 Mathematical model of the system

As it has been established in [4]–[6], the motion equations of the "pendulum–electric motor" can be described by the following deterministic dynamical system:

Received: 20 July 2011 / Accepted: 5 January 2012

ISSN 2241-0503

$$\begin{aligned}\frac{dy_1}{d\tau} &= Cy_1 - y_2y_3 - \frac{1}{8}(y_1^2y_2 + y_2^3);\\ \frac{dy_2}{d\tau} &= Cy_2 + y_1y_3 + \frac{1}{8}(y_1^3 + y_1y_2^2);\\ \frac{dy_3}{d\tau} &= Dy_2 + Ey_3 + F;\end{aligned} \tag{1}$$

where phase variables y_1y_2 describe the pendulum deviation from the vertical and phase variable y_3 is proportional to the rotation speed of the motor shaft. The system parameters are defined by

$$C = -\frac{\delta}{\omega_0}\left(\frac{a}{l}\right)^{-2/3}, D = -\frac{2ml^2}{I}, F = 2\left(\frac{a}{l}\right)^{-2/3}\left(\frac{N_0}{\omega_0} + E\right) \tag{2}$$

where m - the pendulum mass, l - the reduced pendulum length, ω_0 - eigenfrequency of the pendulum, a - the length of the electric motor crank, δ - damping coefficient of the medium resistance force, I - the electric motor moment of inertia, E, N_0 - constants of the electric motor static characteristics.

Since the system of equations (1) is nonlinear, the identification and study of its attractors can only be done through a series of numerical methods and algorithms. The methodology of such studies is suggested and described in [6], [7].

3 Maps of dynamic regimes

A very clear picture of the dynamical system behavior can give us a map of dynamic regimes. It is a diagram on the plane, where two parameters are plotted on axes and the boundaries of different dynamical regimes areas are shown. Since the number of parameters in the system (1) is more than two, the detailed map of dynamic regimes will consist of many sheets.

In fig. 1 several sheets of dynamical regimes maps are shown. Two of four parameters (C, D, E, F) of the system (1) were constants and two others varied within certain limits. The map in fig. 1a was built when $C = -0.1, E = -0.59$. The map in fig. 1b was built when $F = -0.17, E = -0.59$. The last two maps in fig. 1c-d were built when $D = -0.6, F = 0.19$ and $C = -0.1, F = 0.19$ respectively. The dark-grey areas of the maps correspond equilibrium positions of the system (1), the light-grey – to limit cycles and the black – to chaotic attractors.

As we can see, in each map there are extensive areas where the system has chaotic regimes. This means that the deterministic chaos is a typical steady-state regime of the given system.

It should be emphasized that consideration the problem in ideal formulation, i.e. neglecting the pendulum influence on electric motor functioning, can lead to gross errors in describing of the dynamics of system. Indeed, in the ideal formulation of the problem in the system of equations (1) should be put D = 0, then the system of equations disintegrates into two subsystems. The first one

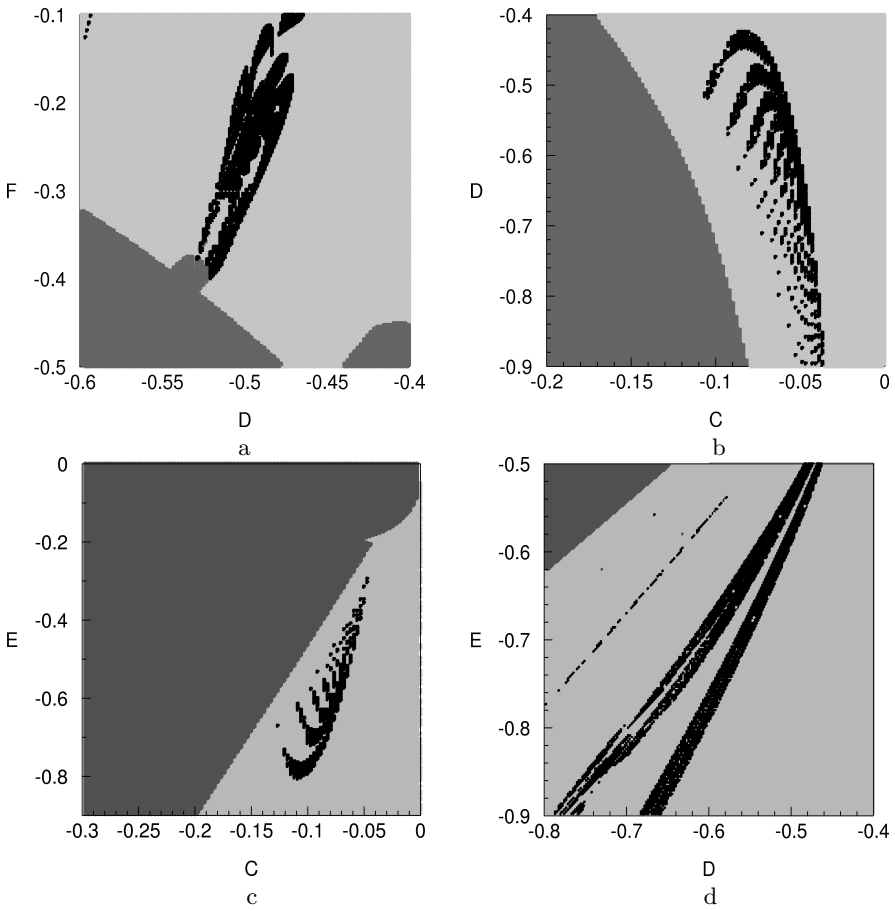

Fig. 1. Maps of dynamic regimes

will consist of the first two equations of (1), and the second one will consist of the one third equation of the system (1). Therefore, in the ideal formulation of the problem, the maximum phase space dimension of the obtained equations will be equal to two. In the spaces of this dimension the existence of chaotic attractors is theoretically impossible [6], [1].

The obtained maps of dynamical regimes allow us to conduct a quick qualitative identification of the type of steady-state regime of the system (1). On the basis of the constructed maps, more detailed studies of emerging dynamic regimes can be carried out. Particularly, the transition from regular to chaotic regimes.

For this purpose, we carry out a vertical (horizontal) section of maps and build other characteristics of the system. For instance, let us carry out a vertical section of the map, that is shown in fig. 1b, along the line $C = -0.07$. In fig 2a a fragment of phase-parametric characteristic ("bifurcation tree") of the system is shown and in fig 2b the dependence of maximal non-zero Lyapunov's characteristic exponent of the system from the parameter F is

depicted. These characteristics correspond to the parameter D change in range of -0.55 to -0.4. The intervals of the parameter D, in which there are separate branches of the bifurcation tree "crown", correspond to the periodic regimes of the system steady oscillations. And the intervals in which the "crown" is represented by saturated black color, correspond to chaotic regimes. As it has been established in [4]–[6], this kind of "bifurcation tree" corresponds to transitions "cycle – chaos" according to the Feigenbaum's scenario from the right side of the bifurcation parameter changes and to intermittency in the sense of Pomeau-Manneville from the left side of the bifurcation parameter changes.

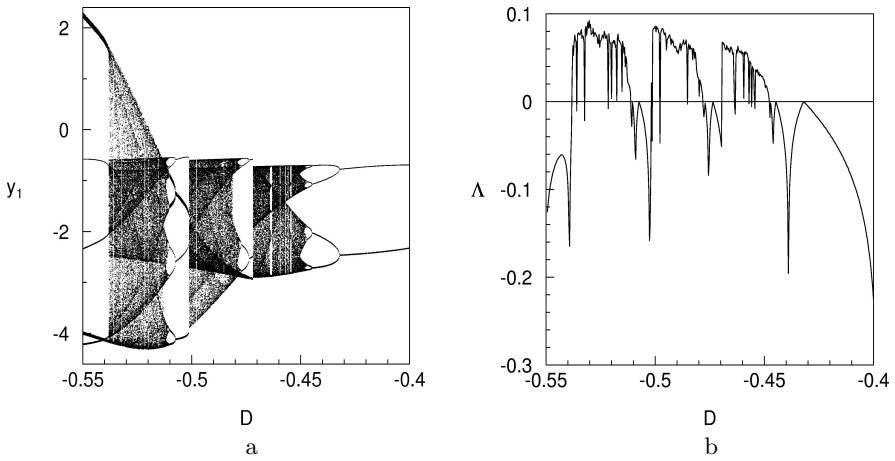

Fig. 2. Phase-parametric characteristic of the system (a), the dependence of maximal non-zero Lyapunov's characteristic exponent (b)

4 The universality class determination

Let us consider the behavior of the system when parameters are $C = -0.1$, $D = -0.5$, $E = -0.59$, and $0.16 \leq F \leq 0.27$. In fig. 3a the dependence of maximal non-zero Lyapunov's characteristic exponent of the system (1) from the parameter F is depicted. As we can see, there are several intervals of variation F where the system has positive Lyapunov's characteristic exponent. The attractor of the system in these intervals is a chaotic attractor. In the region of existence of chaotic attractors, in the left side of the fig. 3a, we can notice several dips of the Lyapunov's exponent graph to negative values. Small intervals of the parameter F in which there are such dips form the so-called windows of periodicity in chaos. In these windows attractors of the the systems are limit cycles. Also in the right side of the fig. 3a we can clearly see the approaches of maximal Lyapunov's exponent to the zero line, which correspond to the points of bifurcation of period-doubling.

In fig. 3b the phase-parametric characteristic of the system is shown. A close examination of this figure shows as the bifurcation points of regular

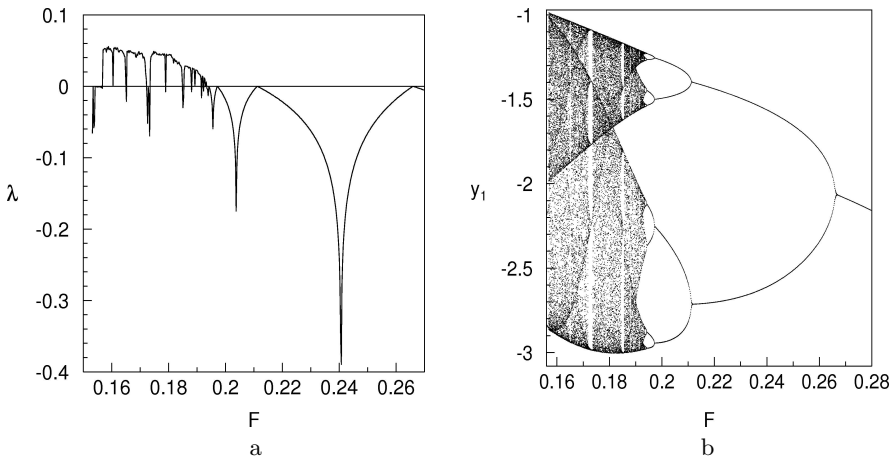

Fig. 3. The dependence of maximal non-zero Lyapunov's characteristic exponent from F (a), phase-parametric characteristic of the system (b).

regimes as well as the bifurcation points, at passing of which, regime changes from regular periodic to chaotic. So in this case, at decreasing the parameter F, transition to chaos happens through the infinite cascade of period-doubling bifurcations according to the Feigenbaum's scenario.

In order to determine the class of universality for the system (1), we need to calculate the Feigenbaum's constant, which is determined by the formula:

$$\delta = \lim_{n\to\infty} \delta_n = \lim_{n\to\infty} \frac{F_n - F_{n-1}}{F_{n+1} - F_n}, \tag{3}$$

where F_n – value of the bifurcation parameter at the n-th point of period-doubling bifurcation.

Bifurcation values of F_n correspond to the approaches of maximal Lyapunov's exponent to the zero line (fig. 3a) or to the cleavage points of separate branches of "bifurcation tree" in fig. 3b. We should mention, that for a correct calculation of the Feigenbaum's constant the bifurcation values of F_n must be determined with a sufficiently high accuracy. Therefore using fig. 3 we initially roughly define the interval of the parameter F variation that contains the first bifurcation point. As can be seen from fig. 3, $0.26 < F_1 < 0.27$. Then we build the dependence of maximal Lyapunov's characteristic exponent from F and phase-parametric characteristic on the interval $(0.26, 0.27)$ and specify the value of the first bifurcation point. Repeating the procedure of decreasing the interval of the parameter F variation and constructing the dependence of maximal Lyapunov's characteristic exponent from the parameter F and phase-parametric characteristic on the smaller scale we can obtain the value F_1 with a sufficiently high accuracy. In order to verify the correctness of the bifurcation point determination we build phase portraits of the system passing the first point of bifurcation and make sure, that the structure of phase portraits changes from single-turn cycle to two-turn cycle. Similar procedures are used for defining the following period doubling bifurcation points.

In our case, the values of bifurcation points were determined with an accuracy to $\varepsilon < 10^{-7}$. At $F = 0.265967$ the attractor of our system is single-turn limit cycle and at $F = 0.265966$ this cycle loses its stability and in the system arises two-turn limit cycle. We take the average of this two values as the first point of period-doubling bifurcation, so that we assume that $F_1 = 0.2659665$. At $F = 0.211192$ the system has two-turn cycle and at $F_2 = 0.2111915$ the second period-doubling bifurcation takes place and four-turn cycle arises in the system as a result of it. This cycle loses its stability at $F_3 = 0.1971565$ and 8-turn limit cycle arises in the system. The fourth and fifth period-doubling bifurcations occur respectively at $F_4 = 0.1942145$ and $F_5 = 0.1935835$. As a result 16- and 32-turn cycles appear in the system. At $F_6 = 0.1934483$ 32-turn limit cycle loses its stability and 64-turn cycle arises in the system. This infinite cascade of period-doubling bifurcations comes to end by origin of a chaotic attractor.

Substituting the obtained values into the formula (3) we get:

$$\delta_2 = 3.90274, \delta_3 = 4.77056, \delta_4 = 4.66244, \delta_5 = 4.66720$$

We take the value $\delta_5 = 4.66720$ as an approximate value of the Feigenbaum's constant.

Let us show that the value of the Feigenbaum's constant remains virtually unchanged at different set of the parameters of the system (1). Let the parameters of the system are $C = -0.1$, $D = -0.5$, $F = 0.14$. As bifurcation parameter we choose E that varies $-0.77 \leq E \leq -0.6$. In fig. 4a,b the dependence of maximal non-zero Lyapunov's characteristic exponent from E and phase-parametric characteristic of the system are shown respectively.

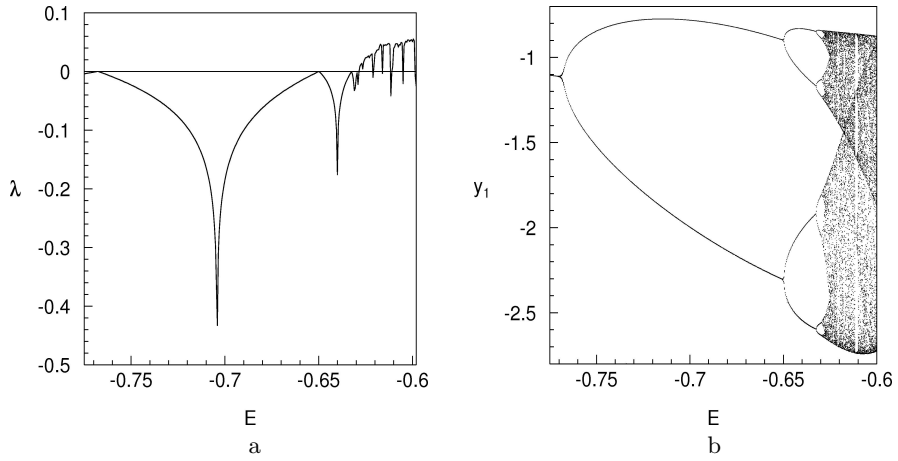

Fig. 4. The dependence of maximal non-zero Lyapunov's characteristic exponent from E (a), phase-parametric characteristic of the system (b).

The qualitative similarity of fig. 3a-b with the respective fig. 4a-b should be noted . As in the previous case, there are several intervals of the parameter change (in this case it is E) in which the system has positive Lyapunov's

characteristic exponent (fig. 4a). Therefore in these intervals the system has chaotic attractors. Again in fig. 4a we can clearly see the approaches of maximal Lyapunov's exponent to the zero line. The form of "bifurcation tree" (fig. 4b) clearly illustrates the Feigenbaum's scenario of transition to chaos. However, as opposed to the previous case, the infinite cascade of period-doubling bifurcations takes place at increasing of the bifurcation parameter.

Let us find the values of the parameter E at which period-doubling bifurcations are happening. The methodology of obtaining these values is similar to that which was used in the previous case for finding bifurcation values of F. At $E = -0.76763$ the attractor of our system is single-turn limit cycle, which loses its stability at $E_1 = -0.767625$ and in the system arises two-turn limit cycle. At $E = -0.64983$ the system still has two-turn limit cycle and at $E_2 = -0.649825$ the second period-doubling bifurcation takes place and four-turn cycle arises in the system as a result of it.

This cycle loses its stability at $E_3 = -0.632405$ and 8-turn limit cycle arises in the system. The fourth and fifth period-doubling bifurcations occur respectively at $E_4 = -0.629315$ and $E_5 = -0.628666$. As a result 16- and 32-turn cycles appear in the system. At $E_6 = -0.628527$ 32-turn limit cycle loses its stability and 64-turn cycle arises in the system. This infinite cascade of period-doubling bifurcations comes to end by origin of a chaotic attractor at $E = -0.62848$. Using the formula (3) and respectively substituting the values E_i instead of F_i into it, we get the following values:

$$\delta_2 = 6.76234, \delta_3 = 5.63754, \delta_4 = 4.76117, \delta_5 = 4.66906.$$

We take the value $\delta_5 = 4.66906$ as an approximate value of the Feigenbaum's constant.

The obtained values quite accurately match with the Feigenbaum's constant, which approximately equals 4.6692. This means that we can state that the system (1) apply to class of universality with the classical Feigenbaum's constant.

5 Analytical approximation of Poincare map

In the previous studies of the "pendulum–electric motor" [4]–[6] it has been established that chaotic attractors that exist in this system, generally, have "quasi ribbon" type of Poincare maps.

This means that the original system of differential equations can be approximately reduced to one of the discrete maps [3], [1]. The study of the dynamics of this discrete map will be much easier than investigation the dynamics of the original system.

Let the system (1) has following values of parameters $C = -0.1$, $D = -0.5$, $E = -0.59$, $F = 0.19$. At these values of the parameters in the system there is a chaotic attractor. Its phase portrait is depicted in fig. 5.

In fig. 6 the Poincare maps of this chaotic attractor are shown. As can be seen from this figure, the Poincare maps on both phase variables have a structure that is close to a line on the plane. Both maps represent some chaotic

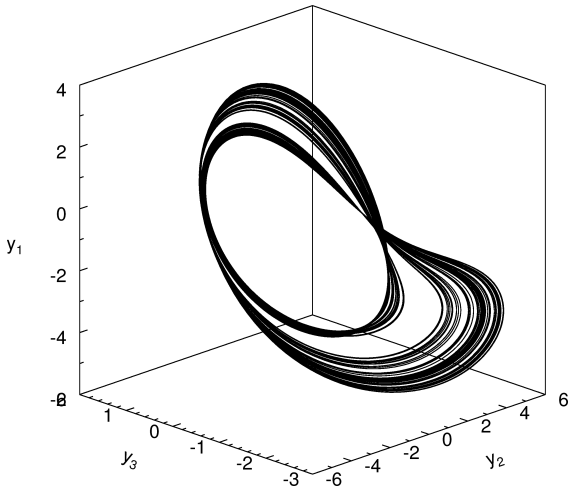

Fig. 5. Phase portrait of the chaotic attractor at $C = -0.1$, $D = -0.5$, $E = -0.59$, $F = 0.19$

set of points. Quantity of these points increases with increasing the time of numerical integration. It is impossible to foresee the order of points placement along "the ribbons" that form the map. However, it is known beforehand that they can only be placed along these ribbons.

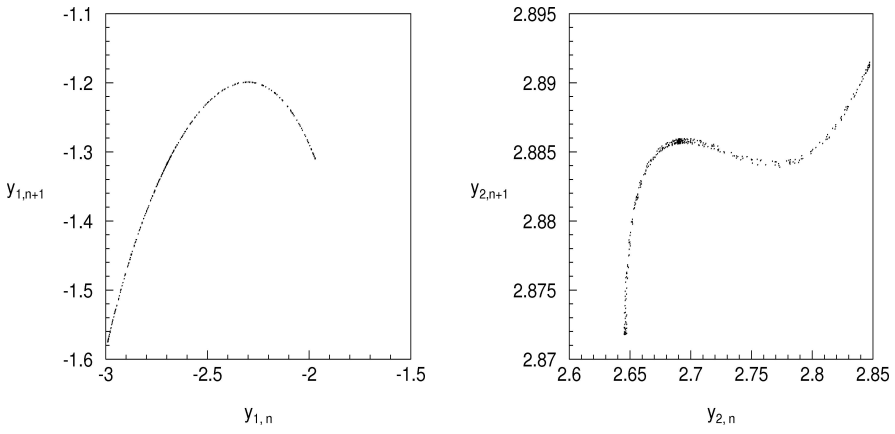

Fig. 6. The Poincare maps of the chaotic attractor.

Let us consider the Poincare map that is shown in fig. 6a. The graph of this map is defined by a set of discrete coordinate values

$$(y_{1,n+1}, y_{1,n}), \quad n = 1, 2, ..., N, \tag{4}$$

where N – is a number of discrete points on which the Poincare map is constructed. Let us set the problem of finding the polynomial whose graph as close

as possible to the points of the Poincare map. For this purpose, the LS method has been used. For set of points (4) we find a m-order polynomial:

$$f^{(m)}(y_1) = p_1 y_1^m + p_2 y_1^{m-1} + ..p_m y_1 + p_{m+1}, \tag{5}$$

the coefficients of which are solution of the minimization problem

$$\min_{p_1,p_2,\ldots,p_{m+1}} \sum_{i=1}^{N} \left(f^{(m)}(y_{1,i}) - y_{1,i+1} \right)^2. \tag{6}$$

The approximation errors have been estimated using the mean-squared error, i.e. $\varepsilon^{(m)} = \sqrt{\min_{p_1,p_2,\ldots,p_{m+1}} \sum_{i=1}^{N} \left(f^{(m)}(y_{1,i}) - y_{1,i+1} \right)^2}$. Applying this method, the following approximations have been obtained:

$$f^{(2)}(y_1) = -0.8377y_1^2 - 3.8947y_1 - 5.7267, \varepsilon^{(2)} = 0.0506;$$

$$f^{(3)}(y_1) = -0.0067y_1^3 - 0.8881y_1^2 - 4.0199y_1 - 5.8292, \varepsilon^{(3)} = 0.0505;$$

$$f^{(4)}(y_1) = -0.5365y_1^4 - 5.3596y_1^3 - 20.778y_1^2 - 36.6289y_1 - 25.7282,$$

$$\varepsilon^{(4)} = 0.0096.$$

Then, the only approximation errors are shown:

$$\varepsilon^{(5)} = 0.0087, \varepsilon^{(6)} = 0.0082, \varepsilon^{(7)} = 0.0081, \varepsilon^{(8)} = 0.0081.$$

It is seen that with the increasing the polynomial order, starting from the order $m = 4$, the approximation accuracy increases insignificantly.

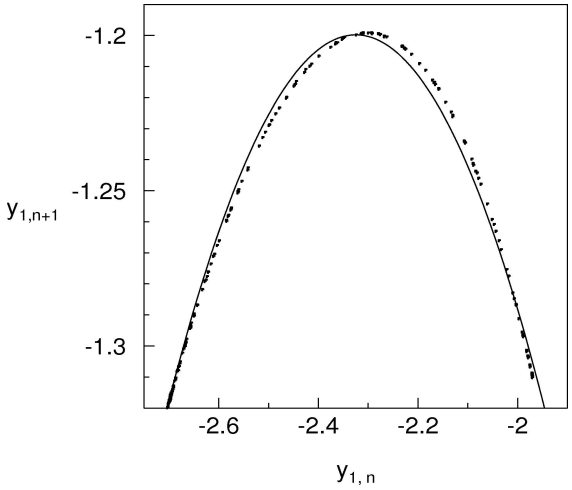

Fig. 7. The Poincare map and its second-order polynomial approximation

The fig. 7 shows an enlarged fragment of the constructed polynomial $f^{(2)}(y_1)$ (continuous line in the figure) that is overlaid on the Poincare map. As can be seen from this figure, these two graphs are close enough to each other. Therefore, this gives us basis to consider the principal possibility to study the continuous system "pendulum–electric motor" (1) using discrete map $y_{1,n+1} = f^{(2)}(y_{1,n})$. More accurate results will be obtained when the maps $y_{1,n+1} = f^{(m)}(y_{1,n}),\ m = 4 \div 8$ are used.

6 Conclusion

At the study of the dynamical system "pendulum–electric motor", the atlas of maps of dynamical regimes has been constructed. It has been established that deterministic chaos is a typical steady-state regime of the given system. The Feigenbaum's constant of system "pendulum–electric motor" is obtained. The class of universality of the given system is defined. The analytical polynomial approximations of the Poincare map have been found.

References

1.V. S. Anishchenko, V. V. Astakhov, A. B. Nieman, T. E. Vadivasova, and L. Schimansky Geier. Nonlinear Dynamics of Chaotic and Stochastic Systems. Springer, Berlin, 2003.
2.V. O. Kononenko. Vibrating System with a Limited Power-supply. Iliffe, London, 1969.
3.S. P. Kouznetsov. Dynamic chaos. Physmatlit, Moscow, 2006, (in russian).
4.T. S. Krasnopolskaya, A. Yu. Shvets. Chaotic interactions in a pendulum-energy-source system. Sov. Appl. Mech., vol. 26, 500—504, 1990.
5.T. S. Krasnopolskaya, A. Yu. Shvets. Chaos in vibrating systems with limited power-supply. Chaos, vol. 3, no. 3, 387—395, 1993.
6.T. S. Krasnopolskaya, A. Yu. Shvets. Regular and chaotical dynamics of systems with limited excitation. R&C Dynamics, Moscow, 2008, (in russian).
7.T. S. Krasnopolskaya, A. Yu. Shvets. Dynamical chaos for a limited power supply oscillations in cylindrical tanks. Journal of Sound and Vibration, vol. 322, no. 3, 532—553, 2009.

Chaotic Modeling and Simulation CMSIM) 1: 205-217, 2012

Detection of jet axis in a horizontal turbulent jet via nonlinear analysis of minimum/maximum temperature time series

A. Charakopoulos[1], T.E. Karakasidis[1*], P.N. Papanicolaou[2]

[1] Department of Civil Engineering, University of Thessaly, 38334 Volos, Greece
[2] Department of Civil Engineering, National Technical University of Athens, Athens Greece

(E-mail: *thkarak@uth.gr)

Abstract: We have analyzed experimental temperature time series from a horizontal turbulent heated jet, in order to identify the jet axis location using non linear measures. The analysis was applied on both, the original time series as well as on the extreme value (minimum and maximum values) time series. In our analysis we employed mainly non-linear measures such as mutual information and cumulative mutual information. The results show that the analysis of the extreme values time series using cumulative mutual information permits to distinguish the jet axis time series from the rest of the jet, as well as discriminate regions of the jet located close to jet axis or close to the boundaries. Furthermore, it is of interest that the application of simple statistical measures and clustering techniques shows that the use of extremes time series let us distinguish with greater confidence the jet axis than the use of the original one.
Keywords: Non-linear time series analysis, turbulence, mutual information, cumulative mutual information, clustering.

1 Introduction

Jet flow is a very important research subject that has attracted scientific interest due to extensive applications in environmental engineering. So far a large number of investigations have been carried out to locate the trajectory and understand the turbulence properties of the flow using statistical methods which do not necessarily lead to understanding the dynamics of the flow [3, 19].
The transition from laminar to turbulent flow in a jet has been extensively studied as a fundamental non linear dynamical problem [4, 5, 17, 25]. The study of dynamical systems by analysis of the time series of a variable measured in a physical system, is of particular interest over the last decades, and gives the possibility of comprehension the underlying system dynamics. Time series analysis may include linear and non linear methods. The linear analysis includes simple statistical measures such as autocorrelation function and power spectrum, while non linear analysis methods based on the reconstruction of phase through spaces include the mutual information and correlation dimension. For a concise review of these methods one can consult the book by Kantz and Schreiber (1995) [10] and Abarabnel (1996) [1]. These more complex methods

Received: 14 July 2011 / Accepted 20 December 2011

ISSN 2241-0503

allow us to extract more detailed characteristics of the underlying dynamical system.

In this paper linear and non linear measures are used to analyze temperature fluctuation time series. Our aim was to study the dynamic characteristics of the temperature fluctuation experiment. More specifically we analyze the temperature fluctuation measurements recorded using fast response thermistors along a horizontal line in order to investigate if one can discriminate time series corresponding to regions close to the jet axis, where conditions of fully developed turbulence are expected, from time series corresponding to regions that are more distant and from those close to the boundary with the ambient water. Horizontal buoyant jet investigations [2, 6, 9, 18] are mainly concerned with the structure of the flow.

The novelty of the present work is that the analysis was applied both on the original time series as well as on the extreme value (minimum and maximum values) time series. The initial time series is reduced to a series (extreme time series) of successive pairs of minimum and maximum values. The objective of our analysis is to investigate whether it is possible that a time series of extreme values can reveal dynamic characteristics of the underlying system in the same or better way as the analysis of the original time series. One can easily understand that the interest is important, since this would permit us to study dynamical systems using reduced information.

The structure of the paper is as follows. In Sec. 2 we discuss briefly the theoretical background and the experimental set-up for the temperature measurements. In Sec.3 we present the methodology employed for data analysis along with the linear and nonlinear measures. The results and discussion are presented in Sec. 4. Finally the conclusions are presented in Sec. 5.

2 Theory and Experimental Set-up

2.1 Theory

A horizontal heated round jet of diameter D and density ρ_o flows out of a nozzle with velocity U in a calm ambient fluid of density ρ_α. The specific volume, horizontal momentum and buoyancy fluxes are defined as

$$\begin{aligned} Q &= \frac{\pi D^2}{4} U \\ M &= QU \qquad\qquad and \\ B &= g_o' Q = \frac{\rho_\alpha - \rho_o}{\rho_\alpha} gQ \end{aligned} \tag{1}$$

respectively, where g is the gravitational acceleration and $g_o^{'}$ the effective gravity that will subsequently produce vertical momentum flux. Fisher et al. (1979) [7] have defined two characteristic length scales as:

$$l_Q = \frac{Q}{M^{1/2}} \qquad and \qquad l_M = \frac{M^{3/4}}{B^{1/2}} \tag{2}$$

the ratio of which is the initial jet Richardson number R_o:

$$R_o = \frac{l_Q}{l_M} = \left(\frac{\pi}{4}\right)^{1/4} \frac{\sqrt{g_o^{'} D}}{U} = \left(\frac{\pi}{4}\right)^{1/4} \frac{1}{F_o} \qquad and \qquad F_o = \frac{U}{\sqrt{g_o^{'} D}} \tag{3}$$

where F_o is the initial densimetric Froude number.

The temperature difference between the jet and ambient fluid produces the density deficiency that is responsible for the initial jet specific buoyancy flux. The dilution S at a point of the jet flow field is defined to be the ratio:

$$S = \frac{T_o - T_a}{T - T_a} \tag{4}$$

Where T_o is the initial jet temperature T_a the ambient temperature and the T the local time-averaged temperature. Jirka (2004) [8] has defined the jet axis to be the point of minimum dilution S_c:

$$S_c = \frac{T_o - T_a}{T_c - T_a} \tag{5}$$

where T_c is the maximum time-averaged (centerline) temperature. We define x_c and y_c the horizontal and vertical distances from the nozzle where the jet axis is located. Near the nozzle $(x/l_M < 1)$ the jet trajectory is horizontal, the flow is mainly driven by the initial momentum flux and it is characterized as jet-like [18]. When $(y/l_M > 2)$ the trajectory of the flow is altered to vertical and the flow is characterized as plume-like. The flow regime $(1 < x/l_M < 5)$ is the transition from jet-like to plume-like flow [18], [21].

2.2 Experimental setup

The experiments were performed at the Hydromechanics and Environmental Engineering Laboratory of the University of Thessaly [20]. The dispersion tank is made of 12.5mm thick Lucite with orthogonal horizontal section 0.90m x 0.60m and 0.80m depth. A perspective view of the experimental setup is shown in Fig.1.

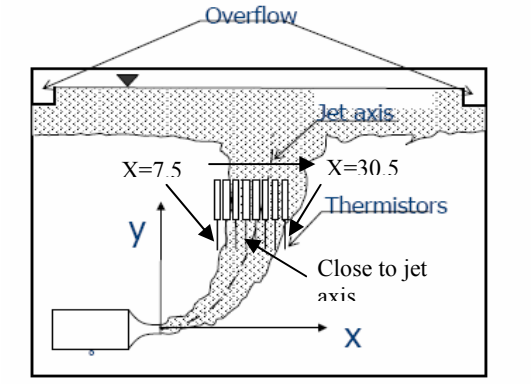

Fig. 1. Perspective view of the experimental setup

The tank was equipped with a peripheral overflow to remove excess water. In this mater the depth of water is fixed at 77 cm. The hot water jet supply consists of a water heater made of stainless steel, which is well insulated and pressurized by air at 2 atm, to provide adequate constant head pressure to drive to jet. During the water heating, a recirculating pump was used to ensure that the hot water is well mixed and there are no temperature gradients. An insulated pipe drives the water from the heater into the jet plenum, through a calibrated flow meter. A jet nozzle of 0.65cm diameter was used. The jet water temperature was around 60 ºC, while the ambient water temperature ranged between 18 to 20 ºC. Temperature measurements were obtained by an array of eight fast response thermistors spaced equally at 1cm apart, positioned at constant elevation from the nozzle, on the plane of symmetry of the buoyant jet. The jet was made visible by means of a slide projector on a semitransparent paper sheet (shadowgraph) in order to place the rake of thermistors properly. In this paper, we use the data recorded at an elevation of 5cm above the nozzle axis. The initial parameters of the flow are shown in table 1. We analyzed 24 recordings of temperature time series, one for each location of measurement, where the sampling time at each location was 30s at a frequency of 200Hz. Comprehensive details about the experimental setup can be found in Karakasidis et al (2009) [11].

Table 1. Experimental conditions

D(cm)	W(cm/s)	T_o(ºC)	T_a(ºC)	M(cm^4/s^2)	B(cm^4/s^3)	Re	l_m(cm)	R_o	y_c/l_m
0.65	29.25	60	17.8	284	149	1646	5.66	0.102	0.883

3. Time series analysis

3.1 Methodology

In an effort to discriminate the jet axis time series from the rest of the jet we used linear and nonlinear measures applied both on the original time series as well as on the extreme value (minimum and maximum values) time series. The initial time series is reduced to a series (extreme time series) of successive pairs of minimum and maximum values following the methodology by D.Kugiumtzis et al., 2006 [14]. The goal of this work was to examine if simple linear and non linear methods such as cumulative mutual information, can discriminate different states of systems from the analysis of the reduced length time series, instead of the full original time series.

3.2 Data set – Extreme time series model

As already mentioned 24 time series of temperatures have been recorded using fast response thermistors along a horizontal line of a fully developed turbulent heated jet. Consequently some of the time series correspond to conditions of turbulent flow (time series derived close to centerline of the jet) while other time series, obtained close to the boundary between the heated jet and the ambient water, have intermittent (laminar and turbulent) flow characteristics. Each time series consist of 6000 observations.

We derived new *extreme time* series of successive maximum and minimum values from each initial time series. Suppose we have a time series of length N, $\chi(t)$, $t = 1,2,....N$. If $y_1 = \chi(t_1)$ the first minimum, $y_2 = \chi(t_{1+...})$ the first turning point (maximum), $y_3 = \chi(t_{2+...})$ the second turning point (minimum) etc we extract from the initial time series the time series $y(t) = y_1, y_2, y_3, ...y_n$ called *extreme time series*. The extracted time series have lengths varying from N=130 to 1500 depending on the structure of the initial time series.

An example of a whole initial and extreme time series is shown in Fig. 2(a). In Fig. 2 (b) a zoom of a segment of the initial temperature time series of Fig 2(a) is presented.

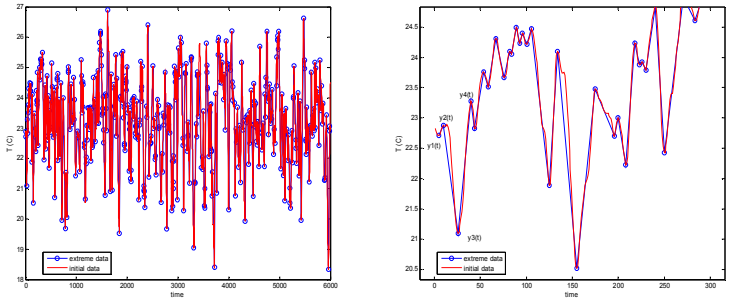

Fig. 2. (a) Initial and extreme time series. (b) Segment of initial and extreme time series.

3.3 Nonlinear measures

The most widely known nonlinear measure, which is used to select the appropriate delay time τ for state space reconstruction is the Mutual Information $I(\tau)$ and is defined as:

$$I(\tau)= \sum_{x(ti),x(ti+\tau)} P(x(ti),x(ti+\tau))*\log[\frac{P(x(ti),x(ti+\tau))}{P(x(ti))*P(x(ti+\tau))}] \quad (6)$$

Where $x(t_i)$ is the i[th] data point of time series, $\tau = k\Delta t(k = 1, 2, ...k_{\max})$; $P(x(t_i))$ is the probability density at $x(t_i)$; $P(x(t_i), x(t_i + \tau))$ is the joint probability density at $x(t_i), x(t_i + \tau)$; τ is the delay time.

The delay τ of the first minimum is chosen as a delay time for the reconstruction of phase space.

We also used a new nonlinear measures the *Cumulative Mutual Information* $M(\tau_{\max})$, defined as the sum of mutual information $I(\tau)$ D.Kugiumtzis et al., 2007 [14] for a number of delay τ.

$$M(\tau_{\max}) = \sum_{\tau=1}^{\tau_{\max}} I(\tau) \quad (7)$$

3.4 Clustering analysis using the Cumulative Mutual Information function

Clustering is an important technique that groups together similar data sets. Several studies used clustering methods based on mutual information [23, 24]. In our study we used single linkage hierarchical clustering algorithm in order to classify our data. The clustering techniques applied both on the original time series as well as on the extreme value (minimum and maximum values) time series. As a measure of similarity we used the *Cumulative Mutual Information*.

One of the main advantages of hierarchical clustering is that a dendrogram can be drawn to find the appropriate number of clusters in a dataset. Briefly we propose the following clustering algorithm steps:

- We compute the Euclidean distance y between pairs of objects in *n*-by-*p* data matrix X. Rows of X correspond to observations; columns correspond to variables.
- We create a hierarchical cluster tree z from the distances in y (y is a Euclidean distance matrix or a more general dissimilarity matrix, formatted as a vector).
- Finally we group the data set into clusters. The most dependent data are grouped together.

4. Results and Discussion

During the experiment the jet axis (at elevation 5cm above the nozzle axis) was located by optical measurements nearly at the midpoint between the jet boundaries (x=16.5 – 17.5 cm). This was also supported by the behavior of the average temperatures observed in these time series, as well as from Recurrence Plot analysis [11]. It is well known from the theory of fluid mechanics that turbulence near the center of the jet is fully developed. There appear many short-lived small scale turbulent structures, while near the jet boundary the large scale flow structures live longer.

We calculated the mutual information function for both, the original as well as for the extreme data series and the results are presented in Figs. 3(a)-(b). In Fig. 3 (b) we observe that for the extreme time series reported at x=16.5 cm and x=17.5 cm (points which are near jet axis) the mutual information function clearly attains the lowest values for any value of the time delay, if compared to the results for the rest of the time series. Such behavior is consistent with what we expected since close to the jet centreline the memory of the flow structures is lost fast.

(a)

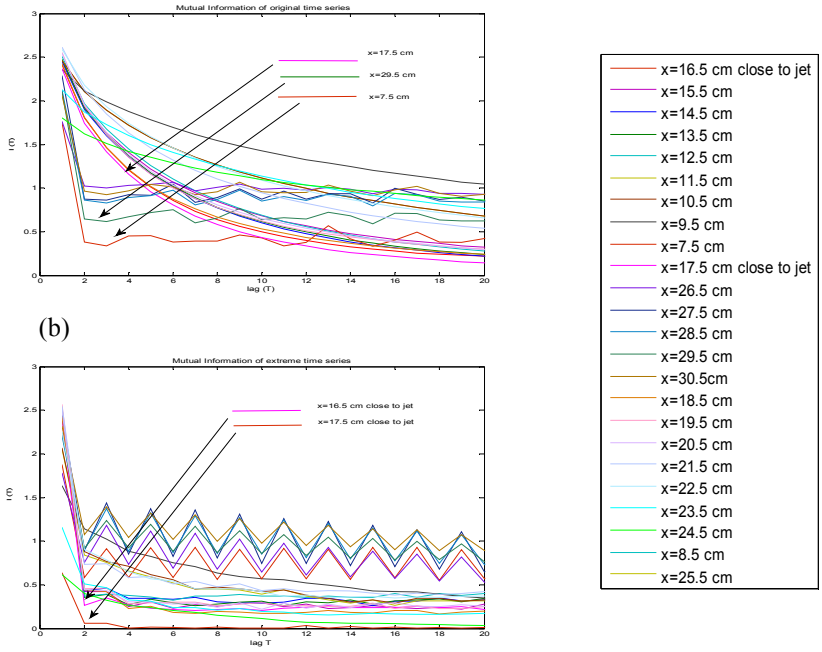

Fig. 3. (a) Mutual information of the Initial time series along the horizontal line.
(b) Mutual information of the Extreme time series along the horizontal line

In Fig. 3(a) we can see that there are time series presenting the smallest local minimum but not the lowest values of average mutual information which

correspond in fact to regions in or close to the ambient water, while time series close to the jet axis (close to x=17.5cm) present the lowest values of average mutual information although for larger lags. As we get far from the jet axis ,but always in the turbulent jet region, average mutual information increases and time lags of the minimum are shifted toward larger times. We must however bear in mind that the time lags are not directly compared for the original and the extreme time series, since the distance between successive points varies.

In Fig.4 (a) and (b) we summarize results for the cumulative mutual information for the original and extreme time series. A close look in Fig. 4(b), where the cumulative mutual information for the extreme time series is presented, indicates that we can discriminate three main regions corresponding to time series. The first region corresponds to a set of time series too far from the centerline of jet (x=7.5cm, x=27.5cm, x=28.5cm, x=29.5cm, x=30.5cm). The second region corresponds to a set of time series very close to the center of jet (x=16.5cm, x=15.5cm, x=17.5cm, x=18.5cm, x=19.5cm). The third region corresponds to a set of time series (x=9.5cm, x=21.5cm, x=22.5cm, x=23.5cm) far from the center of jet but not as much as the time series from the first region.

(a)

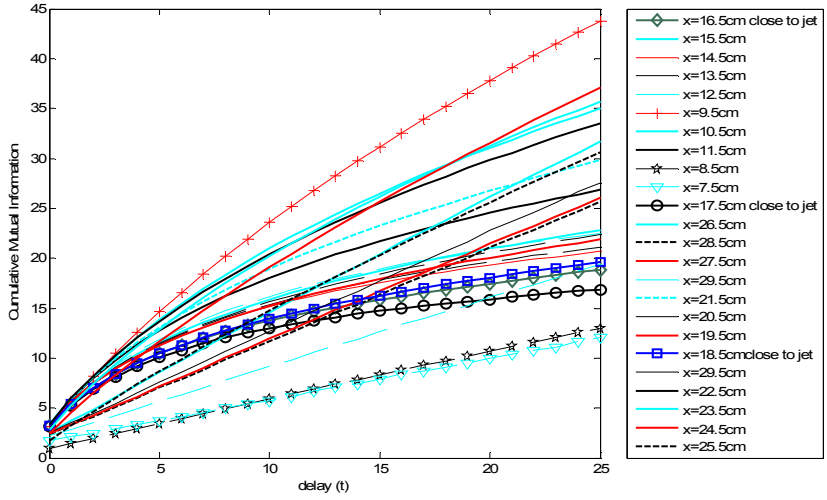

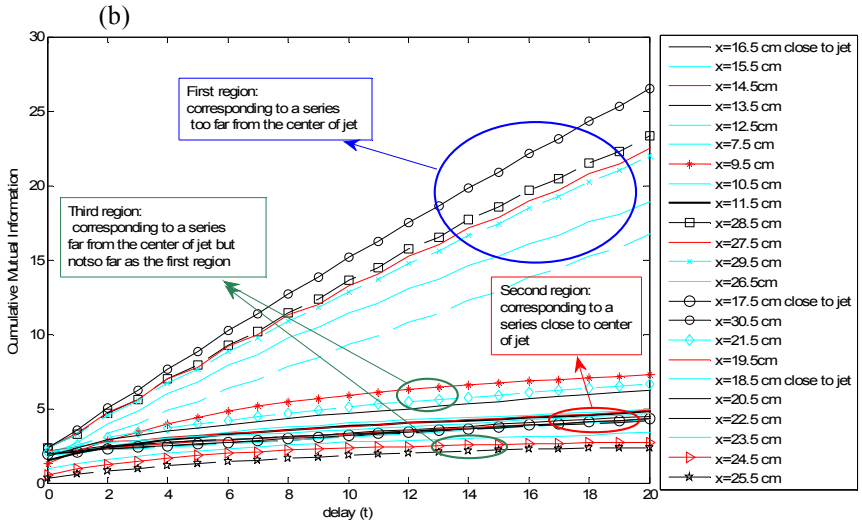

Fig. 4. (a) Cumulative Mutual information of the Initial time series along the horizontal line. (b) Cumulative Mutual information of the Extreme time series along the horizontal line

It is of interest to note that such a detailed discrimination of the three regions is not so straightforward in Fig. 4(a) where the cumulative mutual information from the original time series is presented.

Furthermore we evaluate the discriminating power of cumulative mutual information, applying a clustering algorithm to the set of our cumulative mutual information time series. For the clustering we used the algorithm described in paragraph 3.4. The hierarchy built by the clustering algorithm based on cumulative mutual information from reduced and original time series is represented by the dendrograms given in Fig. 5 and Fig.6.

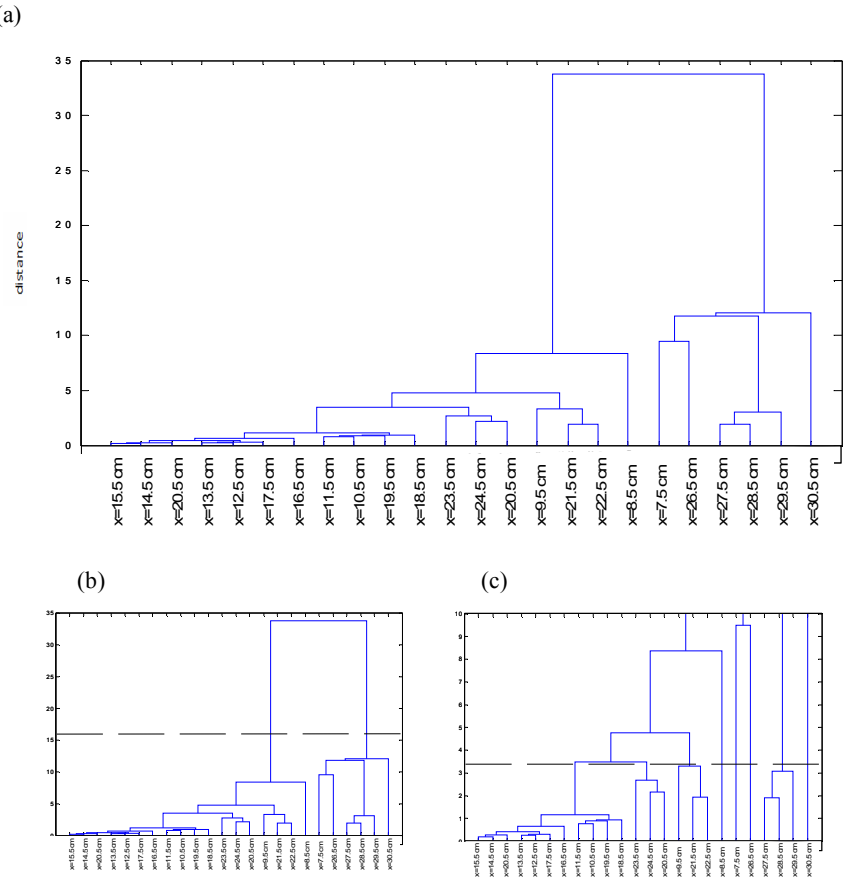

Fig. 5. (a), (b), and (c) Dendrogram Cumulative Mutual information of the Extreme time series along the horizontal line at different cut point

In Figure 5(a) we present the hierarchy clustering of each extreme time series. We decided to make two *´´cuts´´* at the dendrogram at different levels of distance (vertical axis). In Fig. 5(b), the first *´´cut´´* is made at distance~16, where one can clearly see two main partitions. One main group consisted from the time series at x=7.5cm, x=26.5cm, x=27.5cm, x=28.5cm, x=29.5cm, x=30.5cm. This group corresponds to the region too far from the axis of the jet. The second main cluster includes the remaining time series. This first step is important because we can exclude the time series time series corresponding to the edges of the measuring area.

In Fig. 5 (c) we can see the dendrogram which results in from the second *´´cut´´* at distance~3.5. We can see more clearly some major cluster and some smaller. Specifically the time series at x=23.5cm, x=24.5cm, x=20.5cm and at x=9.5cm,

x=21.5cm, 22.5cm join and at x=21.5cm, x=10.5cm, x=19.5cm is joined with x=18.5cm. These above partitions correspond to a set of time series far from the center of jet but not as much as the time series from the first step (x=7.5cm, x=26.5cm, x=27.5cm, x=28.5cm, x=29.5cm, x=30.5cm).
Moreover in Fig. 5 (c) we can distinguish other some small clusters which include the time series at x=15.5cm, x=14.5cm, x=20.5cm and x=13.5cm, x=12.5cm, x=17.5cm. We can notice that the time series at x=16.5cm correspond close to the centerline of jet is separate from other.

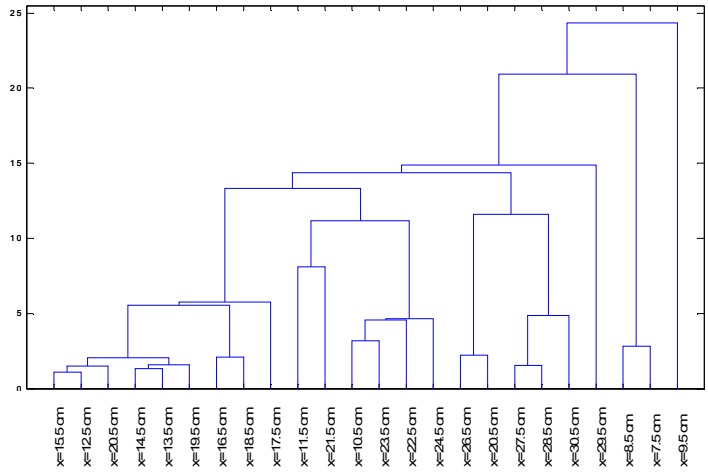

Fig. 6. Dendrogram Cumulative Mutual information of the Initial time series along the horizontal line.

As we can see in Fig 6 where the results for the cumulative mutual information resulting from the analysis of the original time series are presented, there are several clusters without the same discriminating structure observed from the analysis of the extremes time series (Fig.5).

5. Conclusions

In this work we have investigated a new approach in order to detect the jet axis of temperature time series derived from experimental data. The novelty of this study is that the analysis was applied both on the original time series as well as on the extreme value (minimum and maximum values) time series. More specifically we focus to a new measure the *Cumulative Mutual Information*, and we showed that it can discriminate the underlying dynamics from one time series to another. Another important issue is that the performance of the *Cumulative Mutual Information* was applied to a reduced length time series (extreme time series) and showed that it has higher discriminating power than in the original time series. This issue is very important if we take into account the

size of the computational analysis of original data due to the length of the time series.

6. References

1. Abarabnel H.D.I. Analysis of observed chaotic data. Springer, Berlin. 1996.
2. Anwar, H.O., 1969. Behavior of a buoyant jet in a calm fluid, Proc. ASCE, J. Hyd.
3. Div.. 95(4), 1289-1303.
4. Bradshaw P. Turbulence, Topics in Applied Physics, 12, Springer, 1978
5. Broze G. and Hussain F. Transitions to chaos in a forced jet: intermittency, tangent
6. bifurcations and hysteresis. *J. Fluid Mech.* 331, 37-71, 1996.
7. Crow S. C, and Champagne F. H. Orderly structure in jet turbulence. *J. Fluid Mech.* 48, 3, 547-591, 1971.
8. Fan, L-N., 1967, Turbulent buoyant jets into stratified or flowing ambient fluids, Rep. No. KH-R-15, W.M. Keck Laboratory of Hydraulics and Water Resources, California Institute of Technology, Pasadena, California
9. Fischer H. B, List E. J, Koh R. C. Y, Imberger J, and Brooks N. H. Mixing in Inland and Coastal Waters (Academic Press), 1979.
10. Jirka G. H. Integral model for turbulent buoyant jets in unbounded stratified flows. Part I: Single round jet. Env. Fluid Mech. 4, 1-56, 2004.
11. Johnston A. J., Phillips C. R. and Volker R.E. Modeling horizontal round buoyant jets in shallow water. *Journal of Hydrauling Engineering* . 120, 1994.
12. Kantz H. and Schreiber T. Nonlinear time series analysis. Cambridge University Press, Cambridge, 1995.
13. Karakasidis T. E., Liakopoulos A., Fragkou A. and Papanicolaou P. N. Recurrence Quantification Analysis of Temperature Fluctuations in a Horizontal Round Heated Jet. *International Journal of Bifurcation and Chaos*, 19, 2487-2498. 2009.
14. Kraskov A, Stogbauer H, Andrzejak R. G, and Grassberger P. Hierarchical clustering using mutual information. *Europhysics Letters,* 70(2), 278-284, 2005
15. Kugiumtzis D, Kehagias A and Aifantis E. C. Statistical analysis of the extreme values of stress time series from Portevin-Le Chatelier effect. *Physical Review E,* 70, 036110, 2004.
16. Kugiumtzis D, Papana A, Tsimpiris A, Vlachos I, and Larsson PG. Time series feature evalyation in discriminating preictal EEG states. *Lecture Notes in Computer Science ,* 4345, 298-310, 2006.
17. Kugiumtzis D, and Vlachos I. Turning point prediction of oscillating time series using local dynamic regression models. arXiv:0809.2229v1, 12 Sep 2008
18. Kugiumtzis D, Vlachos I, Papana A, and Larsson PG. Assessment of measures of scalar time series analysis in discriminating preictal states. *International journal of Bioelectromagnetism,* 9(3), 134-145, 2007.
19. Mataoui A, and Schiestel R. Unsteady phenomena of an oscillating turbulent jet flow inside a cavity: Effect of aspect ratio. *Journal of Fluids and Structures.* 25, 60-79, 2009.
20. Michas S. N. and Papanicolaou P.N. Horizontal round heated jets into calm uniform ambient. *Desalination.* 248, 803-815, 2009.

21. Monin A. S, and Yaglom A .M. Statistical Fluid Mechanics, 2 (MIT Press, Cambridge) 1975
22. Palamitzoglou G. *Diploma Thesis,* Department of Civil Engineering, University of Thessaly. 2005.
23. Papanicolaou P. N. and List E. J. Investigations of round vertical turbulent buoyant jets. *J. Fluid Mech.* 195, 341-391, 1988.
24. Papanicolaou P. N. and List E. J. Statistical and spectral properties of tracer concentration in round buoyant jets. *Int. J. Heat Mass Transfer.* 30, 2059-2071, 1987.
25. Priness I, Maimon O, and Ben-Gal I. Evaluation of gene-expression clustering via mutual information distance measure, *Bioinformatics,* 8(6), 111, 2007
26. Tourassi G, Frederick E, Markey M, and Floyd C. Application of the mutual information criterion for feature selection in computer-aided diagnosis, *Med. Phys,* 28(12), 2394-2402, 2001.
27. Wang X, and Keat Tan S. Environmental fluid dynamics-jet flow. *Journal of Hydrodynamics,* 22(5), 1009-1014, 2010.

Chaotic Modeling and Simulation (CMSIM) 1: 219-227, 2012

Multifractal Analysis of the Psychorelaxation Efficiency for the Healthy and Pathological Human Brain

Olga E. Dick [1]

[1] Pavlov Institute of Physiology of Russian Academy of Science, St. Petersburg, Russia (E-mail: glazov.holo@mail.ioffe.ru)

Abstract: Changes in EEG time series before, during and after removing a pain syndrome by applying the psychorelaxation technique are examined for healthy subjects and patients with chronic psychogenic pain disorders connected with disruptions of interrelations between cortex and subcortex on the thalamic and the brain-stem level. The degree of psychorelaxation and decrease of the pain syndromes is estimated as a change in the multifractality degree gained by the wavelet transform modulus maxima method. For the healthy subjects we observe the reliable decrease of the multifractality degree and the enhancement of the anticorrelated dynamics of consecutive EEG values during the pain and their recovery up to the previous values during psychorelaxation. The all healthy subjects notice that the pain syndrome disappears. The analogous dynamics in the multifractality and the improvement of the functional state are observed only for 70% "thalamic" patients. For other 30% patients of the group the multifractality degree remains less than for the healthy subjects. For all the "brain-stem" patients during relaxation the multifractality degree remains high and the singularity spectrum corresponds to both the correlated and anticorrelated dynamics. The study demonstrates that the changes in the multifractality give a good ability to estimate the psychorelaxation efficiency for the healthy and pathological human brain.
Keywords: EEG, Psychorelaxation technique, Multifractal analysis.

1 Introduction

It is well known that bioelectrical activity of the human brain recorded from the head surface as electroencephalography signal (EEG) can be considered as oscillatory processes exhibiting clearly defined variability and having the chaotic and fractal properties [2, 9]. Fractal dynamics of EEG is supported by the form with step-like features and some sort of self-similarity at least stochastically. In other words, on small scales EEG patterns are not identical to the whole signal but the self-similarity remains after averaging by statistically independent samples of the signal. Multifractality of the human brain is found in EEG time series in both healthy and pathologic states [5, 7]. The present work is devoted to the comparative analysis of the multifractality degree in EEG patterns of normal and pathological brain activities. Impairments connected with anxious phobic disorders are considered as pathology. Chronic pain complaints are specific for patients suffering these disorders. These complaints frequently

Received: 14 September 2011 / Accepted 20 December 2011

ISSN 2241-0503

are not confirmed by medical research and accompanied by emotional disturbances leading to a significant reduction in the level of social functioning [4]. Neural disorders of this type are rather resistant to medicinal treatment. That is why the development of various psychotherapeutic methods is of interest to clinical practice. These methods sometimes allow removing pain symptoms. One of the methods is psychorelaxation technique [3] in which the psychorelaxation is in switching attention from the pain sense on the perception of color spots arising spontaneously in the state of concentrating on the pain locus with closed eyes. Switching attention from the pain intensity to the color spots is accompanied by decreasing the pain symptoms up to their complete disappearance.

The aim of the work is to estimate the psychorelaxation efficiency for treatment of psychogenic pain in patients with anxious phobic disorders by the method of multifractal analysis. For solving the task we analyze EEG fragments recorded during the perception of psychogenic pain and during its removal by the psychorelaxation technique.

2 Experimental procedure

The scalp EEG data were recorded during 50 minutes with Ag/AgCl electrodes placed at the frontal F3, F4, Fz and occipital O1, O2, Oz sites from 15 healthy subjects and 18 patients with neural impairments connected with anxious phobic disorders. For healthy subjects the pain was evoked by a tactile stimulation on the midpoint between the first and second fingers during 1 minute. The pain was removed by psychorelaxation technique. For patients with psychogenic pain its reduction was perfomed during 10 - 20 psychorelaxation trials. So, the recordings were obtained for three states: before tactile pain stimulation (10 minutes), during it (20 minutes) and during relaxation (20 minutes) for the healthy subjects and during psychogenic pain and in relaxation state for the patients with neural disorders. The psychorelaxation technique [3] was is in switching attention from the pain sense on the perception of color spots arising spontaneously when concentrating on the pain locus with closed eyes. Thus, in the psychorelaxation state the pain sense transformed into a color image by the patient brain. The observed color spots could appear as achromatic (black or grey) colors or chromatic (red, orange, yellow or blue) ones and they could change the color. As attention was shifted from the pain to the color spots and their color was changed, the patient's condition could be improved up to the complete disappearance of pain symptoms.

The data were sampled at a rate 256 samples/sec with a resolution of 12 bits/sample. Then the data were digitally filtered using 1–45 Hz band pass filter. The each state included 256000 samples and it was divided into 20 segments of the duration 50 seconds. After repeated recordings 60 non- artifact segments of equal duration were randomly chosen from the sets: "before pain", "during pain" and "during psychorelaxation".

3 Estimation of EEG multifractality

To estimate multifractal scaling properties of EEG time series we applied the wavelet transform modulus maxima (WTMM) method [1]. The algorithm of the method consists of the following procedures.

1) The continuous wavelet transform of the time series describing the examined signal $x(t)$:

$$W(a,t_0)=\frac{1}{a}\int_{-\infty}^{+\infty}x(t)\psi^*\left(\frac{t-t_0}{a}\right)dt,$$

is used. Here a and t_0 are the scale and space parameters, $\psi((t- t_0)/a)$ is the wavelet function obtained from the basic wavelet $\psi(t)$ by scaling and shifting along the time, symbol * means the complex conjugate. As the basic wavelet we use the complex Morlet wavelet:

$$\psi(t)=\pi^{-1/4}e^{i\omega_0 t}e^{-t^2/2}.$$

The value ω=2π gives the simple relation between the scale a and the frequency f: f=1/a.

2) A set $L(a)$ of lines of local modulus maxima of the wavelet coefficients is found at each scale a.

3) The partition functions are calculated by the sum of q - powers of the modulus maxima of the wavelet coefficients along the each line at the scales smaller the given value a:

$$Z(q,a)=\sum_{l\in L(a)}\left(\sup_{a^*\le a}\left|W(a^*,t_l(a^*))\right|\right)^q,$$

$t_l(a^*)$ determines the position of the maximum corresponding to the line l at this scale.

4) By the fact that the partition function is $Z(q,a)\sim a^{\tau(q)}$ at $a\to 0$ [1], the scaling exponent can be extracted as $\tau(q)\sim \log_{10} Z(q,a)/\log_{10} a$.

5) Choosing different values of the power q one can obtain a linear dependence $\tau(q)$ with a constant value of the Hölder exponent $h(q)=d\tau(q)/dq=const$ for monofractal signals and nonlinear dependence $\tau(q)=qh(q)-D(h)$ with large number of the Hölder exponents for multifractal signals.

6) The singularity spectrum (distribution of the local Hölder exponents) is calculated from the Legendre transform [1]: $D(h)=qh(q)-\tau(q)$.

Using the WWTM algorithm for the different EEG segments we obtain the multifractal parameter, namely, the width of the singularity spectrum $\Delta h = h_{max} - h_{min}$, where $h_{max} = h\ (q = -5)$ and $h_{min} = h\ (q = 5)$ are the maximal and minimal values of the Holder exponent corresponding to minimal and maximal fluctuation of the brain activity, respectively. Smaller Δh indicates that the time series tends to be monofractal and larger Δh testifies the enhancement of multifractality. To examine the differences between the mean values of the parameter obtained for all the segments of different sets of one subject the non-parametric Mann-Whitney test ($p < 0.05$) was applied.

4 Results and discussion

Power spectra of EEG of all the healthy subjects have no significant differences in three different states, namely, background (before the pain stimulation), during the pain stimulation and during psychorelaxation. Alpha activity [7 - 14] Hz dominates.

Multifractal analysis enables us to distinguish the EEGs in the three states. For the all examined electrode sites the width of the singularity spectrum (Δh) decreases during the pain stimulation and recovers up to previous values after pain removing. In the all states h_{max} <0.5 (Fig. 1), hence, the singularity spectrum corresponds to anticorrelated dynamics of consecutive EEG values.

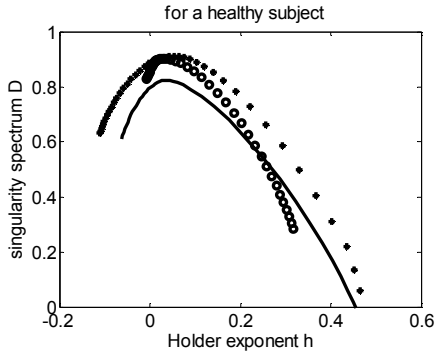

Fig. 1. The examples of singularity spectra of a healthy subject in three functional states (the curve denoted as "*" symbol corresponds the state before the tactile pain stimulation, the curve specified as "o" describes the state during the pain stimulus and the solid line corresponds to the psychorelaxation state.

Thus, persistent sequences are characterized by stochastically "up - down" patterns. The decrease of h_{max} during the pain stimulation testifies about the enhancement of the anticorrelation degree, so that the signal becomes less smooth and more singular and the randomness of the fluctuations increases. Therefore, the interval time series tend to become more random during the pain stimulation and recover during relaxation.

The decline of the width of the singularity spectrum during the pain stimulation shows a reduction of nonuniformity of the signal and a fall in the multifractality degree. This fall is due to weak fluctuations (for $q<0$, $h>0$), and at strong fluctuations ($q>0$) the time series become monofractal (uniform by scaling characteristics) and the singularity spectrum transfoms into a point (h=const).

In the state of concentration of the attention on the pain sense the all healthy subjects noticed achromatic colors (black or grey) and the short-wavelength colors (blue or green) in the relaxation state. The pain syndrome disappeared. The results agree with the previous data in which each color image caused a specified shift in the psychophysiological state of a subject and determined the presence of psychoemotional stress [6]. In the work [3] it has been revealed that psychotherapeutic influence relieving the stress, is accompanied by a reliable enhancement of colors of the short-wavelength part of visible light.

The patients with neural disorders were separated into two groups accordingly to the classification [8]. For the first group of patients (10 subjects) the disruptions of interrelations between cortex and subcortex on the thalamic level were found in the rest state. It was expressed in changing thalamo – cortical (vertical) and thalamo – thalamic (horizontal) links. Except for alpha activity describing optimal cortico – subcorctical relations, the EEG time series of the patients included theta activity specified pathological changes in these relations.

During the pain sense the power spectra are characterized by the increase in theta activity. It testifies about an enhancement of unstability of neurodynamic processes. During psychorelaxation theta activity falls in occipital sites of 45% of the group and remains or increases both in frontal and occipital sites (55% of the group). Improvement of psychophysiological state did not correlate with a decrease of theta activity. In other words, there were no reliable changes in power spectra.

During concentrating on the pain locus the patients observed mainly the long-wavelength colors (red, orange, yellow). These colors remained during the psychorelaxation for the 30% patients of the group. The other 70% patients noticed the transformation of color spots to the short-wavelength blue and the complete removal of the pain sense.

Multifractal analysis shows the reliable changes in the electrical brain activity. In all states of the patients with disruptions on the thalamic level the Holder exponent values and the width of the singularity spectrum are less than the values obtained for the healthy subjects. It means that the degree of anticorrelation of persistent sequences of EEG is higher and the randomness of "up – down" patterns increases. It corresponds to the enhancement of unstability of neurodynamic processes in the brain of the patients as compared with the healthy subjects.

During the pain sensation by the patients the multifractal parameter reduces in all electrode sites. During psychorelaxation the recovery of the Holder exponent values up to the values corresponding to the healthy subjects corresponds to the transformation of color spots to the short-wavelength blue (70% patients of the group) (Fig. 2). For other 30% patients the maximal values of the Holder exponent increase weakly during psychorelaxation and they do not reach the

values obtained for the healthy subjects. The width of the singularity spectrum remains less than for the healthy subjects.

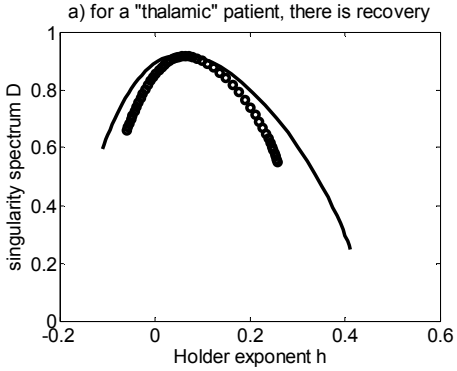

Fig. 2. The examples of singularity spectra of a subject with disruptions of cortico – subcortical links on the thalamic level during the pain sense and during the psychorelaxation (the curve specified as “o” describes the state during the pain sensation and the solid line corresponds to the psychorelaxation state)

Thus, the removal of pain syndromes for the first group patients corresponds to the fall in the degree of anticorrelation of persistent EEG sequences and decline of the randomness of “up – down” patterns observed in all electrode sites. Hence, the improvement of the functional state testifies about a decline of unstability of neurodynamic processes of the brain and optimization of cortico – subcortical links.

For the patients of the second group (8 subjects) disruptions in cortico – subcortical relations manifest on the brain-stem level that leads as a rule to distortion of the stem – cortical and cortico – thalamic (vertical) links. It results to the significant suppression of the alpha component and emergence of the theta acitivity. It is accompanied by the large unstability of neurodynamic processes and amplification of the psychoemotional stress. So, the theta acitivity is prevalent in the all states of this group of the patients . The spectra decline with increasing frequency remembering the spectrum of the pink noise with its inverse proportionality to frequency (~1/f).

The Holder exponent values and the width of the singularity spectrum are larger than the values obtained for the healthy subjects in all studied electrode sites. That is why the multifractality degree of the persistent sequences of EEG far exceeds the degree obtained for the healthy subjects.

During the pain sense the singularity spectrum ($0.1<h<0.9$) corresponds to the both correlated dynamics ($h>0.5$) and anticorrelated dynamics ($h<0.5$) (Fig.3). During relaxation at strong fluctuations ($q>0$) the Holder exponent values decline but the multifractality degree remains high and the singularity spectrum corresponds to both “up - down” and “up - up” patterns.

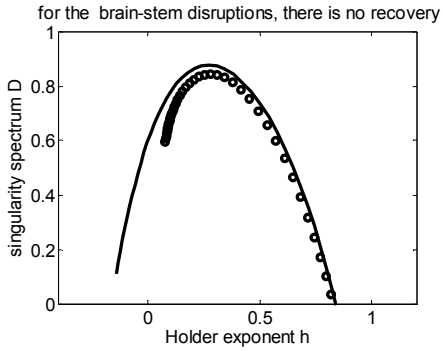

Fig3. The examples of singularity spectra of a subject with neural disorders on the brain stem level during the pain sense and during the psychorelaxation (the curve specified as "o" describes the state during the pain sensation and the solid line corresponds the psychorelaxation state)

The transformation of achromatic dark color spots is not observed for 81% patients. For others 19% achromatic dark colors change into long - wavelength red or orange (distant from colors for the healthy subjects). The both cases are characterized by the similar changes in the singularity spectra and the absence of the improvement of the psychophysiological state.

state	color image	width Δh, Qz	width Δh, Fz	pain removal
healthy subjects:				
before pain		0.59±0.05	0.48±0.05	
during pain	achromatic grey	0.32±0.03	0.26±0.03	
relaxation	blue or green	0.55±0.05	0.62±0.05	yes, in 100%
patients with thalamic disorders:				
during pain	red or yellow	0.28±0.03	0.21±0.03	
relaxation	red, orange or yellow	0.35±0.03	0.32±0.03	no, in 30%
relaxation	blue	0.52±0.05	0.59±0.06	yes, in 70%
patients with brain – stem disorders:				
during pain	achromatic black	1.22±0.11	1.15±0.11	
relaxation	black, red or orange	1.03±0.10	1.07±0.10	no, in 100%

Table 1. Comparison of the mean values of the width of the singularity spectrum obtained by averaging over subjects in different physiological states. The data are given for the Qz and Fz sites.

Training such patients to concentrate their attention on the pain locus and to switch attention on color spots arising spontaneously during 20 repeated trainings did not allow to remove the pain symptoms completely.

The averaged data represented in Table 1 illustrate that the pain removal is accompanied by the recovery of the Holder exponent values up to the values corresponding to the healthy subjects. Thus, there is the relationship between the change of the multifractal parameter and the improvement of the psychophysiological state during psychorelaxation for the patients suffering psychogenic pain.

5 Conclusions

The study demonstrates that power spectra of the patients with neural disorders do not always reflect variations of the psychorelaxation degree. Contrastingly, the changes in the multifractal parameter give a good ability to estimate changes in the healthy and pathological brain activity. Multifractality of the healthy brain is statistically stable as well as stable its neurodynamics. The both cases of unstability in two studied groups of the patients with anxious phobic disorders are connected with deviation (in different sides) of the multifractal parameter from the values specified for the healthy brain. The recovery of the values correlates to the improvement of the psychophysiological state of the patients during psychorelaxation trials. That is why the multifractal analysis can be applied for estimating the psychorelaxation efficiency of the human brain.

Acknowledgements

I thank V. A. Ishinova and I. A. Svyatogor, the physicians of St. Petersburg Albrecht Reabilitation Center and Pavlov Institute of Physiology for their help with EEG recordings.

References

1. E. Bacry, J. F. Muzy and A. Arneodo. Singularity spectrum of fractal signals: exact results. *J. Statist. Phys*. 70: 635-674, 1993.
2. E. Bullmore, et al. Generic aspects of complexity in brain imaging data and other biological systems. *NeuroImage.* 47. 1125- 1135, 2009.
3. V. A. Ishinova, I. A. Svyatogor, T. N. Reznikova. Features of color reflection in psychogenic pain in patients with somatoform disorders during psychotherapeutic treatment. *Spanish J. of Psychology,* 12, 715-724, 2009.
4. B. D. Karvasarsky. Encyclopedia of psychotherapy. St. Petersburg, Ed. Piter, 2002
5. D. Popivanov, et. al. Multifractality of decomposed EEG during imaginary and real visual-motor tracking. *Biological Cybernetics* 94: 149-156 , 2006
6. J. Schultz. Das autogene Training. [The Autogenic Training]. 14th Edition. Stutgart. Ed. Thieme. 1973

7. I. H. Song and D. S. Lee. Fluctuation Dynamics in Electroencephalogram Time Series. In: Mira J, and Alvarez JR(eds) *Lecture Notes in Computer Sci.* Springer-Verlag, Berlin, pp.195-202, 2005.

8. I. A. Svyatogor. Classification of EEG patterns and their neurophysiological interpretation for desadaptation disorders. *Biologicheskaia obratnaia sviaz.* 3. 10 - 19, 2000.

9. A. M. Wink, et al. Monofractal and multifractal dynamics of low frequency endogenous brain oscillations in functional MRI. *Human Brain Mapping* 29: 791-801, 2008.